Earth-Science Reviews 232 (2022) 104112

Contents lists available at ScienceDirect

Earth-Science Reviews

journal homepage: www.elsevier.com/locate/earscirev

Invited Review

Impact Earth: A review of the terrestrial impact record

Gordon R. Osinski [a,b,*], Richard A.F. Grieve [a,b], Ludovic Ferrière [c], Ania Losiak [d], Annemarie E. Pickersgill [e], Aaron J. Cavosie [f], Shannon M. Hibbard [a,b], Patrick J.A. Hill [a,b,g], Juan Jaimes Bermudez [a,b], Cassandra L. Marion [a,b,h], Jennifer D. Newman [a,b,g,h,i], Sarah L. Simpson [a,b,k]

[a] Department of Earth Sciences, University of Western Ontario, 1151 Richmond Street, London, Ontario N6A 5B7, Canada
[b] Institute for Earth and Space Exploration, University of Western Ontario, 1151 Richmond Street, London, Ontario N6A 5B7, Canada
[c] Natural History Museum Vienna, Burgring 7, A-1010 Vienna, Austria
[d] Institute of Geological Sciences, Polish Academy of Sciences, Podwale 75, 50-449 Wroclaw, Poland
[e] School of Geographical and Earth Sciences, University of Glasgow, Molema Building, Lilybank Gardens, Glasgow G12 8QQ, UK
[f] School of Earth and Planetary Science, Curtin University, GPO Box U1987, Perth, Western Australia 6845, Australia
[g] Department of Earth and Atmospheric Sciences, University of Alberta, Edmonton, Alberta T6G 2E3, Canada
[h] Canada Aviation and Space Museum, Ingenium, 11 Aviation Parkway, Ottawa, Ontario, Canada
[i] Centre for Terrestrial and Planetary Exploration, University of Winnipeg, Winnipeg, Manitoba R3B 2E9, Canada
[j] Astromaterials Research and Exploration Science Division, NASA Johnson Space Center, 2101 NASA Road One, Houston, TX 77058, USA

ARTICLE INFO

Keywords:
Impact craters
Impact structures
Impact cratering
Shock metamorphism
Impactites
Glass
Igneous rocks
Tektites
Spherules

ABSTRACT

Over the past few decades, it has become increasingly clear that the impact of interplanetary bodies on other planetary bodies is one of the most ubiquitous and important geological processes in the Solar System. This impact process has played a fundamental role throughout the history of the Earth and other planetary bodies, resulting in both destructive and beneficial effects. The impact cratering record of Earth is critical to our understanding of the processes, products, and effects of impact events. In this contribution, we provide an up-to-date review and synthesis of the impact cratering record on Earth. Following a brief history of the *Impact Earth Database* (available online at http://www.impactearth.com), the definition of the main categories of impact features listed in the database, and an overview of the impact cratering process, we review and summarize the required evidence to confirm impact events. Based on these definitions and criteria, we list 188 *hypervelocity impact craters* and 13 *impact craters* (i.e., impact sites lacking evidence for shock metamorphism). For each crater, we provide details on key attributes, such as location, date confirmed, erosional level, age, target properties, diameter, and an overview of the shock metamorphic effects and impactites that have been described in the literature. We also list a large number of *impact deposits*, which we have classified into four main categories: tektites, spherule layers, occurrences of other types of glass, and breccias. We discuss the challenges of recognizing and confirming impact events and highlight weaknesses, contradictions, and inconsistencies in the literature.

We then address the morphology and morphometry of hypervelocity impact craters. Based on the *Impact Earth Database*, it is apparent that the transition diameter from simple to complex craters for craters developed in sedimentary versus crystalline target rocks is less pronounced than previously reported, at approximately 3 km for both. Our analysis also yields an estimate for stratigraphic uplift of $0.0945D^{0.6862}$, which is lower than previous estimates. We ascribe this to more accurate diameter estimates plus the variable effects of erosion. It is also clear that central topographic peaks in terrestrial complex impact craters are, in general, more subdued than their lunar counterparts. Furthermore, a number of relatively well-preserved terrestrial complex impact structures lack central peaks entirely. The final section of this review provides an overview of impactites preserved in terrestrial hypervelocity impact craters. While approximately three quarters of hypervelocity impact craters on Earth preserve some portion of their crater-fill impactites, ejecta deposits are known from less than 10%. In summary, the *Impact Earth Database* provides an important new resource for researchers interested in impact craters and the impact cratering process and we welcome input from the community to ensure that the *Impact*

* Corresponding author at: Department of Earth Sciences, University of Western Ontario, 1151 Richmond Street, London, Ontario N6A 5B7, Canada.
E-mail address: gosinski@uwo.ca (G.R. Osinski).

https://doi.org/10.1016/j.earscirev.2022.104112
Received 7 February 2022; Received in revised form 29 June 2022; Accepted 5 July 2022
Available online 21 July 2022

Earth website (http://www.impactearth.com) is a living resource that is as accurate and as up-to-date, as possible.

1. Introduction

The surface of the Earth has been shaped by numerous geological processes over the past four and a half billion years. We tend, however, to think mostly about the processes that have been experienced in human history, such as erosive forces, volcanism, and earthquakes, which remind us that our planet is geologically active. Even with volcanic eruptions, however, there have thankfully been no globally significant, super eruptions as part of humanity's experience; although the 1815–16 Tambora eruption appears to have come very close (e.g., Oppenheimer, 2003). This also holds true for significant meteorite impact events, which is likely as a major reason as to why, until the latter part of the 20th century, the importance of impacts as a planetary geological process was not recognized. The advent of planetary exploration demonstrated, however, that impact craters are a dominant geological feature on the Moon and, as we have learned over the subsequent five decades, on the majority of the rocky planets, dwarf planets, moons and asteroids throughout the solar system. Since the 21st century, the realization that asteroids and comets have impacted planetary bodies throughout geological time has revolutionized our understanding of solar system history and evolution. Indeed, it is now widely recognized that impact cratering is one of the most important and fundamental geological processes in the solar system. The large fireball event and meteorite shower of February 15th 2013 over the Chelyabinsk Oblast, Russia (Brown et al., 2013) also served as a reminder that impact events are not a phenomenon past geological eras but continue today.

Our understanding of how impacts have shaped the geological and biological evolution of Earth and other solar system bodies is constantly evolving. What is clear is that the rates of bombardment were much higher in the first half a billion years of solar system history (e.g., Bottke and Norman, 2017; Gomes et al., 2005; Morbidelli et al., 2012; Zellner, 2017). During this time-period, there is strong evidence that planetary-scale impacts occurred. For example, data from Apollo samples, lunar meteorites, and numerical models support the Giant Impact Hypothesis for the origin of the Earth–Moon system (e.g., Canup, 2012; Ćuk and Stewart, 2012; Herwartz et al., 2014). Planetary-scale impacts have also been invoked to account for the crustal scale dichotomy between the northern and southern hemispheres on Mars (e.g., Golabek et al., 2011; Marinova et al., 2008), the delivery of water to terrestrial planets from beyond the ice line (e.g., Daly and Schultz, 2018; O'Brien et al., 2014), and the tilted rotation axis of Uranus (Kegerreis et al., 2018; Kurosaki and Inutsuka, 2018). As the formation of igneous rocks during major impact events is ubiquitous (Dence, 1971; Grieve and Cintala, 1992; Osinski et al., 2018; Pierazzo et al., 1997), several workers have proposed that primary impact melts and, to a lesser extent, subsequent adiabatic melting due to uplift and exhumation of lithospheric and mantle rocks from depth, are a major contributor to the formation of early planetary crusts on the terrestrial planets (Elkins-Tanton, 2012; Elkins-Tanton et al., 2004; Grieve et al., 2006; Latypov et al., 2019).

Motivated by the discovery of extraterrestrial platinum group metals in sedimentary rocks that mark the Cretaceous–Paleogene boundary (Alvarez et al., 1980), considerable attention has been paid to the destructive environmental effects of impacts and their role in, at least, one of the top five mass extinction event on Earth (e.g., Kring, 2003; Pierazzo and Artemieva, 2012; Schulte et al., 2010). That major impact events can have a deleterious effect on the biosphere, coupled with the high impact rates early in solar system history, have led to the common assertion that impacts would have precluded or extinguished the first attempts at terrestrial life (e.g., Chyba, 1993; Maher and Stevenson, 1988; Sleep et al., 1989). More recently, however, studies have shown that impacts can also be beneficial for life, from delivering and/or generating many of the necessary chemical ingredients for life to creating habitats for life in the form of hydrothermal systems, crater lakes, and substrates such as glasses, clays, and porous rocks (see recent review by Osinski et al., 2020a). Many of the worlds impact craters are also known to host ore deposits or hydrocarbon reservoirs, such that the beneficial effects of impacts extend from creating conditions suitable to life to economic resources (Grieve, 2012; Reimold et al., 2005).

In summary, the impact of extraterrestrial objects with planetary bodies is a fundamental geological and biological process and is one that occurs from the very beginning of the formation and evolution of any solar system. Unfortunately, or fortunately for the survival of humans, the uniformitarian principle that "The Present Is the Key to the Past" does not hold particularly well for major impacts that are relatively rare stochastic events and for which there is no historically recent large example to study. Our understanding of impact events, therefore, comes primarily from numerical simulations, experiments, satellite and rover observations from other planetary bodies, the study of Apollo samples from the Moon and other extraterrestrial samples in the form of meteorites, as well as the geological record of impact cratering on Earth. Despite the incompleteness of the terrestrial record, with its complications due to overprinting by other terrestrial geological processes, such as erosion, tectonism, etc., the impact cratering record of Earth is critical to our understanding of the processes, products, and effects of impact events. Impact craters on Earth afford the only present opportunity to conduct fieldwork, deep drilling, detailed geophysical surveys, and obtain *in situ* samples, that are necessary to characterize the nature and properties of the impactites, develop ideas, test hypotheses, and refine our understanding of impact process. In this contribution, we provide an up-to-date review and synthesis of the impact cratering record on Earth through the initiative known as *Impact Earth*.

The goal of the *Impact Earth* initiative (http://www.impactearth.com) is to provide a holistic view of impacts, from fireballs, to meteorite falls, to the largest crater-forming events (Osinski and Grieve, 2019). At its core is a new searchable database of all confirmed impact sites on Earth and many of their most salient attributes, such as age, size, etc. This database is provided here in Appendix A and is discussed in subsequent sections. The origin of the *Impact Earth Database* can be traced back over 65 years to when the systematic search for impact structures in Canada was initiated in 1955 by Dr. Carlyle S. Beals, who was the Dominion Astronomer at the Dominion Observatory (Ottawa, Canada) at the time. This initial effort was enabled by the first national Canadian aerial photograph campaigns. Some early reports are provided by Beals (1958), Beals et al. (1960), Innes (1964), and Beals (1965), culminating with the publication by Dence (1965) that listed 10 possible Canadian impact structures, all of which were subsequently confirmed. This Canadian-focused effort was subsequently taken up by the Earth Physics Branch of the Department of Energy, Mines and Resources in 1970 and expanded to be global in scope, with the first published version being provided by Dence (1972), who listed 63 "certain (authenticated) meteorite impact craters"; although this represented only 12 separate impact sites, with many (e.g., Henbury, Sikhote Alin) comprising multiple "craters", and the largest being the 1.2 km diameter Barringer or Meteor Crater, USA. Dence (1972) also listed 42 "probable impact craters", all but one of which were subsequently confirmed to be of impact origin. It is worth noting that the first published world-wide listing of terrestrial impact structures was by Spencer (1933) who listed "five more or less certain examples of known meteorite craters": Barringer, Henbury, Kaali, Odessa, and Wabar. Other early lists were published by Krinov (1963) and Monod (1965).

Over the course of the next two decades, additional structures were added to the Canadian database, as were other data on their nature and

Table 1
Recommended nomenclature for impact features.

Term	Definition	Meteorite fragments?	Shock metamorphism?	Notes
Impact pit	Terminal pits formed by the impact of an extraterrestrial object, with insufficient velocity to induce a shock wave within target material. A large portion of the impactor is buried beneath or at the bottom of the pit.	Yes	No	Also called penetration craters, penetration funnels, or terminal pits in the literature. The conditions during formation of terminal pits are within the temperature-pressure conditions characteristic for other Earth surface processes. This type of feature is often formed in association with larger meteorite falls next to impact craters or hypervelocity impact craters. Pits can range in size from dm (e.g., the Mukundpura meteorite formed a small pit 43 cm wide and 20 cm deep from which 2.5 kg of carbonaceous chondrite was recovered (Thombre et al., 2019)) to m (e.g., the largest known stony meteorite, the 1770 kg Jilin meteorite, was found in a pit 6 m deep (Begemann et al., 1985)).
Impact crater	An impact crater is a general term that encompasses all impacts of an extraterrestrial object including cases where either shock metamorphism did not occur or has not been recognized in the target materials.	Common	No	No large meteorite mass found in the pit/crater, but fragments of extraterrestrial material associated with the structure. No evidence for shock metamorphism documented. "Craters" such as Carancas (Kenkmann et al., 2009), Campo del Cielo (Cassidy and Renard, 1996) and Morasko (Szokaluk et al., 2019) would fall into this category. The lack of identified signs of shock metamorphism in the case of very small impact craters developed in unconsolidated targets is caused by: a small volume of sufficiently shocked target, a different portioning of energy between craters made in consolidated and unconsolidated materials (see Section 4.3 for other examples and further discussion).
Hypervelocity impact crater	Restricted to impacts where evidence of shock metamorphism in the target materials has been detected.	Depends on size. Common for small structures, rare for larger (>2 km diameter) structures	Yes	Requires the documentation of one or more unambiguous shock metamorphic indicators (see Section 4.2 and Table 2).
Impact deposit	Deposits with evidence of extraterrestrial material and/or geochemical signature and/or shock metamorphism. The source crater may or may not be known.	Rare	Yes and No	This includes tektites, various occurrences of impact glass, sometimes as spherules, and various breccias and distal ejecta in the stratigraphic record that may be recognised based on geochemical (e.g., Alvarez et al., 1980) or mostly petrological means (e.g., Lowe et al., 2014).
Impact crater strewn field	An impact site with more than one distinct crater.	Common	Rare	Impact crater strewn fields are a group of structures formed at the same time (e.g., Losiak et al., 2018, 2020) by a disruption of a single asteroid during its atmospheric entry (Bland and Artemieva, 2006). Strewn fields can comprise a mix of hypervelocity impact craters, impact craters, and impact pits. The separation of structures within the strewn field is up to a few 10s of km. This should not be confused with tektite or meteorite strewn fields, which are accumulations spread out over considerable geographical areas of tektites (see Section 5.4.1.) and meteorites, respectively.

characteristics, and a searchable digital database was created and maintained initially at the Earth Physics Branch and later by the Geophysics Division of the Geological Survey of Canada in Ottawa from 1986 onwards. Periodic reviews provided updates during this time period and include Grieve et al. (1987), which listed 116 confirmed impact craters, and Grieve (1991) and Grieve and Shoemaker (1994), which listed 130 and 145 confirmed impact structures, respectively. Following the termination of a systematic program of impact research at the Geological Survey of Canada in 1997, the database was transferred to the University of New Brunswick, where an abbreviated version was made public on the internet. A number of individual researchers and citizen scientists have also compiled their own (working) lists of confirmed and possible impact structures (e.g., the recent compilation by Kenkmann, 2021), a few of which were made accessible online at some point in time, but many were not maintained and/or are no longer available on the internet. The lack of an agreed-upon and consistent set of criteria for confirming an impact site – which we discuss in Section 4 – has also led to many of these previous lists in having many ambiguous or suspect entries.

The *Impact Earth Database* we present and review here and that is available at http://www.impactearth.com is an outgrowth of these earlier Canadian government-led efforts but is a full relational-database, with enhanced available attributes and search capabilities. The starting point of this work was the original database, provided to us by the Geological Survey of Canada. For the first part of this contribution, we assessed this existing database and carried out a comprehensive scoping review (following the recommendations of Paré et al. (2015) and references therein) of the literature on all confirmed and potential impact features. For clarity, in Section 2, we discuss what actually constitutes a "meteorite impact crater", provide an overview of the impact process (Section 4), and outline the criteria that we used and recommend for how *impact craters*, *hypervelocity impact craters*, and *impact deposits* on Earth are confirmed (Section 4). As there are likely omissions and even errors in this database due to the diversity and breadth of the current literature on terrestrial impacts, we welcome input from the entire community. In the second part of this contribution, we provide a critical

review of the *Impact Earth Database* and discuss weaknesses, contradictions, and inconsistencies in the literature. We provide recommendations as to how to determine important attributes such as age and diameter. For each impact feature, we provide important attributes, including when it was first confirmed as due to impact, age, diameter, level of preservation, and what types of impactites and shock metamorphic features have been reported in the literature.

One of our main aims is that the *Impact Earth Database* will provide an important new resource for researchers interested in impact craters and that it will stimulate future research endeavours. The *Impact Earth* website (http://www.impactearth.com) will be a living resource for those who wish to track what has changed over time. We note that we do not cover post-impact processes, such as impact-generated hydrothermal systems (Kirsimäe and Osinski, 2012; Osinski et al., 2013), the destructive environmental effects (Schulte et al., 2010), or the positive beneficial effects for microbial life (Osinski et al., 2020b) and generation of economic resources (Grieve, 2012; Reimold et al., 2005). Finally, we also acknowledge that the Canadian context is preferentially used here to illustrate some of the properties and challenges of the terrestrial record (e.g., in determining rim diameter, even in relatively fresh structures), which is related to the first two authors having conducted the bulk of their field and laboratory studies at Canadian impact sites.

2. What constitutes an impact crater?

In the literature, sites proposed to be of extraterrestrial origin are referred to by various terms: "craters", "impact craters", "hypervelocity impact craters" or "meteorite impact craters". The first attempt to introduce consistent terminology and a classification scheme for craters was by Krinov (1963) and Dence (1965), and subsequently synthesized by Dence (1972). These authors defined four main types of craters: 1) *Impact pits* formed by meteorites that remain intact; 2) *Impact craters* formed by meteorites that break up and deform but the target materials are not subjected to shock metamorphism; 3) *Simple hypervelocity craters*, comprising uplifted and overturned rim rocks, a breccia lens, but most importantly, evidence of shock metamorphism in the target materials; and 4) *Complex hypervelocity craters* that are relatively shallow with respect to their depth-diameter ration, with a central uplifted area and slumped or depressed rim structure.

Stöffler and Grieve (2007) also noted that the term "impact" should more correctly be "hypervelocity impact", defined as "the collision of two (planetary) bodies at or near cosmic velocity, which causes the propagation of a shock wave in both the impactor and target body (Melosh, 1989)". The key defining factor then is *shock metamorphism*, which refers to material engulfed by and, therefore, affected by the passage of a *shock wave* (Stöffler and Grieve, 2007). The problem arises with the use of the term "impact crater", without the prefix "hypervelocity". To some, the terms "impact crater" and "hypervelocity impact crater" may be interchangeable. For example, French, in his book *Traces of Catastrophe*, writes that "the general term 'impact crater' is used here to designate a hypervelocity impact crater" (French, 1998). This definition is not the same as Dence (1972), who explicitly stated that "impact craters" do *not* form through the passage of a shock wave and are *not* hypervelocity in origin. French (1998) then refers to *pits* as low-velocity impacts, forming craters typically less than a few 10s m in diameter. Importantly, pits do not form from hypervelocity impact and shock metamorphism does not occur in the target rocks or impactor.

Table 1 provides definitions of the terminology used in this review and the *Impact Earth* database and website. Importantly, most terrestrial impact sites, both impact craters and hypervelocity impact craters, are eroded to some degree such that the original crater-form is modified or even no longer present. As such, the term *impact structure* as a general term is preferred for most terrestrial hypervelocity impact craters, except in the rare cases where the original crater morphology is preserved.

3. The impact cratering process

Tens to hundreds of metric tons of material from space is acquired by the Earth every day. The bulk of this material is micrometer to mm size and disintegrates and/or melts in atmosphere. On planetary bodies that lack an atmosphere, such as the Moon, this material does impact the surface, forming microcraters and is the dominant process causing erosion of exposed lunar rock surfaces (Hörz et al., 1971). Centimeter- to m-size objects (i.e., *meteoroids*) that are coherent enough and can survive atmospheric passage and make it to the Earth's surface intact are termed *meteorites*. During passage through the Earth's atmosphere, these meteoroids leave visible paths in the form of *meteors* or "shooting stars". A *fireball* is an unusually bright meteor that reaches a visual magnitude of −4 or brighter (American Meteor Society, 2022). As discussed in the previous section, large meteorites can penetrate some distance into the surface of the target materials to form *impact pits* (Table 1), where the pit is only slightly larger than the meteorite itself. An example of one of the largest impact pits is one formed by the Sterlitamak IIIAB iron meteorite in 1990 in Russia, where a 315 kg meteorite with dimensions 50 × 45 × 28 cm was found within a 10 m diameter pit at 12 m depth (Petaev, 1992). Meteorites, even those that form m-size impact pits, will have lost most or all of their original velocity and kinetic energy by atmospheric retardation and suffered some degree of disintegration and ablation (French, 1998).

In some cases, for example the 1908 Tunguska (Vasilyev, 1998) and the more recent 2013 Chelyabinsk (Brown et al., 2013) events, extraterrestrial objects in the m- to few 10s m size range can be completely disrupted during passage through the Earth's atmosphere and explode at heights that can affect the Earth's surface. It is becoming increasingly apparent that such events, referred to interchangeably as airbursts, aerial bursts, or bolides, are common and pose significant threats to humans. The Center for Near Earth Object Studies at NASA's Jet Propulsion Laboratory manages an up-to-date database of all fireballs (reported by US government sensors) since 1988. Ground- and satellite-based observations combined with theoretical calculations of airbursts suggest that the Earth is struck annually by a objects with energies equivalent to 2–10 kt TNT equivalent, with Tunguska-size events occurring once every 1000 years (Brown et al., 2002). Wasson (2003) further suggested that airbursts larger than Tunguska must surely have occurred throughout geological time. The issue is that such events are predicted to not form craters or leave other clear and long-lasting signs on the Earth surface, so they are hard to identify and confirm. Numerical modelling by Boslough and Crawford (2008) suggests that during large low-altitude airbursts, a high-temperature jet is formed that, if it makes contact with the Earth's surface, will expand radially outwards in the form of a fireball. Pressures are insufficient to produce shock metamorphism in surface materials; however, temperatures exceed the melting temperatures of silicate minerals which, following rapid quenching, will create abundant glass deposits that may be preserved in the geological record (Boslough and Crawford, 2008).

If the extraterrestrial object – i.e., an asteroid or comet – is large enough to pass through the atmosphere with little to no deceleration, it impacts the Earth's surface at a combination of its original cosmic velocity (i.e., the velocity at which an object is moving through space) and the Earth's escape velocity, generating a shock wave and forming a *hypervelocity impact crater*. For Earth, the minimum impact velocity for the formation of a hypervelocity impact crater is 11.2 km/s, which is the escape velocity of our planet. Average impact velocities, however, are substantially higher, with ~18 km/s for asteroids and ~ 30–50 km/s for comets. Such extreme velocities translates into staggeringly high amount of kinetic energy deposited into the Earth's crust. Taking the average impact velocity for an asteroid (~18 km/s), a 45° impact angle (the most likely), and assuming projectile and target densities of 3000 kg/m^3, 100 m and 1 km-diameter projectiles release ~10^{17} and 10^{20} J, respectively, and produce craters ~1.1 km and 13.8 km in diameter, respectively (Collins et al., 2005). For comparison, the largest

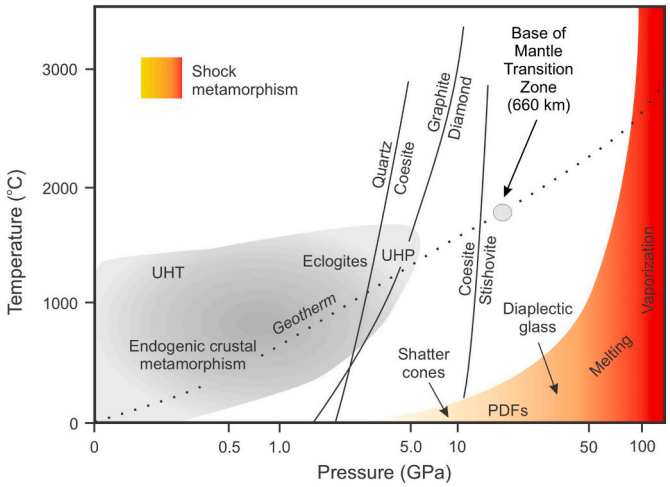

Fig. 1. Pressure–temperature (P–T) plot showing comparative conditions for shock metamorphism and 'normal' endogenic crustal metamorphism. Note that the pressure axis is logarithmic. While there is some overlap in pressure between eclogites and Ultra High Pressure endogenic metamorphic rocks and low pressure shock metamorphic effects (i.e., shatter cones that form at ~2 GPa and higher), the temperature conditions are distinctly different. Modified from French (1998) and Osinski and Pierazzo (2012).

earthquake ever recorded (i.e., the M9.5 1960 Chile earthquake) and the largest known volcanic eruptions (e.g., the explosive ~27 Ma La Garita Caldera eruption and largest single Colombia River basalt lava flows at ~15 Ma), released energies of the order of 10^{19} J (Gudmundsson, 2014). The formation of a hypervelocity impact crater is, in addition, further unlike any other endogenic geological process (Fig. 1), due to the extreme pressures (100 s and likely exceeding 1000 GPa; cf., the pressure at the centre of the Earth of ~360 GPa) and temperatures (10,000 s ^{o}C; cf., the temperature at the centre of the Earth of ~6000 °C), their virtually instantaneous nature (i.e., seconds to minutes), the extreme strain rates involved (~10^{4} to 10^{6} s^{-1}; cf., the average geological strain rates of ~10^{-14} (Fagereng and Biggs, 2019)), and the fact that this energy is released at an essentially single location on the Earth's surface.

The formation of a hypervelocity impact crater has historically been considered to encompass three main stages (Ahrens and O'Keefe, 1977; Gault et al., 1968; Melosh, 1989) (Fig. 2): (1) contact and compression, (2) excavation, and (3) modification. This adequately conveys the formation of hypervelocity impact craters, but does not convey the significant impact-induced processes, environmental, and geological effects, that may continue for thousands to millions of years after the impact event. Such post-impact stages and processes are beyond the scope of this contribution, but include the *hydrothermal phase*, where impact-generated hydrothermal systems and crater lakes can develop, the *post-impact succession phase*, and the *ecological assimilation phase* (Osinski et al., 2020c).

The so-called *thermobaric phase* of an impact event is when the hypervelocity impact crater is formed (Osinski et al., 2020c), comprising the three formation stages listed above. Details of the physics of crater formation are given in Melosh (1989) and are only presented here in narrative form. Crater formation begins with the initial *contact and compression stage* (Fig. 2a), when the impactor contacts the surface of the target, and ends, when the shock compression of the impactor has been completely unloaded (i.e., it is vaporized, melted, and/or ejected from the cavity). During this stage, the impactor penetrates ~1–2 times its diameter into the target rocks and transfers its considerable kinetic energy to the target rocks. Shock waves are generated at the target-impactor interface and propagate both into the target rocks and back into the impactor. The "free" upper surface of the impactor cannot be subjected to compression and, thus, the shock wave is reflected back into the impactor as a rarefaction or tensional wave (Ahrens and O'Keefe, 1972). It is the passage of this rarefaction wave through the impactor that causes it to unload from high shock pressures. Under shock compression, there is considerable pressure-volume work performed within the target rocks and their internal energy is increased. If porosity is present in the target rocks (e.g., in most sedimentary rocks) the pores are closed by relatively low shock pressures (Güldemeister et al., 2013; Kieffer et al., 1976; Wünnemann et al., 2008). As with the impactor, shock pressures cannot be maintained at the free surface of the target rocks and a rarefaction wave propagates into the shock compressed target rocks. This combination of the shock and rarefaction waves in the target materials ultimately results in *shock metamorphism* (Fig. 1) of target rocks and the production of distinctive *shock metamorphic effects*, which are discussed in detail in Section 4. It is notable that the pressure–temperature space in which shock metamorphism occurs is distinctly different from any form of endogenic metamorphism (Fig. 1). On decompression by the rarefaction wave, not all the pressure-volume work due to shock compression is recovered. The unrecovered pressure-volume work that remains is expressed as waste heat, which can result in the melting (see review by Osinski et al., 2018) and, even, vaporization of the impactor and a portion of the target rocks (Melosh, 1989) (Fig. 1).

During the subsequent *excavation stage*, the kinetic energy imparted to the target rocks by the interaction of the shock and rarefaction waves leads to particle velocities in the target rocks, with trajectories that define an "excavation flow-field" (Fig. 2b). This flow-field, combined with downward and outward physical compression of the target rocks, result in the formation of a so-called "transient cavity". It is important to note that the transient cavity is a conceptual construct and only exists as a physical entity in the smallest of impacts. Fig. 1b, which shows the concept of a transient cavity, can be regarded as a provenance map for what happens to the target rocks and where they end up (Dence, 1968; Grieve and Cintala, 1981). This figure illustrates the consequence of the different trajectories of target rocks, which results in the division of the transient cavity into an upper "excavated zone" and a lower "displaced zone" (Fig. 2b). During the excavation stage, material in the upper zone, comprising a mixture of fragmented target rocks with varying proportions of impact melt, is ejected ballistically beyond the transient cavity rim to form the *continuous ejecta blanket* (Oberbeck, 1975). A portion of the melt and fragmented target rock mixture that originates beneath the point of impact is deflected upwards and outwards parallel to the base of the transient cavity, but must travel further and possesses less kinetic energy than material in the excavated zone, so that ejection is not achieved (Grieve et al., 1977) (Fig. 2b). This material remains in the transient cavity into the modification stage (Figs. 2c, d). The end of the excavation stage is the point in time when motions associated with the passage of the shock and rarefaction waves can no longer excavate or displace target rocks and melt (Fig. 2c). As noted below, however, the excavation and modification stages may begin and end at different times in different parts of the transient cavity and these two stages can overlap in time, particularly in larger craters.

Towards the end of the excavation stage, however, the next stage of the cratering process is determined by the scale of the impact event, through a combination of the size of the transient cavity, planetary gravity and, and to a lesser extent, by the strength of the target rocks. Below a certain size, the transient cavity is only mildly unstable, and the third and final *modification stage* involves only inward collapse and slumping of the transient cavity wall, and a *simple hypervelocity impact crater* is formed (Fig. 3a). Simple hypervelocity impact craters comprise a bowl-shaped cavity, with an uplifted and commonly overturned rim or "flap" that approximates the transient cavity rim (Fig. 2e). The overturned flap is overlain by allochthonous impact ejecta deposits and the crater interior is partially filled, to approximately half the depth of the original transient cavity, with crater-fill impactites largely derived from the inward collapse of a portion of the transient cavity wall. The term "impactite" is "a collective term for all rocks affected by one or more hypervelocity impact(s) resulting from collision(s) of planetary bodies" and comprises three main classes of rocks: shocked rocks, impact melt

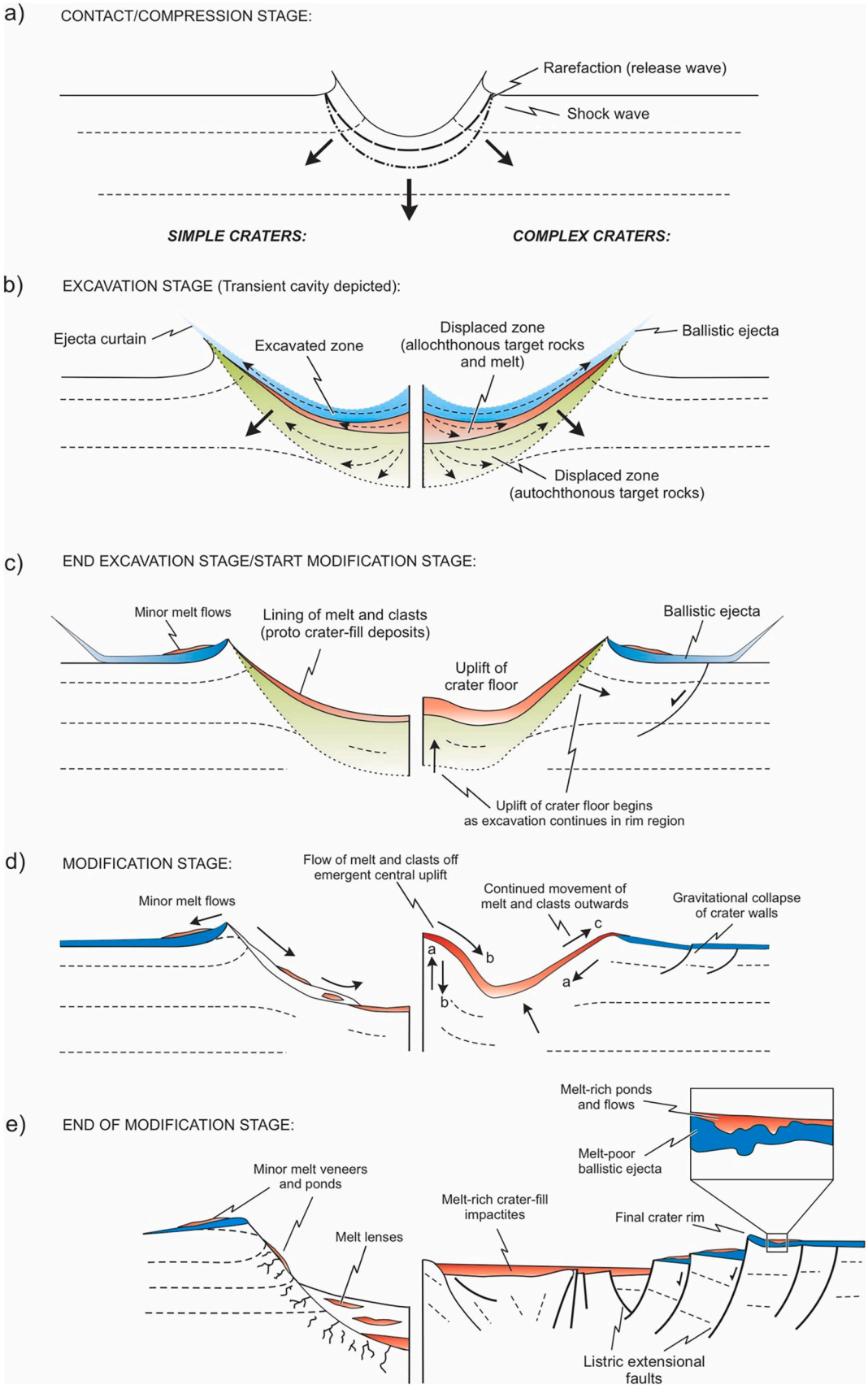

(caption on next page)

Fig. 2. Schematic diagrams showing the formation of simple and complex hypervelocity impact craters. It should be noted that these diagrams are for continental non-marine impacts. For marine impacts, the subsequent resurge of water into the crater cavity affects many aspects of the cratering process and products (see Sections 8 and 10.3. for details). a) The initial contact/compression stage of crater formation. b) During the excavation stage, a transient cavity forms by the excavation and displacement of target materials. The emplacement of ballistic impact ejecta occurs during this stage. c) At the end of the excavation stage, the transient cavity is lined with a mix of melt and clastic material. The transition to the modification stage in complex craters (right) occurs when the uplift of the crater floor occurs, which in larger craters can occur while excavation is still ongoing in the outermost regions of the transient cavity. d) During the modification stage, minor slumping occurs in simple craters (left) and in complex craters (right) the uplift of the crater floor and inward collapse of the transient cavity rim occurs. In this schematic, the arrows represent different time steps, labelled "a" to "c". Initially, the gravitational collapse of crater walls and central uplift (a) results in generally inwards movement of material. Later, melt and clasts flow off the central uplift (b). e) Final crater form after the end of the modification stage. Modified from Osinski et al. (2011) and Osinski and Pierazzo (2012).

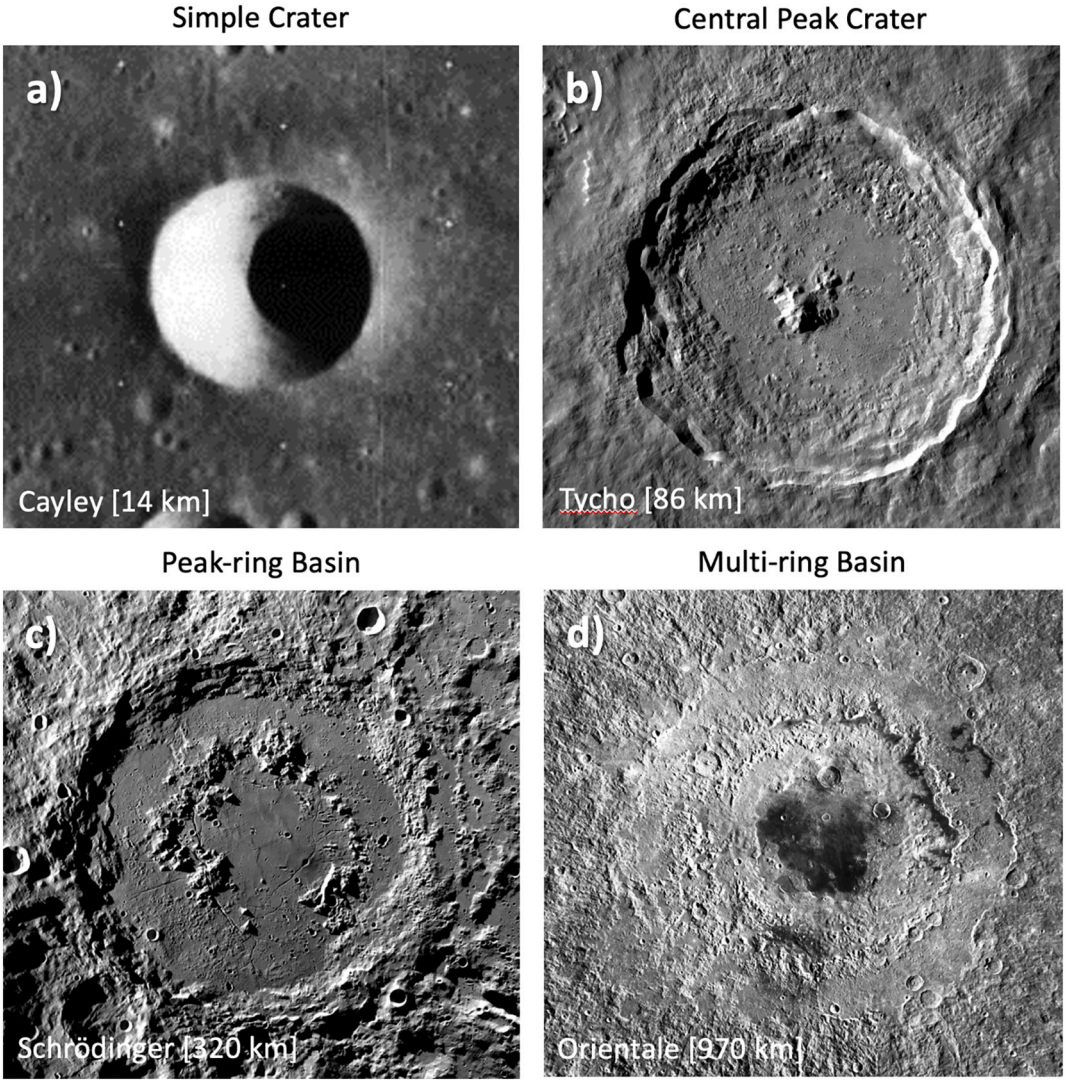

Fig. 3. Images of lunar craters showing the change in morphology with increasing diameter. All images are portions of Lunar Reconnaissance Orbiter Camera Wide Angle Camera mosaics. Image credits: NASA/GSFC/Arizona State University.

rocks, and impact breccias (Stöffler and Grieve, 2007). Studies at the Barringer and Brent simple craters demonstrate that the crater-fill impactites in simple craters is mostly impact breccia with overall low shock levels, consistent with an origin via slumping of the (low shock) transient cavity walls (Grieve and Cintala, 1981), intermixed with volumetrically relatively small lenses and zones of more highly shocked and shock melted material that originated closer to the point of impact and lined the floor and walls of the transient cavity, prior to the collapse of the cavity walls.

Above a certain threshold size, the transient cavity is considerably more unstable and the modification stage drastically changes the character of the final crater, producing so-called *complex hypervelocity impact craters* (e.g., Fig. 3b). The actual transition diameter from simple to complex hypervelocity impact craters on the terrestrial planets is approximately inversely proportional to the gravitational acceleration (g) of a given planet (Pike, 1980). Historically, the simple to complex transition diameter for the Moon was proposed to occur at ~19 km (Pike, 1977), but more recent analyses using higher-resolution imagery and elevation data from the Lunar Reconnaissance Orbiter mission place the transition diameter at ~20 km for highland craters and ~ 18 km for mare craters (Krüger et al., 2018). On Earth, the transition has been cited traditionally as occurring at ~2 km for craters in sedimentary and ~ 4 km in crystalline targets, respectively (Dence, 1972) – we revisit these transition diameters for terrestrial craters in Section 9.1.

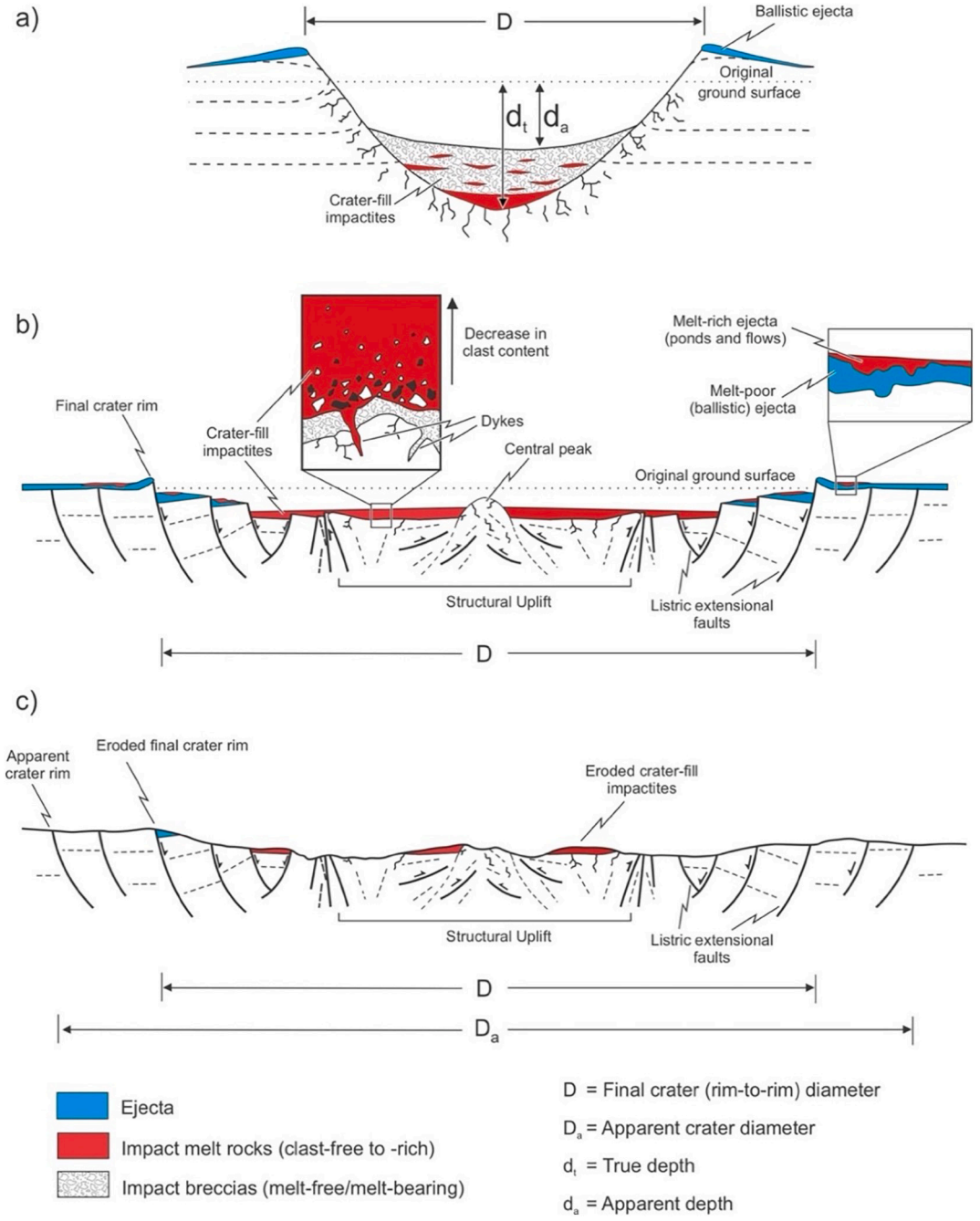

Fig. 4. Schematic cross sections of simple and complex hypervelocity impact craters developed in crystalline target rocks and in continental non-marine settings. Note that for craters developed in mixed sedimentary-crystalline and purely sedimentary target rocks, the lithological character of the crater-fill impactites and ejecta deposits differ (see Section 10). a) Simple impact craters comprise a relatively deep crater fill by a mix of impact breccias and intercalated impact melt rocks. Ballistic ejecta deposits occur outside the topographic final crater rim. b) Complex impact structures have shallower depth-to-diameter ratios than simple impact craters. Crater-fill impactites typically follow a sequence from the bottom up of melt-free to -poor impact breccias overlain by impact melt-bearing breccias and/or impact melt rocks. Ballistic ejecta can occur inside the final crater rim in the faulted terraced region. Most terrestrial complex craters preserve a two-layered ejecta stratigraphy with melt-rich ejecta overlying the ballistic ejecta deposits (Osinski et al., 2011).

During the modification stage in complex craters, the originally bowl-shaped transient cavity is modified by two competing processes (Figs. 2c – e); uplift of the floor of the transient cavity floor in the center of the cavity and the complete downward and inward collapse of the rim area. In larger craters, this structural uplift can occur before excavation ceases at the outer reaches of the transient cavity and can also overshoot above the original target surface and then collapse back downwards and outwards (Fig. 2d). It is also important to note that the transition from simple to complex crater morphologies is not abrupt. For example, there is a group of so-called *transitional impact craters* on the Moon that range from 15 to 42 km in diameter. Such transitional craters comprise a relatively flat crater floor instead of the bowl-shaped form of simple craters, possesses one or more discrete terrace and/or rock slides, but lack an emergent topographic structural uplift (Osinski et al., 2019).

On the Moon and other planetary bodies with well-preserved craters, the structural uplift is manifest as a topographic central peak (Fig. 3b), or cluster of peaks, that rises above the surrounding crater-fill deposits. With increasing crater diameter on the Moon (~200 km), a peak ring

structure appears in addition to the central peak, forming proto-basins or central-peak basins (Pike and Spudis, 1987). At even larger diameters, central peaks are no longer visible and peak-ring basins (>300 km diameter) (Fig. 3c) and eventually multi-ring basins (>600 km diameter) (Fig. 3d) form, which comprise two or more concentric topographic rings, respectively (Hartmann and Kuiper, 1962). At terrestrial hypervelocity impact craters the original topography and morphology of the centrally uplifted region is typically not preserved due to erosion, and the generic term *structural uplift* is preferred (Grieve et al., 1981). However, as discussed in Section 9.3., the central uplifts of terrestrial complex impact craters appear to be more subdued in their morphology and morphometry and may never have looked like fresh lunar complex craters.

The second major process occurring during the modification stage in complex craters is the inward and initially downward collapse of the transient cavity walls (Fig. 2d). In fresh planetary craters, the rim region comprises a series of fault-bounded terraces (Fig. 3b). Field studies of craters on Earth reveal the degree of structural complexity that is typically hidden from view in remote-sensed data on fresh planetary craters. These terrestrial studies show that crater collapse occurs along a series of interconnected faults, oriented both radially and concentrically to the point of impact (Kenkmann et al., 2014); concentric faults are often listric in nature and can be oriented both inwards and outwards (Osinski and Spray, 2005). Radial faults accommodate movement along concentric faults and deformation is also accommodated via radially and concentrically-oriented fold structures (Kenkmann et al., 2014; Kenkmann and von Dalwigk, 2000; Osinski and Spray, 2005). Due to these considerably more substantial modification processes, complex craters have smaller depth-diameter ratios than simple craters, typically ~1:10 to 1:20 for lunar craters (Pike, 1977). For complex craters, the modification stage is the longest stage in the impact cratering process, approaching a few minutes in duration in the largest impacts (Melosh, 1989).

As noted above, throughout the modification stage, the transient cavity is lined by a melt and fragmented target rock mixture that was not ejected during the excavation stage (Figs. 2c, d). Due to the dynamic nature of the modification stage, this material can undergo significant transport during this final stage of formation of complex craters. A portion of this material remains within the interior of the final crater, forming crater-fill deposits (Figs. 2e, 4b). Such crater-fill impactites in complex craters formed in crystalline target rocks are dominated by impact melt rocks and melt-bearing breccias (Grieve and Therriault, 2012). Observations of terrestrial and planetary craters also reveal that a portion of this material is transported as ground-hugging flows during modification stage outwards beyond the transient and final crater rims in a second major phase of ejecta emplacement (Hawke and Head, 1977; Osinski et al., 2011). In complex craters, the transient cavity is essentially collapsed and destroyed during the modification stage. As a result, ejecta deposits occur both within the final crater, in regions which were exterior to the initial transient cavity, but are now interior to the final crater rim, and in regions exterior to the final crater rim (Fig. 2e). The end of the modification stage equates to the point in time where all major transport and movement of target material as the result of the deposition of the kinetic energy of the impactor ceases. The modification of terrestrial craters through post-impact isostatic and structural readjustment, particularly movement along the major faults, can continue for geologically significant time after the initial impact event, particularly if there is subsequent tectonic activity.

4. Criteria required to confirm impact events

4.1. A historical perspective

Throughout the 19th century, the increasing recognition of meteorites led to a growing appreciation that extraterrestrial objects can strike Earth (see Marvin, 2006, and references therein). In 1891, the discovery of the Cañon Diablo iron meteorite "near the base of a nearly circular elevation, which was known locally as "Crater Mountain" in northern Arizona (Foote, 1891), marked the beginning of the debate as to the origin of the structure we now know as Meteor or Barringer Crater. At about the same time, Gilbert (1893) proposed the impact origin for lunar craters. Three years later, Gilbert (in)famously concluded that this same crater in Arizona, which he referred to by its more official local name of Coon Mountain or Coon Butte, was not of extraterrestrial origin (Gilbert, 1896). It wasn't until a few years later that Daniel M. Barringer, a mining engineer and businessman, first proposed an impact origin for this structure, making the connection between the presence of iron meteorites and a crater (Barringer, 1905).

For the subsequent few decades after the recognition of Meteor or Barringer Crater, only the presence of meteorite fragments was deemed as evidence for an impact event. There were, however, researchers suggesting the impact origin of other structures in the absence of meteoritic fragments. A notable early example is Spencer (1933), who recognized the link between circular topographic depressions and the presence of meteoritic material and unusual silica glasses at the Odessa craters in Texas (Barringer, 1928), the Henbury crater field in Australia (Alderman, 1932), Kaali in Estonia (Reinwald, 1939), and the Wabar craters in Saudi Arabia (Philby, 1933). The author appears to also have been the first to suggest the impact origin of Campo del Cielo craters in Argentina.

Boon and Albritton (1936) built upon the observations of Spencer (1933) and hypothesized that given the presence of larger multi-km size impact craters on the Moon that the same should be the case for the Earth. These authors were among the earliest to suggest the impact origin of larger structures that lacked meteorite fragments. Their descriptions of circular structures with central uplifted areas surrounding downfaulted rocks and a rim comprising outward dipping layers essentially describes what we now know as *complex impact structures*. These authors appear to have also been the first to make the connection to so-called "cryptovolcanic structures" on Earth. Boon and Albritton (1936) noted "cryptovolcanic structures" possessed a circular outline, a central uplift, set in a larger exterior down-faulted area and evidence for "violent action". The term "cryptovolcanic" was first used to describe what is now known as the Steinheim impact crater in Germany (Branco and Fraas, 1905). Bucher (1936) described several similar "cryptovolcanic structures" in the USA, and defined them as "disturbances produced by the explosive release of gases under high tension, without the extrusion of any magmatic material, at locations where there had previously been no volcanic activity". Boon and Albritton (1936) concluded that "that some of the structures which have been assigned to volcanic origin are equally as well interpreted as meteorite structures". All but one of the cryptovolcanic structures they cited, as reported by Bucher (1936), were subsequently confirmed as complex hypervelocity impact structures: Decaturville, Flynn Creek, Kentland, Serpent Mound, Upheaval Dome, and Wells Creek. The one structure not currently confirmed is Jeptha Knob, but its impact origin remains a possibility (Cressman, 1981; Fox, 2014; Seeger, 1968) (see Section 4.4. for further discussion). Similarly, Fredriksson and Wickman (1963) suggested that 5 unusual geological structures in Sweden (Dellen, Hummeln, Mien, Siljan, and Tvären) were possible "fossil astroblemes"; all of these were subsequently confirmed as hypervelocity impact structures.

The presence of meteoritic fragments, however, remained the only widely accepted diagnostic criterion to confirm an impact event until the early 1970s. Indeed, as noted above, in his compilation of known impact craters, Dence (1972) listed only 12 "certain (authenticated) meteorite impact craters" (Aouelloul, Barringer, Boxhole, Campo del Cielo, Dalgaranga, Haviland, Henbury, Kaälijarvi, Odessa, Sikhote Alin, Wabar, Wolfe Creek), all, except one (Aouelloul) were confirmed by the presence of meteorite fragments. Dence (1972) did provide a list of 42 "probable impact craters", many of which were previously interpreted as "cryptovolcanic structures", based on "possible" evidence for shock metamorphism. While some early workers did suggest a link between

Table 2
Criteria that can be used to confirm the presence of a hypervelocity impact crater.

Feature	Description and notes	Setting(s) in crater	Rock or mineral type(s)	References
Shatter cones	Meso- and/or macroscopic linear, conical striations on fracture surfaces that are best developed in fine-grained, structurally isotropic rocks that have been affected by relatively low levels of shock metamorphism, ~2 to 10 GPa (Fig. 6a).	In-situ in central uplift; lithic clasts in crater-fill deposits, ejecta deposits and dykes in crater floor (Fig. 5).	All consolidated rock types; more difficult to discern in coarse-grained lithologies.	(Baratoux and Reimold, 2016; Dietz, 1968; Milton, 1977; Osinski and Ferrière, 2016; Wieland et al., 2005).
Planar Fractures (PFs)	Microscopic, multiple parallel sets of open planar fractures greater than 3 μm wide, spaced more than 15–20 μm apart, produced by low level shock pressure (~5–8 GPa). Importantly, due to the production of features that resemble PFs in endogenic settings, to be considered diagnostic on their own, PF's must occur as sets of 2 or 3 across a single grain, in a significant number of grains, and with distinct crystallographic orientations (Figs. 6b,c).	Crater fill deposits, ejecta deposits, dykes in crater floor, and *in-situ* target rocks affected by low levels of shock (Fig. 5).	All rock types; tectosilicates (quartz, feldspars), nesosilicates (garnet, titanite), zircon, apatite.	(Cox et al., 2020; L. Ferrière and Osinski, 2012; French, 2004; French and Koeberl, 2010; Stöffler and Langenhorst, 1994; Timms et al., 2019).
Planar Deformation Features (PDFs)	Microscopic, parallel, narrow planar features (usually less than 200 nm thick) spaced 2–10 μm apart in individual mineral grains (e.g., quartz, feldspar) comprised originally of lamellae of amorphous material, produced by shock pressures ~10 to 30 GPa. PDF's often occur as multiple, intersecting sets with distinct crystallographic orientations. In many cases, the original isotropic material has annealed over time and the PDFs are discerned as parallel lines of microscopic inclusions and are described a "decorated PDFs" (Fig. 6d).	Crater fill deposits, ejecta deposits, dykes in crater floor, and *in-situ* target rocks affected by shock metamorphism (Fig. 5).	Quartz, feldspars, zircon.	(Carter, 1965; Chao, 1967; Engelhardt and Bertsch, 1969; Grieve et al., 1996; Robertson et al., 1968; Stöffler and Langenhorst, 1994).
Feather features (FFs)	Thinly spaced, short, parallel to subparallel lamellae that branch off of PF's. These microstructures are poorly understood but are somewhat crystallographically controlled and likely develop at ~7 to 10 GPa (Figs. 6b,e).	Crater fill deposits, ejecta deposits, dykes in crater floor, and *in-situ* target rocks affected by shock metamorphism (Fig. 5).	Quartz.	(Poelchau and Kenkmann, 2011).
Diaplectic glass	Natural glass formed by solid state transformation (i.e., without melting) at shock pressures >30 to 50 GPa (Figs. 6f,g).	Crater fill deposits, ejecta deposits, *in-situ* target rocks affected by shock metamorphism (rare) (Fig. 5).	SiO_2, feldspars.	(Bunch et al., 1967; Fritz et al., 2019; Grieve et al., 1996; Stöffler, 1984).
FRIGN zircon	Former reidite in granular neoblastic (FRIGN) zircon, a ~ 1 μm diameter, neoblastic, granular zircon grain indicative of pressures ≥30 GPa and temperatures ≥1673 °C.	Crater fill deposits and ejecta deposits (Fig. 5).	$ZrSiO_4$	(Cavosie et al., 2018a)
Stishovite	High pressure polymorph of SiO_2, forming at shock pressures ≥10 GPa.	Crater fill deposits, ejecta deposits, and dykes in crater floor (Fig. 5).	SiO_2	(Chao et al., 1962; Stöffler and Langenhorst, 1994)
Reidite	High pressure polymorph of $ZrSiO_4$, forming at shock pressures ≥20 GPa.	Crater fill deposits, ejecta deposits, and dykes in crater floor (Fig. 5).	$ZrSiO_4$	(Glass et al., 2002; Wittmann et al., 2006; French and Koeberl, 2010)
TiO_2-II	High pressure polymorph of TiO_2, forming at shock pressures ~5 to 12 GPa.	Crater fill deposits, ejecta deposits, and dykes in crater floor.	TiO_2	(Bendeliani et al., 1966; Spektor et al., 2013)
Unnamed (La, Ce, Th)PO_4 polymorph	High pressure polymorph of unnamed phosphate mineral, (La, Ce, Th)PO_4.	Crater fill deposits (Fig. 5).	(La, Ce, Th)PO_4	(Erickson et al., 2019)
Orthorhombic-ZrO_2 polymorph	High pressure, orthorhombic polymorph of ZrO_2, forming at shock pressures ~70 to 90 GPa.	Crater fill deposits (Fig. 5).	ZrO_2	(Haines, 1997; Wittmann et al., 2006)

what are now known as shock metamorphic features and impact events, most notably Robert Dietz and his pioneering recognition of shatter cones (Dietz, 1946, 1947), the occurrence of shock metamorphism was not generally recognized until the 1960s. This represented a paradigm shift in the understanding and recognition of meteorite impact craters.

The first study, to our knowledge, to recognize microscopic planar microstructures or lamellae in quartz that we now refer to as planar fractures (PFs) and planar deformation features (PDFs) was by McIntyre (1962) in an abstract presented at the First Western National Meeting of the American Geophysical Union held in December 1961 – and later published in McIntyre (1968). Carter (1965) provided one of the first peer-reviewed articles to document planar microstructures in quartz, based on studies of samples from Barringer Crater and the West Clearwater Lake and Vredefort impact structures. Stöffler (1966) also documented PFs and PDFs at the Ries impact structure and was one of the first studies to document increasing levels of shock toward the point of impact. Another early report was by Chao (1967), who studied samples from the confirmed craters Aouelloul, Barringer, Henbury, Wabar, and the suspected craters of Bosumtwi and Ries, who documented PFs and PDFs in quartz, so-called diaplectic glass, whole rock glass, and the high-pressure polymorphs coesite and stishovite. This publication built upon the landmark conference "Shock Metamorphism of Natural Materials" that was held at the NASA Goddard Space Flight Center in Maryland, USA, April 14–16, 1966. The conference proceedings published two years later (French and Short, 1968) cover a wide variety of topics on shock metamorphism, many of which are still considered groundbreaking. Despite the overwhelming evidence that shock metamorphic features, such as PDFs in quartz and shatter cones, can only be formed from hypervelocity impact, there were proponents that clung to the idea of a cryptovolcanic origin. For example, in Canada, the Manicouagan

(Currie, 1972), Mistastin Lake (Currie, 1971), Slate Islands (Sage, 1978), and West Clearwater (Bostock, 1969) impact structures were variably referred to as resurgent cryptovolcanic calderas and diatremes. Even more recently, Nicolaysen and Ferguson (1990) continued to espouse the hypothesis of cryptoexplosion craters, proposing that several well-known impact structures (e.g., Brent, Crooked Creek, Charlevoix, Vredefort, etc.) were formed from the explosive venting of fluids associated with alkaline ultramafic magmas.

4.2. The current perspective

As discussed in Section 2, the presence of meteorite fragments cannot be used to differentiate between impact pits and very small impact craters. As such, the presence of meteorite fragments can only be used to confirm an *impact crater* (see Table 1 for definition). In addition, there are no impact structures that have been confirmed solely by the presence of the geochemical or isotopic traces of an impactor, although it has been extremely useful in building the case for the impact origin for several structures and impact deposits, including many of the Archean spherule layers (Simonson and Glass, 2004). It was also the initial identification of extraterrestrial platinum group metals in sedimentary rocks that mark the Cretaceous–Paleogene boundary (Alvarez et al., 1980) that initiated the search for the source impact crater of that age, which proved to be the Chicxulub impact structure, Mexico (Hildebrand et al., 1991). The presence of the chemical or isotopic traces of extraterrestrial objects also remains an important tool used to confirm the impact origin of deposits in the geological record, for which the source crater is unknown. This is particularly important for the origin of extensive spherule beds in the Phanerozoic and Precambrian record (Glass and Simonson, 2012) (see also Section 5.4. below). For a review of the various extraterrestrial chemical and isotopic tracers and their utility, the reader is referred to Goderis et al. (2012).

Thus, given the defining characteristic of hypervelocity impact being the passage of a shock wave through the target rocks (see Section 2.1; cf., Melosh, 1989; Stöffler and Grieve, 2007), the confirmation of a *hypervelocity impact crater* can only be achieved through the identification of "shock-metamorphic effects" or "shock effects" in rocks and minerals. As shown in Fig. 1, shock metamorphic effects occupy a distinctly different pressure–temperature space than any form of endogenic metamorphism. These interchangeable terms cover all types of solid state shock-induced changes to minerals and rocks, including phase transformations, but not melting. It is outside the scope of this contribution to provide a comprehensive treatise of shock metamorphism and the reader is referred to reviews by French and Koeberl (2010) and Ferrière and Osinski (2012). Table 2 provides an overview of the criterion that we propose can be used to unambiguously confirm a *hypervelocity impact crater* or *impact deposit*. Our synthesis builds upon the review by French and Koeberl (2010), with the addition of more recently discovered and/or accepted diagnostic shock effects, most notably reidite, former reidite in granular neoblasts (FRIGN) zircon, and so-called feather features (FF).

Reidite, the tetragonal high-pressure polymorph (scheelite-type structure) of zircon ($ZrSiO_4$), is now accepted as a diagnostic indicator of impact cratering (Rochette et al., 2019; Wittmann et al., 2006). It has only been replicated in shock experiments at pressures >32 GPa (Fiske et al., 1994), which is a condition that only occurs in crustal material during hypervelocity impacts. Reidite has been identified in impactite samples from only a handful of impact structures (e.g., Xiuyan (Chen et al., 2013), Ries (Gucsik et al., 2004), Chesapeake Bay (Glass and Liu, 2001), and the impact deposit at Stac Fada (Reddy et al., 2015)), and is considered a rare shock mineral (Wittmann et al., 2006). Recent studies have reported a new indicator termed "former reidite in granular neoblasts" or FRIGN zircon, which records both high-pressure and high-temperature conditions (Cavosie et al., 2018c). These granular zircons exhibit orientation relations that indicate a transformation and reversion process from zircon to reidite and back to zircon (Cavosie et al., 2016, 2018c; Rochette et al., 2019; Zhao et al., 2021). For this to occur, the zircon grain would need to experience pressure conditions >30 GPa, followed by post-shock temperatures >1200 °C; although some studies (Kovaleva et al., 2021) suggest that FRIGN zircon may be also a result of a rapid crystallization from the melt.

Feather features are microstructures formed in quartz that are short (typically <100 μm) thinly spaced (2–10 μm) parallel to subparallel lamellae branching off of a PF (Fig. 6b). They were first described as "feather features" (FF) by French and Cordua (1999); although the earliest descriptions seem to be in Carter (1968) and in Robertson et al. (1968). Both PFs and FFs have measurable crystallographic orientation, with these three being most common: (0001), $\{10\bar{1}1\}$, and $\{11\bar{2}2\}$. Poelchau and Kenkmann (2011) found them to form in pressure range ~ 7–10 GPa, which makes them particularly useful at the lower end of the shock scale.

As noted in Section 3, a distinctive characteristic of impact events is the melting of target rocks and the production of a range of glassy to crystalline igneous rocks and breccias (see review by Osinski et al., 2018). High-temperature glasses and melts are often considered diagnostic of hypervelocity impact (e.g., French and Koeberl, 2010). Common products include lechatelierite (pure SiO_2 glass) formed by melting of quartz at temperatures ≥1750 °C (Grieve et al., 1996) and MgO and CaO-rich (up to 20–30 wt%) silicate glasses formed through the impact melting of carbonates (Osinski and Spray, 2001). Other examples include the melting of accessory minerals such as titanite, which requires temperatures of >1380 °C (Hayward and Cecchetto, 1982), the decomposition of zircon to baddeleyite, which occurs at >1850 °C (Timms et al., 2017a), and the transformation of baddeleyite (monoclinic-zirconia) to cubic zirconia, which occurs at temperatures >2370 °C (Timms et al., 2017b). However, these impact products are not produced directly by high shock pressures and are, therefore, not actually "diagnostic" of shock, even if it was high shock pressures that resulted in the high temperatures. Thus, while their presence can help to *infer* the presence of a hypervelocity impact crater, high-temperature glasses and melts alone cannot be used to confirm such a feature.

4.3. The challenge of small craters

As discussed in Section 4.2., the confirmation of a hypervelocity impact crater requires the identification of "shock-metamorphic effects" or "shock effects" in rocks and minerals. Unfortunately, in the case of very small impact craters (<100–200 m diameter), the affected volume of target rocks is usually very limited and later distributed over a large surface area. For example, during the formation of the largest Morasko craters (~100 m in diameter) ~1000 m^3 was shocked above 5 GPa, ~300 m^3 above 10 GPa, and ~ 1 m^3 (if any) was shocked above 30 GPa (Bronikowska et al., 2017). As a result, a year's long hunt for grains with planar deformation features (requiring >10–30 GPa) was unsuccessful (A. Muszynski, pers. comm., 2021). Experimental impacts into (unconsolidated) quartz sand showed that material with even modest signs of shock-affected material forms up to ~0.15% of proximal ejecta (and up to 2.5% of material lining up the inside of the crater) (Wünnemann et al., 2016). These values represent the absolute upper limit of the melted/shocked material because: 1) experiments were performed at higher velocities than expected for a formation of most terrestrial craters <100 m in diameter), and 2) because of the selected experimental setup (shocked particles were approximated by the weight percent of particles with different than initial grain sizes most of the increase in particle size was due to gluing of the quartz grains by the shock melted plastic and aluminium impactors). In the paper the presence of PDFs was reported, but not illustrated on any of the photos, and their abundance was not provided.

Additionally, highly porous, and unconsolidated materials respond differently to the passage of shock waves than non-porous materials. The target porosity reduces crater volumes and cratering efficiency relative to nonporous rocks to 20–40% of the expected nonporous volume

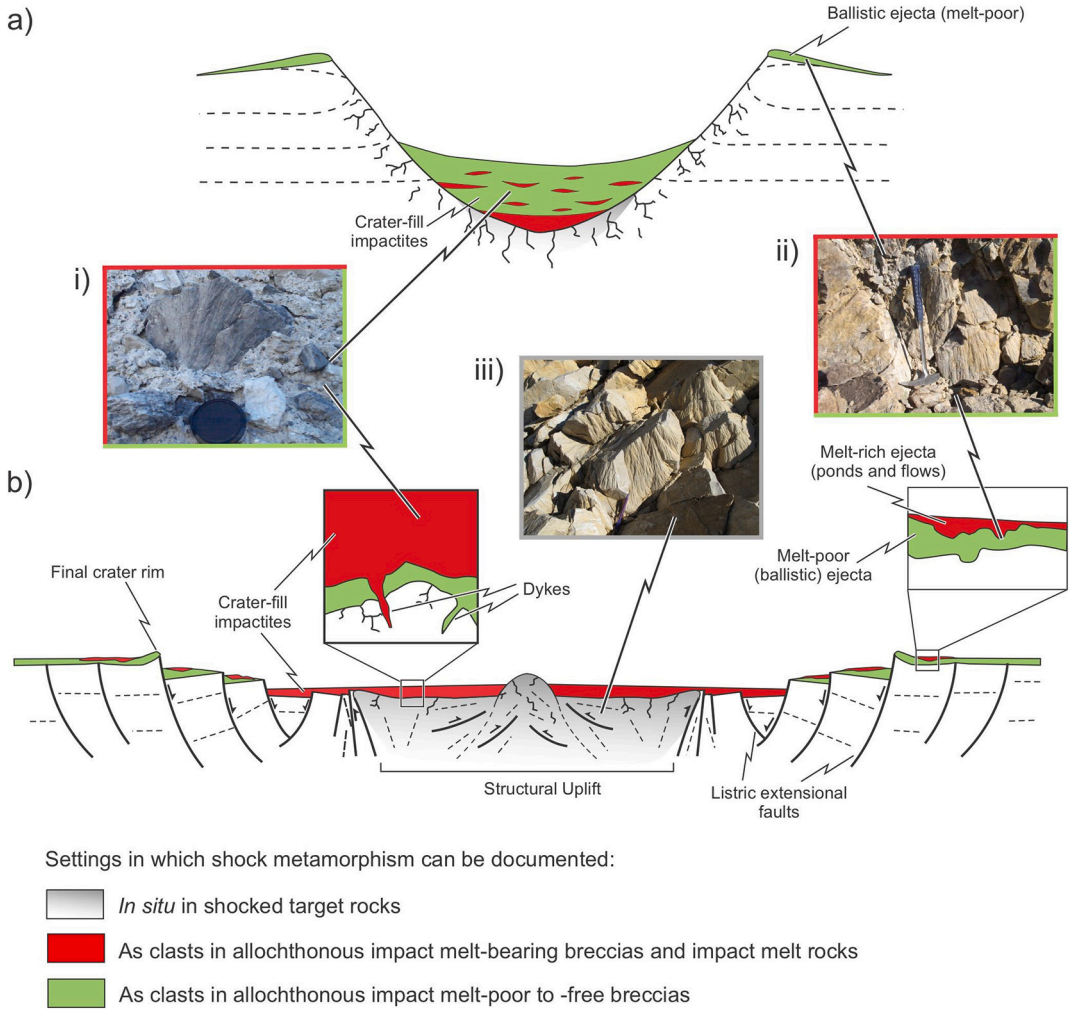

Fig. 5. Schematic cross sections of simple and complex craters showing the settings in which shock metamorphism can be documented. a) *In situ* evidence for shock metamorphism in simple impact craters is restricted to a very small volume of the crater floor immediately under the point of impact (grey shaded region). It is most common to find shock metamorphic indicators in clasts of target rock incorporated into allochthonous crater-fill impactites (i) and ejecta deposits (ii) (red and green units). b) In complex craters, shock metamorphic indicators such as shatter cones (iii) are found *in situ* through the central uplift area (grey shaded region); recorded shock pressures increase in the central uplift inwards and upwards. As with simple craters, shock metamorphic indicators are also common in clasts of target rock incorporated into allochthonous crater-fill impactites (i) and ejecta deposits (ii) (red and green units). See text for further details. (For interpretation of the references to colour in this figure legend, the reader is referred to the web version of this article.)

(Poelchau et al., 2013). This effect is caused by shock wave energy being absorbed by crushing of pore space, leading to a faster decay of the shock wave, but also leading increasing post-shock temperatures (Kieffer, 1971). As a result, most very small impact craters are not associated with identified shock metamorphic effects. Indeed, as discussed in Sections 2 and 4.1, the main, and in most cases only, recognition criteria applied to small impact craters (<100–200 m diameter) is finding meteorite fragments. All 14 known Holocene-age impact craters smaller than 200 m in diameter are identified based on association with meteorite fragments. Eight of them are confirmed solely based on the presence of meteorite fragments (Haviland, Dalgaranga, Whitecourt, Campo del Cielo, Veevers, Morasko, Kaali and Boxhole). A formation of two was witnessed (Sikhote Alin in 1947 and Carancas in 2007). Two other cases (Odessa and Henbury) are also associated with the presence of melt. However, distinguishing impact melts from some atypical wildfire melts is challenging (Roperch et al., 2017; Schultz et al., 2004, 2014). Only two sites (Kamil and Wabar) are characterized by the presence of unequivocal shock metamorphic indicators (PDFs in quartz) that are required to confirm hypervelocity impact craters, and out of those two only Wabar is thought to be formed in unconsolidated materials (Gnos et al., 2013).

All, except one, of the meteorites associated with very small impact craters are irons or stony irons (except the witnessed, somehow atypical case of Carancas, in Peru, formed by the fall of a stony meteorite). This can be explained either by stony meteorites not forming very small impact craters because they disintegrate and decelerate during their atmospheric passage (Artemieva and Shuvalov, 2019; Bland and Artemieva, 2006), or by our inability to find stony meteorites associated with impact craters. Challenges with finding stony meteorites near impact sites may be explained by the meteorite survival and/or the difficulty of finding fragments. First, stony meteorites are much weaker than iron ones and rarely survive atmospheric passage in large enough pieces to form a true impact structure (Bland and Artemieva, 2006). Until 2007, it was assumed that small impact sites cannot be formed by stony asteroids, but due to the witnessed formation of Carancas crater in 2007 by the impact of an H4–5 ordinary chondrite (Kenkmann et al., 2009) this opinion has changed. If the event had not been observed and the structure was discovered years later, it would have been very difficult, or even impossible, to find fragments of the Carancas meteorite because the impactor was fragmented into very small pieces during its atmospheric passage and impact: the largest found piece was only 350 g.

Additionally, weathering unevenly affects different types of meteorites. Iron meteorites tend to quickly develop an oxide and hydroxide

weathering crust around them that effectively seals the inside from deeper water penetration – this mechanism is quite efficient in significantly limiting further damage (Muszynski et al., 2012). Due to this, the oldest known non-Antarctic meteorites are iron meteorites, with terrestrial exposure ages of up to 2.7 Ma (Jull, 2001). Stony meteorites (especially those containing significant amount of Fe-Ni alloy) weather quickly, particularly in contact with water. Weathering-produced minerals such as Fe oxides and hydroxides as well as quickly forming sulphates (Jull et al., 1988) have a higher volume than the original phases, which leads to rock disintegration and further acceleration of weathering. In desert conditions, fragments can be identifiable for ~50 ka, and rare examples can survive for ~1 Ma (Jull, 2001). In humid climates, even hundreds of years can be long enough to change chondrites into undistinguishable piles of rusty rocks. Pieces of achondrites can be nearly as resistant to weathering as terrestrial rocks, but once they lose the fusion crust, they may be very hard to recognise from the surrounding material (especially in the post-glacial areas where a wide variety of rock types are present). This may potentially explain the formation of Ilumetsa (Losiak et al., 2020) and Sobolev (Khryanina, 1981) structures that have properties consistent with them being formed by an impact of an asteroid, but where no clear signs of extraterrestrial material was identified. Currently both of those features are classified as potential impact craters (see section 5.3).

4.4. The question of context

The recent discovery of the Hiawatha impact structure in Greenland (Kjær et al., 2018) highlights a potential quandary in identifying specific impact structures. In this case, there is evidence of a very circular topographic depression, with no indication for volcanism, but the structure is completely buried underneath the Hiawatha Glacier. The evidence for impact comes from PDFs in quartz grains that are not *in* situ but were collected from a glacial outwash plain that originates and/or flows through the crater feature. However, the confirmation of an impact crater based on shock effects in a sample that was not collected *in situ* is not unique. An excellent analogy to Hiawatha is the Mjølnir impact structure in the Barents Sea. This ~40 km structure is buried by ~400 m of sediment and lies at a water depth of 350–400 m and is, thus, inaccessible for direct study, like Hiawatha. Originally suggested to be of impact origin based purely on extensive geophysical data (Gudlaugsson, 1993), its impact origin was subsequently confirmed based on the detection of PDFs in quartz grains in ejecta-bearing strata ~30 km NNE of the structure "within a stratigraphic interval corresponding to the seismically defined deformation event at Mjølnir" (Dypvik et al., 1996). *In situ* sampling has since taken place through drilling of the central uplift and confirmed the occurrence of shock metamorphism (Sandbakken et al., 2005).

In addition, there are several well-known and long-confirmed impact structures in Canada, where, despite being exposed, the shock metamorphic evidence for impact comes solely from glacial cobbles, boulders, and moraines, e.g., Lac Couture (Beals et al., 1967), La Moinerie (Gold et al., 1978), Pingualuit (New Quebec) (Meen, 1957), Pilot (Dence et al., 1968), and Wanipitei (Dence and Popelar, 1972). In all of these instances, the glacial float is linked to roughly circular lakes and/or more irregularly shaped lakes with sub-circular structures revealed via bathymetry. There are other examples in Fennoscandinavia, including Hummeln (Alwmark et al., 2015) and Mien (Svensson and Wickman, 1965), another region that has been heavily glaciated. In summary, the samples in which shock metamorphic criteria are determined need not be *in situ*, as long as there is a clear topographic crater form and evidence (e.g., glacial flow directions) to connect the two.

4.5. Outstanding questions and challenges in confirming impact craters

In general, the more a structure has undergone erosion, the more difficult it is to confirm an impact origin. Topography, a key initial indicator of a potential impact crater, is the first attribute to be modified (e.g., Fig. 4c). In addition, the main reservoir of shocked materials is the crater-fill and ejecta deposits (Fig. 5). These allochthonous impactites record shock effects over a large range in pressures and temperatures up to, and including, whole rock glasses and impact melt rocks. Once these deposits are gone, which is the case for many terrestrial craters (see Section 10), there are two other "reservoirs" of shocked material. The largest volumetrically is the central uplift in complex impact craters (Fig. 5), where lower pressure (sub-solidus) shock effects are recorded (e.g., shatter cones, feather features, PFs, PDFs, diaplectic glasses, etc.). The second type of impactite are dykes of breccia and/or impact melt rock that intruded downwards from the overlying (and now removed by erosion) crater-fill deposits (Fig. 5). Such dykes are common in the eroded central uplifts and crater floors of complex craters of all sizes (Dressler and Reimold, 2004) and they preserve a wider range of shock effects than their host target rocks. A recent example of this is the Tunnunik impact structure, Canada. This structure was confirmed based on the presence of spectacular shatter cones but is heavily eroded (Dewing et al., 2013). Follow up fieldwork, led to the discovery of over two dozen breccia dykes where PDFs in quartz and whole rock glass were discovered (Newman and Osinski, 2017).

Crater size is also a factor. As discussed above in Section 4.3., the smaller the crater, the smaller the volume of material shocked to a given shock pressure. Furthermore, unlike in complex craters, where exposed target rocks in the central uplift are shocked, the exposed target rocks in the rim of simple craters are not shocked to sufficient to pressures to record shock metamorphic effects (Fig. 5). In simple craters, the dominant source of shocked material is in the crater-fill and ejecta deposits. In rare instances and if recovered by drilling or exposed by erosion, the parautochthonous rocks of the crater floor in simple craters, however, do record shock (e.g., at Brent; Robertson and Greive, 1977). The smallest of craters present another challenge. They are most commonly formed in unconsolidated overburden materials, which behave differently to coherent rock and generally result in smaller volumes of shocked material and/or more ambiguous shock products (see Section 4.3).

The identification of impact craters formed in rocks for which known shock effects are lacking or rare (e.g., carbonates and evaporates) presents a distinct problem. For example, apart from shatter cones, there are no currently accepted diagnostic shock metamorphic effects in carbonates (Osinski et al., 2008b). At high shock pressures, impacts into carbonates do result in impact melts, with very unusual compositions and textures, which when combined with other evidence, can provide strong evidence for an impact event. For example, at the Haughton impact structure, Canada, silicate impact glasses with CaO and MgO contents up to ~20 and ~ 30 wt%, respectively, occur. They are unlike any glass formed via endogenic igneous processes but are consistent with the melting of the limestone and dolomite-dominated target rocks (Osinski et al., 2005b; Osinski and Spray, 2001). At Haughton and other structures, the unusual composition of calcite and associated silicate phases (e.g., clinopyroxene and olivine), and the presence of vesicles and immiscibility textures can also only be explained by melting (see Osinski et al., 2008a, and references therein). As noted above, however, these melt products are concentrated in the crater-fill and ejecta deposits and many of the aforementioned textures also require some proportion of silicate-rich sedimentary rocks in the target rocks. Thus, confirming the origin of deeply eroded and/or pure carbonate targets, remains an ongoing problem in cratering studies. There is promise in using XRD and Raman spectroscopy to determine shock levels in carbonates via peak broadening (Lindgren et al., 2009; Skála and Jakeš, 1999) but at present, this is not yet considered unambiguous evidence for shock. As a result, heavily eroded structures in carbonates such as Jeptha Knob, USA, remain in the list of "suspected" impact structures.

A final outstanding problem in cratering studies is what to do with buried structures for which no samples are available, but for which detailed geophysical information consistent with an impact origin is

Table 3
List of confirmed impact craters and their main attributes. See Supplementary Data for additional attributes.

Crater name	Location			Date Confirmed	Age (Ma)	Crater Morphology		Target Properties	Impactor	
	Latitude Decimal Degrees N(+), S (−)	Longitude Decimal Degrees E (+), W(−)	Country			Maximum crater size (km)	Number of Craters		Type	Ref/Notes
Boxhole	−22.37	135.12	Australia	1937	0.030 ± 0.005	0.17	1	Crystalline	Iron, IIIAB	Shoemaker et al. (1988).
Campo del Cielo	−27.38	−61.42	Argentina	1933	0.00338–0.00405	0.115	20+	Sedimentary	Iron, IAB	Specimens of meteorite material range from coarsest octahedrite to granular hexahedrite (Bunch and Cassidy, 1968). Buried crater pits contain magnetic meteorite material and were found using this method (see Geophysics-magnetics) (Cassidy and Renard, 1996).
Carancas	−16.4	−69.03	Peru	15 September 2007	Recent	0.0143	1	Sedimentary	Ordinary chondrite, H4–5	Ordinary chondrite of type H4/5 with diameter of at least 1 m fell (Brown et al., 2008).
Dalgaranga	−27.38	117.17	Australia	1938	<0.003	0.024	1	Crystalline	Mesosiderite, A	Fragments of ferruginous materials have been examined and reveal a composition of a stony iron, mesosiderite (McCall, 1965).
Haviland	37.35	−99.1	U.S.A.	1933	0.02 ± 0.002	N/A	0.01	Sedimentary	Pallasite, PMG	Brenham pallasite (Peck, 1979).
Henbury	−24.34	133.08	Australia	1932	0.0042 ± 0.0019	0.146	12	Sedimentary	Iron, IIIAB	Craters formed by an iron meteorite shower (Compston and Taylor, 1969) (Gibbons et al., 1976). IIIAB octahedrite.
Kaalijarv	58.24	22.4	Estonia	1938	0.003237 ± 0.000010	0.11	9	Sedimentary	Iron, IAB	Oxidized iron meteorites (generally less than 5 g) have been found in most of these small craters (Aaloe and Tiirmaa, 1982). Type IA. Iron meteoroite (IAB) weighing between 400 and 10,000 tons (Losiak et al., 2016). [Note: Group is IAB not IA since group classifications were revised after initial classification.]
Morasko	52.29	16.54	Poland	1964	~0.005	0.09	7	Sedimentary	Iron, IAB	Coarse octahedrite fragments (Classen, 1978). A total of 400 kg hasb een found to-date (Korpikiewicz, 1978).
Odessa	31.45	−102.29	U.S.A.	1928	<0.05	0.168	5	Sedimentary	Iron, IAB	Hundreds of tiny fragments of meteorite iron (Odessa octahedrite, IA type) were collected on the surface of the crater wall and in the meteorite pits (Krinov, 1966). [Note: Group is IAB not IA since group

(*continued on next page*)

Table 3 (*continued*)

Crater name	Location			Date Confirmed	Age (Ma)	Crater Morphology		Target Properties	Impactor	
	Latitude Decimal Degrees N(+), S (−)	Longitude Decimal Degrees E (+), W(−)	Country			Maximum crater size (km)	Number of Craters		Type	Ref/Notes
										classifications were revised after initial classification.
Sikhote Alin	46.07	134.4	Russia	12-Feb-1947	Recent	0.0265	122	Crystalline	Iron, IIAB	Two large specimens, 270 and 100 kg, and a total of 332 kg of meteoritic material collected (Krinov, 1971; Kolesnikov et al., 1972).
Veevers	−22.58	125.22	Australia	1985	~0.004	0.0725	1	Sedimentary	Iron, IIAB	Iron Fragments were found associated with this depression (Shoemaker and Shoemaker, 1985) (Bevan et al., 1995). Chemical group IIAB (Wasson et al., 1989).
Whitecourt	54	−115.36	Canada	2008	<0.0011	0.036	1	Sedimentary	Iron, IIIAB	Herd et al. (2008). Meteorites recovered. Over 5000 meteorites recovered for a total known mass of ~230 kg (Newman and Herd, 2015).

available. Such structures are currently not listed in the Impact Earth database. Stewart (2003) presents an interesting discussion of this topic, highlighting the fact that the proliferation of three-dimensional seismic data due to hydrocarbon exploration has produced unprecedented high-resolution subsurface information in many sedimentary basins and outlining a set of geometrical criteria that "appear to be sufficient to uniquely identify an astrobleme imaged via three-dimensional seismic data". Further investigation of this topic is suggested, as there are undoubtedly many buried impact structures that may be well-preserved, thus offering better opportunities to study, for example, crater morphology and morphometry.

5. Confirmed impact craters, hypervelocity impact craters and impact deposits

Tables 3, 4 and 5 provide up-to-date lists of all confirmed *impact craters*, *hypervelocity impact craters* and *impact deposits*, respectively. Given, however, the lack of any international standards or committee, such as exists for meteorites, we invite input from the community about the accuracy of the current Impact Earth database and as it continues to evolve in the future. (For meteorites, the Meteorite Nomenclature Committee of the Meteoritical Society is "responsible for establishing guidelines for the naming of meteorites, for the approval of new names, for decisions regarding pairing or separation of meteorites previously named, and for dissemination of this information in the Meteoritical Bulletin and the Meteoritical Bulletin Database"). There are some notable exceptions to our list compared to previous compendia, which are discussed below in Section 5.3.

The locations of all confirmed *impact craters*, *hypervelocity impact craters* and *impact deposits* is provided in Fig. 7. It is notable that relatively little has changed in terms of the spatial distribution of impact structures on Earth over the past 30 years, since reviews by Grieve et al. (1987) and Grieve (1991). Then and now, approximately two-thirds of impact craters and hypervelocity impact craters are located in the ancient cratonic areas of Australia, Europe, and North America, where (relative) tectonic stability and low rates of erosion favour preservation. These are also areas with more active research programs and that are generally more easily accessible.

It is noteworthy that the total number of impact craters and hypervelocity impact craters on Earth is unknown and there are reasons to suspect that the terrestrial small crater record is incomplete (cf., Kenkmann, 2021). It is likely that there are several dozen structures with diameters ~100–150 m in diameter waiting to be discovered (Bland and Artemieva, 2006), largely because of a lack of clear recognition criteria that can be applied to small impact structures (see Sections 4.3. and 4.5.). It is also notable that the past decade has seen an upswing in the number of confirmed impact structures (Fig. 8). Notably, several hypervelocity impact structures discovered in the past decade are over 10 km in diameter (Hiawatha, Lake Raeside, Luizi, Pantasma, Saqqar, Tunnunik). The reason for this upswing is unclear but this suggests that the conclusion that all craters >6 km in diameter exposed at the surface have been discovered (Hergarten and Kenkmann, 2015) may be incorrect.

5.1. Impact craters

Table 3 lists 12 impact craters all >10 m diameter. Many were discovered in the 1920s and 1930s (Fig. 8) and all were identified based on the presence of meteorite fragments and/or unusual glasses. At present, unambiguous evidence for shock metamorphism (see Table 2) has not been documented at these sites, despite significant efforts (e.g., as discussed in Section 4.3. for Morasko). (Recall from Section 4.2. that high-temperature glasses and melts are not produced via shock metamorphism and, thus, cannot be used to confirm unequivocally a hypervelocity impact crater.) As such, while some or all of these may be hypervelocity impact craters, until such a time when evidence for shock metamorphism is documented, these sites should all be referred to as impact craters.

Approximately half of these sites are individual craters: the ~13.5 m diameter Carancas crater in Peru, the ~24 m diameter Dalgaranga crater in Australia, the ~15 m diameter Haviland cater in the USA, the ~36 m diameter Whitecourt crater in Canada, the ~80 m diameter Veevers crater in Australia, and the ~170 m diameter Boxhole crater in Australia. Six of these sites comprise crater strewn fields: Campo del

Table 4
List of confirmed hypervelocity impact craters and their main attributes. See Supplementary Data for references and additional attributes.

	Location			Date Confirmed	Buried (Y/N)	Erosional Level	Age (Ma)	Crater Morphology			Target Properties
	Latitude Decimal Degrees N (+), S(−)	Longitude Decimal Degrees E (+), W(−)	Country					Final diameter (km)	Apparent diameter (km)	Type	
Acraman	−32.1	135.27	Australia	1986	No	7	635–541	N/A	90	Complex	Crystalline
Agoudal	31.98	−5.51	Morocco	2014	Partially	6	≤174	N/A	0.5	Simple	Sedimentary
Amelia Creek	−20.51	134.53	Australia	2003	No	7	660–1660	N/A	20	Complex	Mixed
Ames	36.15	−98.12	U.S.A.	1992	Yes	2	478–458	N/A	16	Complex	Mixed
Amguid	26.5	4.23	Algeria	1980	No	2	0.01–0.1	N/A	0.45	Simple	Sedimentary
Aorounga	19.06	19.15	Chad	1992	No	6	0.0035–383	N/A	16	Complex	Sedimentary
Aouelloul	20.15	−12.41	Mauritania	1966	No	3	3.1 ± 0.3	N/A	0.39	Simple	Sedimentary
Araguainha	−16.47	−52.59	Brazil	1973	No	6	248–264	N/A	40	Complex	Mixed
Avak	71.15	−156.38	U.S.A.	1992	Yes	4	94–90	N/A	10	Complex	Sedimentary
Barringer	35.2	−111.1	U.S.A.	1905	No	1	0.0611 ± 0.0048	1.19	N/A	Simple	Sedimentary
Beaverhead	44.36	−113	U.S.A.	1990	No	7	900–470	N/A	60	Complex	Mixed
Beyenchime-Salaatin	71.5	123.3	Russia	1975	No	3	1.8–66	N/A	8	Complex	Sedimentary
Bigach	48.3	82	Kazakhstan	1986	No	2	2–8	N/A	8	Complex	Mixed
Bloody Creek	44.45	−65.14	Canada	2009	Yes	7	0.012–388	N/A	0.4	Simple	Crystalline
Boltysh	48.45	32.1	Ukraine	1973	Yes	2	65.39 ± 0.14	N/A	24	Complex	Crystalline
Bosumtwi	6.3	−1.25	Ghana	1962	No	2	1.13 ± 0.10	10.7	N/A	Complex	Crystalline
B.P. Structure	25.19	24.2	Libya	1974	No	6	<120	N/A	3.2	Complex	Sedimentary
Brent	46.5	−78.29	Canada	1960	Yes	4	453.2 ± 6.0	3.8	3.4	Simple	Crystalline
Calvin	41.5	−85.57	U.S.A.	1994	Yes	5	458–444	N/A	8.5	Complex	Sedimentary
Carswell	58.27	−109.3	Canada	1964	No	7	481.5 ± 0.8	N/A	39	Complex	Mixed
Cerro do Jarau	−30.2	−56.53	Brazil	2018	No	5	≤135	N/A	13.5	Complex	Mixed
Charlevoix	47.32	−70.18	Canada	1966	No	6	453–430	N/A	70	Complex	Mixed
Chesapeake Bay	37.17	−76.1	U.S.A.	1994	Yes	4	34.86 ± 0.32	N/A	90	Complex	Mixed
Chicxulub	21.2	−89.3	Mexico	1991	Yes	2	66.038 ± 0.098	N/A	180	Complex	Mixed
Chiyli	49.1	57.51	Kazakhstan	1989	No	6	56–41	N/A	5.5	Complex	Sedimentary
Chukcha	75.42	97.48	Russia	1992	No	5	<70	N/A	6	Complex	Mixed
Cleanskin	−18.17	137.94	Australia	2012	No	6	1400–520	N/A	15	Complex	Sedimentary
Clearwater East	56.5	−74.7	Canada	1965	No	6	470–460	N/A	26	Complex	Crystalline
Clearwater West	56.14	−74.3	Canada	1964	No	4	286.2 ± 2.6	N/A	36	Complex	Mixed
Cloud Creek	43.07	−106.45	U.S.A.	1999	Yes	3	277–166	N/A	7	Complex	Sedimentary
Colonia	−23.52	−46.42	Brazil	2013	No	3	36–2.5	N/A	3.6	Simple	Crystalline
Connolly Basin	−23.32	124.45	Australia	1991	No	6	66–23	N/A	9	Complex	Sedimentary
Couture	60.8	−75.2	Canada	1967	No	6	429 ± 25	N/A	8	Complex	Crystalline
Crooked Creek	37.5	−91.23	U.S.A.	1954	No	6	485–323	N/A	7	Complex	Sedimentary
Decaturville	37.54	−92.43	U.S.A.	1977	No	5	< 323	N/A	6	Complex	Mixed
Decorah	43.31	−91.77	United States of America	2018	Yes	5	467–464	N/A	5.6	Complex	Sedimentary
Deep Bay	56.24	−102.59	Canada	1968	Yes	5	102–95	N/A	13	Complex	Crystalline
Dellen	61.48	16.48	Sweden	1968	No	6	140.82 ± 0.51	N/A	19	Complex	Crystalline
Des Plaines	42	−87.87	U.S.A.	1986	Yes	6	<299	N/A	8	Complex	Sedimentary
Dhala	25.3	78.13	India	2005	No	5	2500–1700	N/A	11	Complex	Crystalline
Dobele	56.35	23.15	Latvia	1999	Yes	4	359–252	N/A	4.5	Complex	Sedimentary
Douglas	42.68	−105.47	U.S.A	2018	No	3	~280	0.073	N/A	Simple	Sedimentary
Eagle Butte	49.42	−110.3	Canada	1985	Yes	5	<65	N/A	16	Complex	Sedimentary
Elbow	50.59	−106.43	Canada	1998	Yes	6	393–201	N/A	8	Complex	Sedimentary
El'gygytgyn	67.3	172.5	Russia	1978	No	4	3.65 ± 0.08	18	N/A	Complex	Crystalline
Flaxman	−34.6	139.1	Australia	1999	Yes	6	34–541	N/A	10	Complex	Mixed
Flynn Creek	36.17	−85.4	U.S.A.	1968	No	4	~382	N/A	3.8	Complex	Sedimentary
Foelsche	−16.4	136.47	Australia	2002	Partially	4	1496–520	N/A	6	Complex	Sedimentary
Gardnos	60.39	9	Norway	1992	No	5	546 ± 5	N/A	5	Complex	Crystalline
Glasford	40.36	−89.47	U.S.A.	1986	Yes	5	457–453	N/A	4	Complex	Sedimentary
Glikson	−23.59	121.34	Australia	1997	Partially	6	<513	N/A	19	Complex	Sedimentary
Glover Bluff	43.58	−89.32	U.S.A.	1983	No	5	<485	N/A	8	Complex	Sedimentary
Goat Paddock	−18.2	126.4	Australia	1980	No	5	56–48	N/A	5	Transitional	Sedimentary
Gosses Bluff	−23.49	132.19	Australia	1966	No	6	383–165	N/A	32	Complex	Sedimentary
Gow	56.27	−104.29	Canada	1977	No	5	196.8 ± 9.9	N/A	4	Transitional	Crystalline
Goyder	−13.9	135.2	Australia	1996	No	6	1325–150	N/A	7	Complex	Sedimentary
Granby	58.25	14.56	Sweden	2009	Yes	3	468–467	N/A	3	Simple	Sedimentary

(*continued on next page*)

Table 4 (*continued*)

	Location			Date Confirmed	Buried (Y/N)	Erosional Level	Age (Ma)	Crater Morphology			Target Properties
	Latitude Decimal Degrees N (+), S(−)	Longitude Decimal Degrees E (+), W(−)	Country					Final diameter (km)	Apparent diameter (km)	Type	
Gweni-Fada	17.25	21.45	Chad	1996	No	6	≤383	N/A	22	Complex	Sedimentary
Haughton	75.22	−89.41	Canada	1975	No	2	31.04 ± 0.37	16	23	Complex	Mixed
Hiawatha	78.72	−66.3	Greenland	2018	Yes	3	2.6–0.0117	N/A	31	Complex	Crystalline
Hickman	−23.03	119.68	Australia	2008	No	2	0.01–0.1	0.26	N/A	Simple	Mixed
Holleford	44.28	−76.38	Canada	1963	Yes	4	450–650	N/A	2.35	Simple	Crystalline
Hummeln	57.22	16.19	Sweden	2015	No	5	~465	N/A	1.2	Simple	Mixed
Ile Rouleau	50.41	−73.53	Canada	1976	No	6	0.011–1800	~4	4	Complex	Sedimentary
Ilyinets	49.7	29.6	Ukraine	1980	Yes	5	445 ± 10	N/A	4.5	Complex	Mixed
Iso-Naakkima	62.11	27.9	Finland	1993	Yes	6	1200–900	N/A	3	Simple	Crystalline
Janisjarvi	61.58	30.55	Russia	1976	No	6	687 ± 5	N/A	14	Complex	Crystalline
Jebel Waqf as Suwwan	31.03	36.48	Jordan	2008	No	6	2.6–30	N/A	5.5	Complex	Sedimentary
Jeokjung-Chogye Basin	35.55	128.27	South Korea	2021	No	3	0.030–0.063	8	N/A	Complex	Sedimentary
Kalkkop	−32.43	24.34	South Africa	1993	No	3	0.250 ± 0.050	N/A	0.64	Simple	Sedimentary
Kaluga	54.3	36.15	Russia	1980	Yes	2	394–383	N/A	15	Complex	Mixed
Kamenetsk	47.76	32.35	Ukraine	2017	Yes	6	2100–11.63	N/A	1.2	Simple	Crystalline
Kamensk	48.2	40.15	Russia	1980	Yes	5	50.37 ± 0.40	N/A	25	Complex	Sedimentary
Kamil	22.01	26.05	Egypt	2010	No	1	≤0.004	0.045	N/A	Simple	Sedimentary
Kara	69.12	65	Russia	1976	Yes	5	75.34 ± 0.66	N/A	65	Complex	Mixed
Kara-Kul	39.1	73.27	Tajikistan	1993	No	4	<60	N/A	52	Complex	Crystalline
Kardla	58.59	22.4	Estonia	1992	Yes	3	455 ± 1	N/A	4	Complex	Mixed
Karikkoselkä	62.22	25.25	Finland	1996	No	5	260–230	N/A	<2.4	Simple	Crystalline
Karla	54.54	48	Russia	1976	No	5	4–6	N/A	12	Complex	Sedimentary
Kelly West	−19.56	133.57	Australia	1973	Yes	6	1640–500	N/A	6.6	Complex	Crystalline
Kentland	40.45	−87.27	U.S.A.	1947	No	5	300–1	N/A	7	Complex	Sedimentary
Keurusselka	62.14	24.58	Finland	2004	Yes	7	1151 ± 10	N/A	36	Complex	Crystalline
Kgagodi	−22.29	27.35	Botswana	2000	No	4	≤180	N/A	3.4	Simple	Crystalline
Kursk	51.4	36	Russia	1974	Yes	5	359–163	N/A	5.5	Complex	Mixed
Lake Raeside	−28.79	120.96	Australia	2016	Yes	4	250–34	N/A	11	Complex	Crystalline
La Moinerie	57.26	−66.37	Canada	1978	No	7	453 ± 5	N/A	8	Complex	Crystalline
Lappajarvi	63.12	23.42	Finland	1968	No	6	77.85 ± 0.78	N/A	23	Complex	Mixed
Lawn Hill	−18.4	138.39	Australia	1987	No	7	476 ± 8	N/A	16.8	Complex	Mixed
Liverpool	−12.24	134.3	Australia	1971	No	3	1870–541	1.6	N/A	Simple	Sedimentary
Lockne	63	14.85	Sweden	1992	Yes	3	455 ± 1	N/A	7.5	Complex	Mixed
Logancha	65.3	95.5	Russia	1983	Yes	4	66–23	N/A	20	Complex	Mixed
Logoisk	54.12	27.48	Belarus	1979	Yes	3–4	30.0 ± 0.5	N/A	17	Complex	Mixed
Lonar	19.58	76.31	India	1972	No	2	0.576 ± 0.047	1.83	N/A	Simple	Crystalline
Luizi	−10.1	27.55	Congo	2011	No	5	≤573	N/A	15	Complex	Sedimentary
Lumparn	60.15	20.13	Finland	1992	Yes	5	≤458	N/A	10	Complex	Mixed
Malingen	62.91	14.56	Sweden	2014	No	3	455 ± 1	0.7	N/A	Simple	Mixed
Manicouagan	51.23	−68.42	Canada	1969	No	5	215.56 ± 0.05	N/A	100	Complex	Mixed
Manson	42.35	−94.33	U.S.A.	1966	Yes	6	75.9 ± 0.1	N/A	35	Complex	Mixed
Maple Creek	49.48	−109.06	Canada	1998	Yes	6	<72	N/A	5.75	Complex	Sedimentary
Marquez	31.17	−96.18	U.S.A.	1989	Yes	6	58.3 ± 3.1	N/A	12.7	Complex	Sedimentary
Matt Wilson	−15.3	131.11	Australia	2005	No	7	<1344	N/A	7.5	Complex	Sedimentary
Middlesboro	36.37	−83.44	U.S.A.	1966	No	7	<299	N/A	5.5	Complex	Sedimentary
Mien	56.25	14.52	Sweden	1965	No	5	~122	N/A	7	Complex	Crystalline
Mishina Gora	58.4	28	Russia	1974	No	6	<360	N/A	2.5	Simple	Mixed
Mistastin	55.53	−63.18	Canada	1969	No	6	37.83 ± 0.05	N/A	28	Complex	Crystalline
Mizarai	54.01	24	Lithuania	1980	Yes	7	520–480	N/A	5	Complex	Mixed
Mjolnir	73.48	29.4	Norway	1996	Yes	2	141–145	N/A	40	Complex	Sedimentary
Montagnais	42.53	−64.13	Canada	1987	Yes	2	51.1 ± 1.6	N/A	45	Complex	Sedimentary
Monturaqui	−23.56	−68.17	Chile	1966	No	2	0.663 ± 0.023	0.47	N/A	Simple	Crystalline
Morokweng	−26.28	23.32	South Africa	1996	Yes	4	146.06 ± 0.16	N/A	70	Complex	Crystalline
Mount Toondina	−27.57	135.22	Australia	1976	Partially	6	<125	N/A	4	Complex	Sedimentary
Neugrund	59.2	23.4	Estonia	1997	Yes	5	540–530	N/A	20	Complex	Crystalline
Newporte	48.58	−101.58	U.S.A.	1995	Yes	5	500–480	N/A	3.2	Simple	Mixed
New Quebec	61.17	−73.4	Canada	1957	No	3	1.4 ± 0.1	3.44	N/A	Simple	Crystalline

(*continued on next page*)

Table 4 (*continued*)

	Location			Date Confirmed	Buried (Y/N)	Erosional Level	Age (Ma)	Crater Morphology			Target Properties
	Latitude Decimal Degrees N (+), S(−)	Longitude Decimal Degrees E (+), W(−)	Country					Final diameter (km)	Apparent diameter (km)	Type	
Nicholson	62.4	−102.41	Canada	1968	No	6	387 ± 5	N/A	12.5	Complex	Mixed
Oasis	24.35	24.24	Libya	1974	No	6	<120	N/A	15.6	Complex	Sedimentary
Obolon	49.3	32.55	Ukraine	1977	Yes	4	169 ± 7	N/A	19	Complex	Mixed
Ouarkziz	29	−7.33	Algeria	1970	No	5	345–65	N/A	3	Complex	Sedimentary
Paasselkä	62.2	29.5	Finland	1996	No	7	231.0 ± 2.2	N/A	10	Complex	Mixed
Pantasma	13.37	−85.95	Nicaragua	2019	No	3	0.815 ± 0.011	N/A	14	Complex	Crystalline
Pilot	60.17	−111.1	Canada	1968	No	6	450 ± 2	N/A	6	Complex	Crystalline
Popigai	71.4	111.4	Russia	1971	No	3	36.63 ± 0.92	N/A	100	Complex	Mixed
Presqu'île	49.43	−74.48	Canada	1990	No	7	<2729	N/A	15	Complex	Crystalline
Puchezh-Katunki	56.58	43.43	Russia	1984	Yes	4	195.9 ± 1.1	N/A	80	Complex	Mixed
Ragozinka	58.44	61.48	Russia	1986	Yes	2	~59–56	N/A	9	Complex	Mixed
Ramgarh	25.33	76.62	India	2020	No	4	750–165	N/A	10	Complex	Sedimentary
Red Wing	47.36	−103.33	U.S.A.	1996	Yes	4	250–167	N/A	9	Complex	Sedimentary
Riachão	−7.43	−46.39	Brazil	1979	No	4	<299	N/A	4	Complex	Sedimentary
Ries	48.53	10.37	Germany	1961	No	2	14.808 ± 0.038	N/A	24	Complex	Mixed
Ritland	59.41	6.25	Norway	2011	No	6	500–541	N/A	2.7	Simple	Mixed
Rochechouart	45.5	0.56	France	1971	No	6	206.92 ± 0.32	N/A	32	Complex	Crystalline
Rock Elm	44.72	−92.14	U.S.A.	2004	No	7	~485–458	N/A	6.5	Complex	Sedimentary
Roter Kamm	−27.46	16.18	Namibia	1989	No	2	3.8 ± 0.3	N/A	2.5	Simple	Mixed
Rotmistrovka	49.11	32.45	Ukraine	1976	Yes	4	~ 145–94	N/A	2.7	Simple	Crystalline
Saaksjarvi	61.24	22.24	Finland	1969	No	7	602 ± 17	N/A	5	Complex	Crystalline
Saarijarvi	65.17	28.23	Finland	1998	No	7	<600	N/A	2	Simple	Crystalline
Saint Martin	51.47	−98.32	Canada	1970	Yes	4	227.8 ± 0.9	N/A	40	Complex	Mixed
Santa Fe	35.45	−105.55	U.S.A.	2006	No	7	1472–350	N/A	13	Complex	Crystalline
Santa Marta	−10.17	−45.23	Brazil	2014	No	3	<100	N/A	10	Complex	Sedimentary
Saqqar	29.35	38.42	Saudi Arabia	2015	Yes	6	410–70	N/A	34	Complex	Sedimentary
Serpent Mound	39.2	−83.24	U.S.A.	1998	No	7	<359	N/A	8	Complex	Sedimentary
Serra da Cangalha	−8.05	−46.51	Brazil	1979	No	7	≤250	N/A	13.7	Complex	Sedimentary
Shoemaker	−25.52	120.53	Australia	1974	No	7	1300–568	N/A	30	Complex	Mixed
Shunak	47.12	72.42	Kazakhstan	1978	No	2	7–17	N/A	2.8	Simple	Crystalline
Sierra Madera	30.36	−102.55	U.S.A.	1968	No	6	<113	N/A	20	Complex	Sedimentary
Siljan	61.05	15	Sweden	1971	No	7	380.9 ± 4.6	65	75	Complex	Mixed
Slate Islands	48.4	−87	Canada	1976	No	7	~450	N/A	30	Complex	Mixed
Soderfjarden	62.41	21.35	Finland	1985	Yes	6	1880–640	N/A	6.55	Complex	Crystalline
Spider	−16.44	126.05	Australia	1980	No	7	900–580	N/A	13	Complex	Sedimentary
Steen River	59.3	−117.38	Canada	1968	Yes	3	383–108	N/A	25	Complex	Mixed
Steinheim	48.41	10.04	Germany	1967	No	3	~14.8	3.8	N/A	Complex	Sedimentary
Strangways	−15.12	133.35	Australia	1971	No	5	657 ± 43	N/A	26	Complex	Mixed
Suavjarvi	63.07	33.23	Russia	2012	No	6	2700–2200	N/A	16	Complex	Crystalline
Sudbury	46.36	−81.11	Canada	1964	No	5	1849.53 ± 0.21	N/A	200	Complex	Crystalline
Summanen	62.65	25.38	Finland	2018	Yes	5	<1880	N/A	2.6	Simple	Crystalline
Suvasvesi North	62.41	28.11	Finland	1996	Yes	6	~85	N/A	3.5	Complex	Crystalline
Suvasvesi South	62.35	28.17	Finland	2002	No	6	1880–710	N/A	3.8	Complex	Crystalline
Tabun-Khara-Obo	44.06	109.36	Mongolia	1976	No	2	130–170	N/A	N/A	Simple	Crystalline
Talemzane	33.19	4.02	Algeria	1980	No	2	≤3	N/A	1.75	Simple	Sedimentary
Talundilly	−24.83	144.50	Australia	2012	Yes	4	~125	N/A	84	Complex	Sedimentary
Tenoumer	22.55	10.24	Mauritania	1970	No	3	1.57 ± 0.14	N/A	N/A	Simple	Crystalline
Ternovka	48.15	33.3	Ukraine	1979	Yes	7	280 ± 10	N/A	15	Complex	Mixed
Tin Bider	27.36	5.07	Algeria	1981	No	6	<66	N/A	6	Complex	Sedimentary
Tookoonooka	−27.07	142.5	Australia	1989	Yes	3	124–126	N/A	66	Complex	Sedimentary
Tsenkher	43.64	98.37	Mongolia	2019	No	2	4.9 ± 0.9	4.2	N/A	Transitional	Sedimentary
Tswaing	−25.24	28.05	South Africa	1992	No	2	0.220 ± 0.104	1.13	N/A	Simple	Crystalline
Tunnunik	72.28	−113.58	Canada	2013	No	6	~ 450–430	N/A	28	Complex	Sedimentary
Tvaren	58.46	17.25	Sweden	1994	Yes	4	456–458	2	3.1	Simple	Mixed
Upheaval Dome	38.26	−109.54	U.S.A.	2008	No	7	<183	N/A	5.2	Complex	Sedimentary
Vargeao Dome	−26.48	−52.1	Brazil	2004	No	5	123 ± 1.4	N/A	12.4	Complex	Mixed

(*continued on next page*)

Table 4 (*continued*)

	Location			Date Confirmed	Buried (Y/N)	Erosional Level	Age (Ma)	Crater Morphology			Target Properties
	Latitude Decimal Degrees N (+), S(−)	Longitude Decimal Degrees E (+), W(−)	Country					Final diameter (km)	Apparent diameter (km)	Type	
Vepriai	55.05	24.34	Lithuania	1980	Yes	4	155–165	N/A	7.5	Complex	Sedimentary
Viewfield	49.35	−103.04	Canada	1998	Yes	2	170–210	N/A	2.4	Simple	Sedimentary
Vista Alegre	−25.57	−52.41	Brazil	2010	No	6	~134–111	N/A	9.5	Complex	Mixed
Vredefort	−27	27.3	South Africa	1961	No	7	2023 ± 4	N/A	300	Complex	Crystalline
Wabar	21.3	50.28	Saudi Arabia	1933	No	2	~0.0003	0.116	3	Simple	Sedimentary
Wanapitei	46.45	−80.45	Canada	1972	Yes	5	37.7 ± 1.2	N/A	7.5	Complex	Crystalline
Wells Creek	36.23	−87.4	U.S.A.	1959	No	6	323–100	N/A	13.7	Complex	Sedimentary
West Hawk	49.46	−95.11	Canada	1966	Yes	4	351 ± 20	N/A	3.6	Simple	Crystalline
Wetumpka	32.31	−86.1	U.S.A.	1999	No	4	~83.5	N/A	6.25	Complex	Mixed
Wolfe Creek	−19.1	127.47	Australia	1968	No	2	0.120 ± 0.009	0.935	0.8	Simple	Sedimentary
Woodleigh	−26.03	114.4	Australia	2000	Yes	6	2005–168	N/A	60	Complex	Mixed
Xiuyan	40.21	123.27	China	2008	No	4	0.05–5?	1.8	N/A	Simple	Crystalline
Yallalie	−30.34	115.77	Australia	2019	Yes	3	89.8–83.6	N/A	12	Complex	Sedimentary
Yarrabubba	−27.1	119.5	Australia	2003	No	5	2229 ± 5	N/A	70	Complex	Crystalline
Yilan	46.38	129.31	China	2020	No	3	0.0493 ± 0.0032	1.85	N/A	Simple	Crystalline
Zapadnaya	49.44	29	Ukraine	1985	Yes	4	165 ± 5	N/A	3.2	Complex	Crystalline
Zeleny Gai	48.04	32.45	Ukraine	1976	Yes	4	60–100	N/A	3.5	Simple	Crystalline
Zhamanshin	48.24	60.58	Kazakhstan	1977	No	3	0.91 ± 0.14	N/A	13	Complex	Mixed

Cielo in Argentina, Henbury in Australia, Kaalijarv in Estonia, Odessa in the USA, Sikhote Alin in Russia, and Morasko in Poland. All of these impact craters were formed either entirely, or in part, in unconsolidated sediments or soils.

5.2. Hypervelocity impact craters

Table 4 lists the 188 sites for which there is sufficient published evidence of shock metamorphism to warrant being included in a list of confirmed *hypervelocity impact craters* (see also Appendix A). Of the 188 confirmed *hypervelocity impact craters*, all but two are individual craters. The exceptions are the Douglas and Wabar crater strewn fields. For these structures, only the diameter of the largest individual crater is reported in the *Impact Earth* database, with details on all the individual craters and pits provided in Appendix A. Unlike the impact craters discussed in the previous section, both of these hypervelocity impact crater strewn fields have both meteoritic fragments and confirmed shock metamorphic evidence (Appendix A). These are: PDFs in quartz at Douglas (Kenkmann et al., 2018) and coesite and PDFs in quartz at Wabar (Gnos et al., 2013). In addition to these two impact crater strewn fields, a handful of other hypervelocity impact craters have meteoritic fragments. With only one exception (Morokweng), meteorite fragments have only been documented in simple impact craters, such as the 1.2 km diameter Meteor or Barringer Crater, USA, where fragments of iron meteorite were recognized over a century ago (Barringer, 1905). The discovery of coesite (Chao et al., 1960) and stishovite (Chao et al., 1962) provided subsequent confirmation of the hypervelocity impact origin of this structure. An intriguing exception for complex craters is contained in the work of Hart et al. (2002), who concluded that siderophile-rich inclusions in impact melt rocks at the ~70 km diameter Morokweng impact structure, South Africa, represent fragments of a chondritic meteorite. Alwmark and Schmitz (2007) also discovered extraterrestrial chromite grains in the resurge deposit of the 13.5 km diameter Lockne impact structure, Sweden. In addition to physical fragments, approximately a fifth of the confirmed hypervelocity impact craters have known geochemical and/or isotopic signatures of the impactor preserved in impact melt-bearing rocks and glasses (Appendix A).

Of the remaining 186 craters, all but one were confirmed based on the presence of shatter cones and/or PDFs in quartz (Appendix A), which are considered the two most robust evidences for impact (see section 4.2). The ~14 km diameter Pantasma impact structure, Nicaragua, is a notable exception in the database, where confirmation of impact is not based on the presence of PDFs in quartz or shatter cones in various lithologies (Appendix A). The lack of PDFs can be ascribed to its quartz-poor (basaltic) target rocks and the tropical rainforest setting means that outcrops are sparse and heavily weathered, making the identification of shatter cones extremely challenging. Instead, diagnostic evidence for impact comes is from the documentation of FRIGN zircon and an extraterrestrial Cr isotopic signal in impact breccias, with supporting evidence in the form of high-temperature glasses and coesite (Rochette et al., 2019).

As is evident from Appendix A, PDFs in quartz occur in craters of all sizes, down to the Kamil (45 m) crater and the Douglas (66 m largest crater) and the Wabar (116 m largest crater) impact crater strewn fields. In contrast, shatter cones appear to be absent in craters smaller than ~1 km and are less common in buried craters. For the latter, this is likely due to the fact that the probability of finding shatter cones, which requires cm to dm-size pieces of rock, is very low, when the only material available is from drill core. Indeed, shatter cones were only recently reported for the first time at the famous Chicxulub impact structure, Mexico, in rocks drilled from the peak ring (Morgan et al., 2016). In theory, there is no reason why shatter cones should not form in small craters, as the pressures required for their formation would have been generated. Indeed, shatter cones have been formed in nuclear explosion tests (Bunch and Quaide, 1968) and even in experimental craters (Shoemaker et al., 1961). Baratoux and Reimold (2016) suggest that the scarcity of shatter cones in small craters is a result of the lower impact velocity of small objects due to deceleration induced by the atmospheric drag. However, given that impact glass – which requires shock pressures >50–60 GPa, i.e., well above the pressures required for shatter cone formation – is found in craters down to ~45 m diameter (e.g., the Kamil crater in Egypt), we therefore suggest that impact velocity is not a major factor. Instead, we suggest that the scarcity of shatter cones in small simple craters is largely due to the fact that apart from a very small region underneath the point of impact in the crater floor, the majority of the *in situ* target rocks in simple craters available for sampling (i.e., the crater wall and rim) were not subjected to shock pressures capable of forming shatter cones (Fig. 4). Instead, shatter cones in simple craters typically occur only as clasts in breccias in the crater-fill and ejecta. Such deposits are rapidly eroded and/or overlain by sediment, which

Table 5
List of confirmed impact deposits and their main attributes. See Supplementary Data for references and additional attributes.

Deposit name	Location			Date Confirmed	Age (Ma)
	Latitude Decimal Degrees N(+), S(−)	Longitude Decimal Degrees E(+), W(−)	Country		
Tektites					
Australasian strewn field	4.54	99.76	Australia, Indonesia, Malaysia, Vietnam, Cambodia, Laos, Thailand, southern China, Philippines	1900	0.79
Ivory Coast strewn field	4	−7.29	Côte d'Ivoire, Eastern equatorial Atlantic Ocean	1934	1.07 ± 0.05
Central European strewn field	48.25	16.56	Czech Republic, Germany, Austria	1787	14.7 ± 0.7
North American strewn field	26.12	−75.23	United States; microtektites located in Gulf of Mexico, Caribbean, Barbados, NW Atlantic	1996	~35.4
Spherules					
S1	−25.95	30.88	South Africa	1989	3470–3472
S2	−25.9	31.88	South Africa	1986	
S3	−25.92	31.02	South Africa	1986	3243 ± 4
S4	−25.92	31.02	South Africa	1989	3243
S5	−40.76	73.98	South Africa	2010	3234 ± 5
S6	40.76	73.98	South Africa	2010	3308 ± 6
S7	−25.93	30.86	South Africa	2010	3416
S8	−25.9	31.05	South Africa	2014	N/A
Warrawoona	−21	119.5	Western Australia	1977	3470
Monteville impact spherule layer	−29.14	23.14	South Africa	1999	2630
Grænsesø	61.67	−47.8	South Greenland	1960s	~1990
Dales Gorge	−22.33	118.23	Western Australia	1992	2490
Kuruman	−29.14	23.14	South Africa	Late 1970s	N/A
Bee Gorge	−22.23	118.25	Western Australia	1966	2346
Reivilo	−29.05	21.86	South Africa	2004	2580 ± 60
Paraburdoo	−23.06	118.82	Western Australia	2011	2570
Jeerinah	−22.55	119.5	Western Australia	2000	2629 ± 5
Carawine spherule layer	N/A	N/A	Western Australia	1992	2630 ± 6
Nuussuaq spherule bed	70.58	−53.08	Greenland	1991	60.7 ± 1.3
Qidong spherule	32.08	121.5	South China	1992	372
Zaonega spherule layer	62.49	−35.29	Russia	2014	1975–2050
Acraman	31.02	135.45	South Austrailia	1980	450–635
Late Triassic spherule	51.59	−2.41	SW England	1973	214
Sudbury	48.06	−89.51	Canada, USA	1964	1852.5 ± 51
Cretaceous-Paleogene	21.3	−89.54	Mexico	1978	65.07
Eocene clinopyroxene-bearing spherule layer	Global 50.16	Global 4.46	Varies	1973	~35
Senzeille/Hony microtektite	50.54	5.58	Belgium	1992, 1994	367–374
Other glass occurrences					
Dakhleh Glass	25.45	29.19	Egypt	2007	0.145
Darwin Glass	−42.31	145.66	Australia	1972	0.816
Libyan Desert Glass	25.4	25.3	Libya (~Egypt)	1932	28.5
South Ural Glass	53.62	60.17	Russia	1997	183
Edeowie Glass	−31.14	138.31	Australia	2001	0.78
Urengoites	66.12	76.95	Russia	1997	24
Atacama Desert Glass	−24.9	−69.9	Chile	2021	7.83 ± 0.26
Breccia payers					
Alamo breccia	37.67	−115.33	United States	1991	~367
Isle of Skye ejecta	57.22	−6.06	Scotland	2017	337.13
Stac Fada Formation	58.2	−5.35	Scotland	2008	1177 ± 5
Vakkejokk Breccia	68.37	19.26	Sweden	2011	~520
Miocene layer	22.98	154.02	N/A	2019	~11

significantly reduces the chance of finding shatter cones in simple craters. For example, despite a century of study, no shatter cones have been identified at Meteor or Barringer Crater. In contrast, at complex craters, the most common discovery location for shatter cones is in central uplifts, where they occur *in situ* and exposed at the surface (Fig. 4; Appendix A) (cf., Osinski and Ferrière, 2016). Furthermore, with erosion, the exposed area of a central uplift actually increases, such that the possibility of identifying shatter cones also increases.

With respect to target rocks, as noted above, approximately two-thirds of the confirmed terrestrial hypervelocity impact structures occur in the ancient cratonic areas of Australia, Europe, and North America, which comprise metamorphic and plutonic igneous rocks at their cores. However, in a review of the target rock types for both impact craters and hypervelocity impact craters, Osinski et al. (2008b) noted that ~70% of the world's known impact structures occur, in part, in sedimentary target rocks. Despite the number of new hypervelocity impact structures confirmed since this time, an assessment of the *Impact Earth* database shows that exactly 70% of such sites had some amount of sedimentary rock present at the time of impact. In detail, 76 hypervelocity impact craters formed in entirely sedimentary target rocks, 55 in purely crystalline targets (which includes metamorphic and igneous rocks), and with the remainder (57) forming in mixed targets, with some thickness of sedimentary rock overlying crystalline basement rocks. As discussed in Section 7, the abundance of hypervelocity impact structures formed in sedimentary target rocks causes great difficulty when attempting to determine accurate and precise ages for these structures. Target lithology also affects the morphology and morphometry of impact structures (see Section 9) and the impactites produced (see

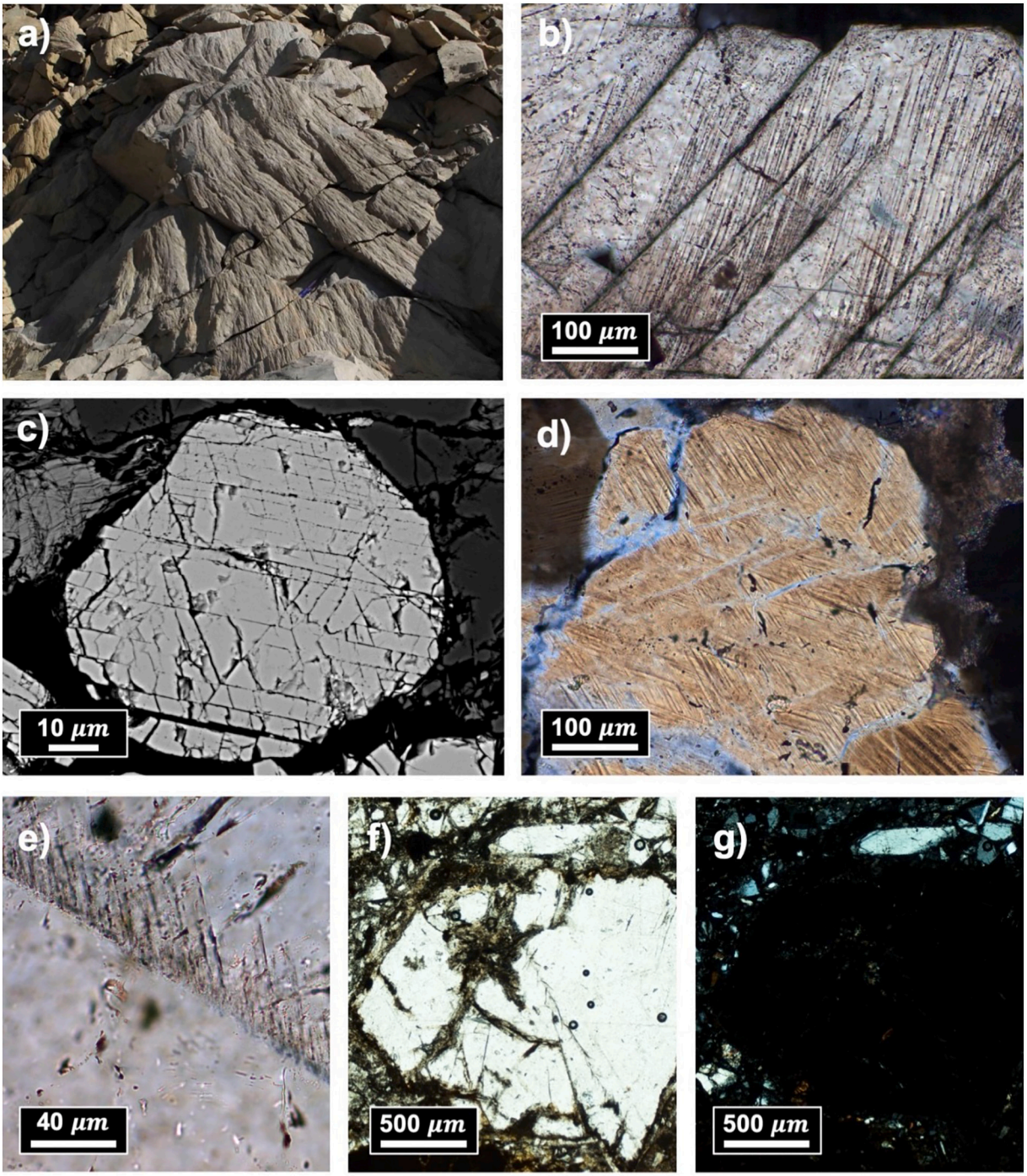

Fig. 6. Images of shock metamorphic indicators. a) Shatter cones in dolomite from the Tunnunik impact structure (hammer for scale). b) Planar Fractures (PFs), Planar Deformation Features (PDFs), and Feather Features (FFs) in quartz from the Chicxulub impact structure. c) Planar Fractures in apatite from the Chicxulub impact structure. d) Two sets of PDFs in quartz from the Bosumtwi impact crater. e) Feather Features emanating from a PF in quartz from the Haughton impact structure. f) and g) Diaplectic plagioclase feldspar (maskelynite) from the Mistastin Lake impact structure. b) and d–f) are plane polarized light photomicrographs; c) is a backscattered electron image; g) is a cross polarized light photomicrograph of f).

Section 10).

Given the fact that two-thirds of the Earth's surface is covered by water, it would be expected that a large number of impact features on Earth formed in such an environment. However, the record is notably sparse. Dypvik and Jansa (2003) in their review of such impacts listed five submarine hypervelocity impact craters (i.e., craters that formed and remain located in the sea/ocean floor) and 11 marine impacts (i.e., craters that formed in the sea/ocean but that are presently exposed on land), with a few other "possible" candidates and impact deposits. Included in the *Impact Earth* database are the more recently discovered Decorah (French et al., 2018), Glasford (Monson et al., 2019), Målingen (Ormö et al., 2014), and Talundilly (Gorter and Glikson, 2012) marine hypervelocity impact structures. In addition, it is also clear that the Sudbury impact structure occurred in a marine setting (Grieve et al., 2010). It is outside the scope of the current contribution to review details of marine impacts, but there is considerable variation in the morphology, morphometry, and products from such events, as recently discussed by Ormö et al. (2021). These differences compared to impacts

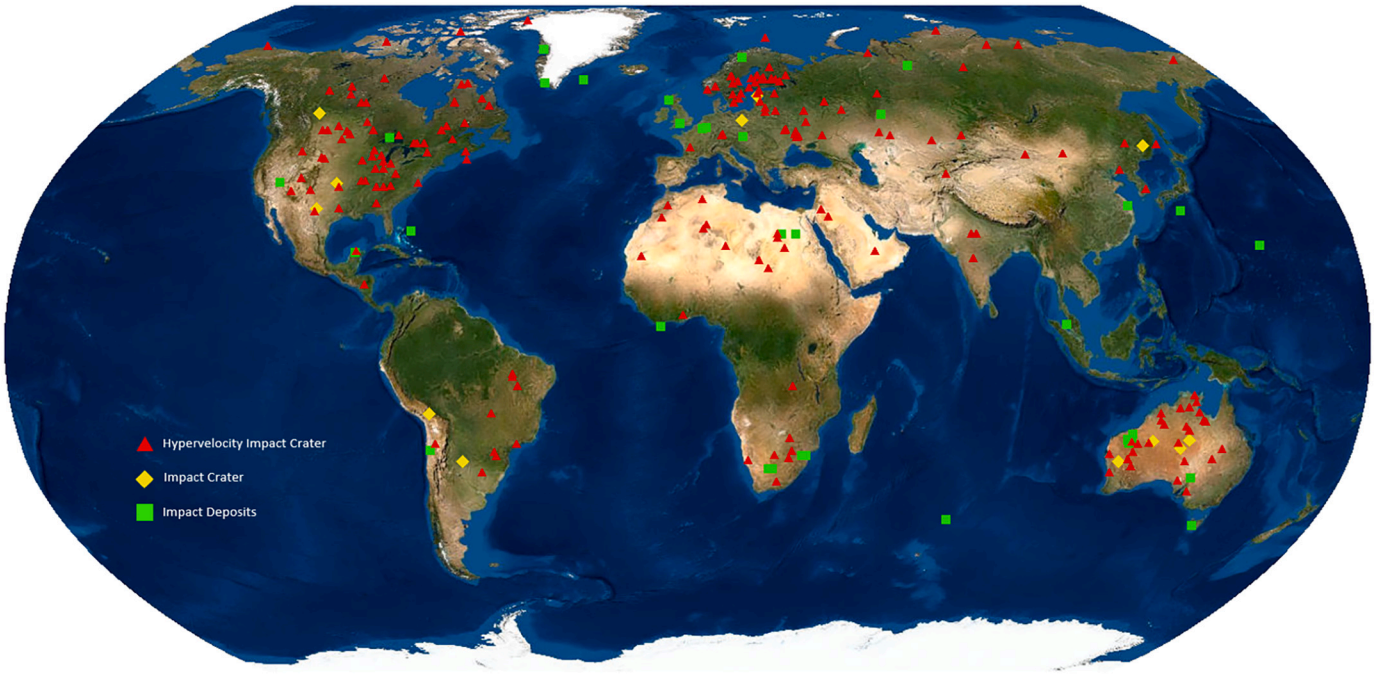

Fig. 7. Location of all confirmed impact craters, hypervelocity impact craters, and impact deposits on Earth.

on land appear to be largely dependent on the size of the impact event with respect to the water depth (Gault and Sonett, 1982; Wünnemann et al., 2007) and complicates estimates of crater diameter (section 8), and greatly affects the morphology and morphometry (Section 9), and types of impactites (Section 10) produced during such impacts.

A final point is that the literature of a considerable number of craters consists only of the original confirmation publication, which, from the point of view of reproducibility, is not ideal. While this includes craters that have been discovered very recently, there are also a number of craters where the impact origin was confirmed decades ago but with no subsequent follow-up studies. There are also examples of structures, which have been proposed as impact craters for some time but for which unequivocal evidence of impact has only more recently been presented. An example is Upheaval Dome, Utah (Shoemaker and Herkenhoff, 1983), which is very accessible in Canyonlands National Park, but for which a small number of PDFs were only identified in 2008 (Buchner and Kenkmann, 2008). This is ascribed to its highly eroded nature, such that virtually all shock diagnostic evidence has been removed.

5.3. *Some notable "impact craters" and "hypervelocity impact craters" not listed here*

While there are undoubtedly many more impact craters, hypervelocity impact craters, and impact deposits lying awaiting discovery or confirmation, the rigorous application of criteria outlined in Section 4 is paramount. With this in mind, there are a small number of structures for

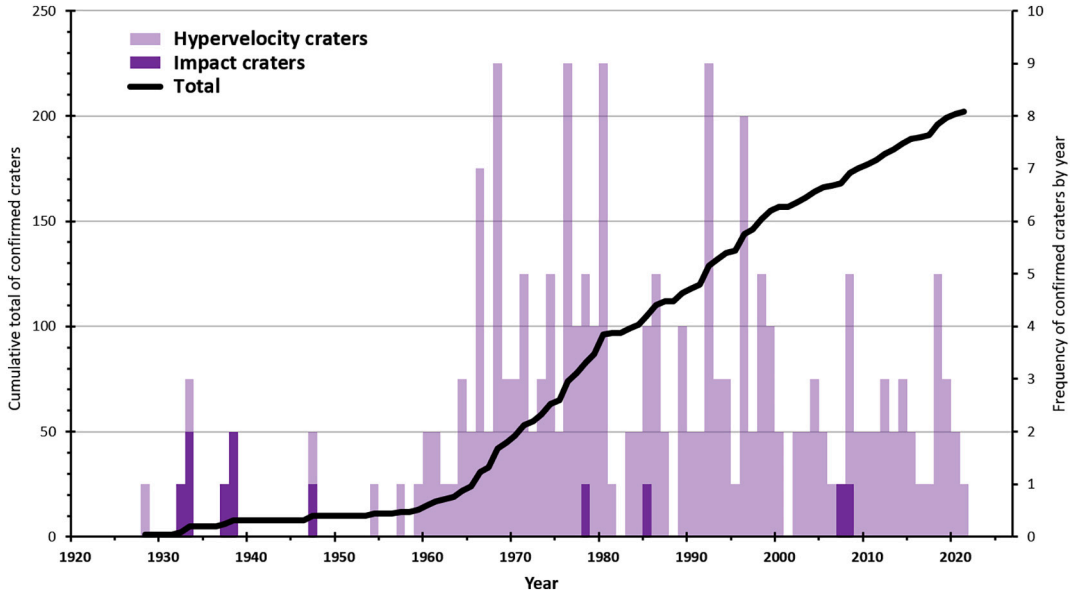

Fig. 8. Plot of the discovery of impact craters and hypervelocity impact craters through time. Note the dramatic change in slope of the cumulative number of known structures in the mid 1960s, which coincides with the "discovery" of shock metamorphic features.

which an impact origin has been previously suggested – and which have appeared in many previous lists of "confirmed" impact structures – that we do not list in the *Impact Earth* database. We briefly outline the reasoning for these decisions below.

Crawford, Australia: The Crawford structure is excluded for two reasons. First, as noted by Haines et al. (1999) "definitive evidence of shock metamorphism is lacking" for this structure. Second, as discussed by Haines et al. (1999) and Haines (2005), the Crawford structure lies within a few 10s km of the Flaxman impact structure and it is unclear at present as to whether this is a separate impact crater or if these structures represent one single structure.

Gusev, Russia: This structure lies close to the confirmed Kamensk impact structure in a similar geological setting (Movshovich and Milyavskiy, 1988). The literature is scarce on this structure, but based on what is presented, there is no evidence showing shock metamorphism nor of an impactor or meteoritic component. Until a time when such evidence is provided, we suggest that the Gusev structure should not be considered a hypervelocity impact structure.

Macha, Russia: The impact origin of Macha is suggested by a single study (Gurov and Gurova, 1998) that seems to be an English-language version of a Russian paper (Gurov et al., 1987). The impact evidence presented is in the form of PDFs in quartz and the chemical composition of metallic particles. However, the presented images of PDFs are either clearly not showing PDFs because they are not planar nor parallel (their Fig. 6), or the quality of images is so low quality that the identification of microstructures is problematic (their Figs. 7 and 8). Additionally, the full indexing of planar deformation features was not performed; instead only frequency distribution of measured angles between poles of planar structures and optical axis in quartz of Macha craters are presented. The provided chemical analysis of three metallic particles is also inconclusive. For example, they contain some nickel (0.084–0.2 wt%) and cobalt (trace to 0.026 wt%), but both of those values are much less than expected from iron meteorites (>5 wt% of Ni and > 0.3% of Co; Jarosewich, 1990; Scott, 2020).

Ilumetsa, Estonia: This site comprises two circular craters 50 m and 80 m in diameter. Based on the presence of two clear circular depressions, ejecta material, charcoal similar to material found in other very small impact craters (e.g., Kaali; Losiak et al., 2016), a post-glacial age that is identical for both structures that are 800 m apart, its formation due to extraterrestrial collision is at least probable. However, there remains no clear signs of extraterrestrial material (except some high-Ni particles of unclear origin, nor signs of shock metamorphism (Losiak et al., 2020)). This exemplifies the challenge of confirming the impact origin of small craters as discussed in Section 4.3.

Piccaninny, Australia: The Piccaninny structure in Australia was noted by Beere (1983) in an aerial survey and considered the possibility of both an impact and cryptovolcanic origin. Shoemaker and Shoemaker (1985) list Piccaninny as a "deeply eroded probable impact structure" but these authors also note that no shock metamorphic evidence has been documented to-date.

Sobolev, Russia: The Sobolev structure was described by a single study (Khryanina, 1981). It is a 53 m single crater-like feature with an overturned sequence at the rim with a paleosoil and a charcoal at the similar geomorphic location as in Kaali (Losiak et al., 2016) or Morasko (Szokaluk et al., 2019) as well as magnetic "melt" spherules with a single reported value of Ni contents up to 2.1%. Shatter cones were also reported from this site, but presented images are not sufficient to confirm their formation in a hypervelocity impact crater.

Suavjärvi, Russia: The Suavjärvi structure has been proposed to be a deeply eroded complex impact structure with a diameter of ~16 km and, potentially, the oldest structure preserved on Earth (Mashchak and Naumov, 2012). However, a recent field expedition found no evidence of previously reported impact breccias and the subsequent analysis of samples also found no evidence of shock metamorphism (Huber et al., 2013).

5.4. Impact deposits

In addition to impact crater strewn fields and individual craters, there are a number of examples of impact deposits that contain material with a confirmed impact origin; however, most have no known source crater. We have classified such impact deposits into five main categories: tektites, spherule layers, occurrences of other types of glass, breccias, and detrital shocked minerals. Below, we outline these five main categories of impact deposits.

5.4.1. Tektites

Impact glass is a common product of meteorite impact events (Osinski et al., 2018; Stöffler, 1984). One of the most well-known types of impact glass are tektites, defined as "an impact glass formed at terrestrial impact craters from melt ejected ballistically and deposited sometimes as aerodynamically shaped bodies in a strewn field outside the continuous ejecta blanket" (Stöffler and Grieve, 2007). Tektites differ in several ways from other types of impact glass (i.e., diaplectic glass, mineral glass, interstitial impact glass, and whole rock impact glass) (Osinski et al., 2018), found in impactites within and around impact craters. Most notably, tektites commonly have splash-form (e.g., teardrop, dumbbell, or bar) shapes and/or aerodynamic shapes with evidence of atmospheric ablation in the form of pits, grooves, or flanged button shapes. The composition of most tektites is also distinctive, with extremely low H_2O contents (often ppm levels) (Beran and Koeberl, 1997; Ferrière et al., 2021), high Fe^{2+}/Fe^{3+} ratios (Heide et al., 2001), and ^{10}Be concentrations that suggest the source region must have been in the upper few hundred meters of the target area (Koeberl, 1994). These properties have led to models of tektite formation that differ from the typical impact glasses emplaced within and around craters. Namely, they are formed in high-velocity (>15–20 km/s) and oblique (30–45°) impacts into silica-rich and possibly unconsolidated targets and originate from the melting of near-surface target materials, which is ejected at high-velocity very early in the crater formation process (Artemieva et al., 2002; Stöffler et al., 2002).

The formation of tektites, however, is not without debate. There are only a few known occurrences. Until very recently, only four large so-called strewn fields of tektites), which have been known since the 1930s (Glass, 1990), have been documented (Table 5): the Australasian, the Ivory Coast or ivoirites, the Central European (Czechoslovakian/Moldavian), also commonly known as moldavites, and the North American (also called bediasites and georgiaites) strewn fields. Two other possible strewn fields have also recently been proposed. The first is in the form of impact glasses from Belize that have been linked to the Pantasma impact crater located ~530 km away (Rochette et al., 2021). We say "possible" as the authors acknowledge that while the Belize impact glasses share many characteristics with known tektites, they also possess "several peculiar features". The second is a new potential tektite strewn field discovered in Uruguay (Ferrière et al., 2017).

5.4.2. Spherule layers

As is evident from Table 5, millimetre-sized spherules are the most common type of distal impact deposit. When found in continuous beds, they are known as known as "airfall beds" or "impactoclastic" deposits (Stöffler and Grieve, 2007). A few have been linked to specific craters, but the majority have no known source crater (Table 5). This is not surprising given the Precambrian ages of the majority of spherule beds (Table 5). Indeed, given the age of the oldest reliably-dated hypervelocity impact structure on Earth (2229 ± 5 Ma for the Yarrabubba impact structure, Australia; Erickson et al., 2020), these spherule beds are the only record of Archean impacts (i.e., >2.5 to <4 Ga) on Earth and provide a unique glimpse into bombardment rates in the inner Solar System during the first 2 billion years of its history (e.g., Bottke and Norman, 2017; Kirchoff et al., 2021). It remains unclear as to the minimum size of impact required to generate these spherule airfall beds; however, given their concentration in the Precambrian and knowledge

of distal deposits from two of the three largest preserved craters (Chicxulub and Sudbury), it is likely that such deposits require >10 km-size impactors and > 200 km-diameter craters.

Numerical modelling presented by Johnson and Melosh (2012) suggests that glassy spherules present in distal ejecta can form in two fundamentally different ways: via "conventional" impact melting or by condensation from a vapour phase. These authors suggested the terms "melt droplets" and "vapour condensate spherules", as the two respective products. Another potential source of confusion that some spherules are sometimes referred to as *microtektites* (if they consist entirely of glass) or *microkrystites* (if they contain primary microlites). It remains unclear if tektites (see Section 5.4.1) and microtektites have the same origins and it is outside the scope of this contribution to revisit the origin of the many spherule layers listed in Table 5.

5.4.3. Other glass occurrences

In addition to tektites and spherules, there are a number of occurrences of glasses that are widely, although not universally, accepted as being of impact origin but for which no source crater has been recognized. Well known examples include Dakhleh Glass (Osinski et al., 2007), Darwin Glass (Meisel et al., 1990), Edeowie Glass (Haines et al., 2001) Libyan Desert Glass (Weeks et al., 1984), and South Ural Glass or Urengoites (Deutsch et al., 1997). Evidence for the impact origin of these glasses typically comes from their unusual compositions, including nearly pure SiO_2, or having CaO and MgO contents >20 wt%, which distinguishes them from volcanic glasses. The origin of these glasses is enigmatic. It is notable that all occur as individual glass bodies and not as clasts in breccias (see section 5.4.4. below for such examples), so they do not represent eroded remnants of crater-fill or proximal ejecta blankets. The size of individual glass bodies ranges from cm to several dm, they lack aerodynamic shapes and other evidence of quenching during passage through the atmosphere (in contrast to tektites), and there is evidence for ponding in a liquid state.

The most plausible formation mechanism for, at least some of, these glasses is through large airbursts. As noted in Section 3, numerical modelling suggests that during large low-altitude airbursts, a high-temperature jet is formed that, if it makes contact with the Earth's surface, will result in the melting of surficial sediments, producing large amounts of impact glass (Boslough and Crawford, 2008). Numerical modelling adds credence to earlier suggestions that airbursts may be responsible for the formation of the ~780 ka Australian tektites (Wasson et al., 1995), the Libyan Desert Glass (Wasson and Boslough, 2000), and the Dakhleh Glass, Egypt (Osinski et al., 2007, 2008c). The recent discovery of condensation spherules in Antarctica has also been explained as being due to a large airbirst event at ~430 ka (Van Ginneken et al., 2021), and widespread glasses in the Atacama Desert, Chile, have also recently been proposed to have formed during nearly simultaneous cometary airbursts near the end of the Pleistocene Period (Schultz et al., 2021). It should be noted, however, that these same Atacama or "Pica" glasses have also been interpreted as the product of natural fires in dried out wetlands (Roperch et al., 2017, 2022). In addition, in the case of the Libyan Desert Glass, Koeberl and Ferrière (2019) have recently reported on the first occurrence of PFs, PDFs, and FFs in quartz grains from bedrock samples from the area of occurrence of the Libyan Desert Glass, and shocked zircon grains have been reported in Libyan Desert Glass (Cavosie and Koeberl, 2019), suggesting that there was a physical impact event, not just an airburst, and that the crater has been almost completely eroded since its formation. Shocked zircon grains have also been reported in Australasian MN-type tektites from southeast Asia (Cavosie et al., 2018b), which also suggests an impact origin involving crater formation.

5.4.4. Breccia layers

In addition to deposits of tektites, spherules, and other glassy bodies described in the previous sections, there are some rare instances in the geological record of lithified rock units that have been proposed to be of impact origin and/or to contain material derived from a hypervelocity impact event. The most famous and longest known example is the Late Devonian age Alamo Breccia. Originally identified in 1990 by J. E. Warme, it was initially described as a catastrophic marine sedimentary megabreccia that covers ~10,000 km^2 in southern Nevada. The discovery of PDFs in quartz in the Alamo Breccia by Leroux et al. (1995) subsequently led to the conclusion that this widespread unit was formed by a hypervelocity impact event. However, it is important to note that the Alamo Breccia does not conform to the definition of an impactite (see Section 10) as it is not part of an ejecta blanket or crater-fill deposit; rather, it represents a sedimentary deposit whose formation was triggered by the impact event and that contains some shocked material mixed in with local non-impact material (Warme and Kuehner, 1998).

Other examples include the Vakkejokk Breccia, Sweden, and the Stac Fada Formation, Scotland, both of which were confirmed through the presence of PDFs in quartz. The ≤27 m thick Vakkejokk Breccia outcrops for ~7 km on the northern side of Lake Torneträsk in Sweden and is interpreted to be the primary ejecta deposit of a crater formed ~520 Ma that is now obscured by later Caledonian overthrusts immediately north of the main breccia section (Ormö et al., 2017). The Stac Fada Member is an 1177 ± 5 Ma age (Parnell et al., 2011) distinctive glass-bearing breccia that outcrops at several locations over ~50 km along the coast of northwest Scotland. Originally interpreted to be volcanic in origin (Lawson, 1973; Young, 2002), before being interpreted as the primary ejecta blanket of a now eroded or buried impact structure (Amor et al., 2008), more recent work suggest that this deposit formed via the interaction of hot impact melt with water – akin to what occurs during phreatomagmatic volcanic eruptions – and represents material emplaced as high-energy ground-hugging sediment gravity flows beyond the extent of the continuous ejecta blanket (Osinski et al., 2020c) (see also Section 10.3.).

5.4.5. Detrital shocked minerals

Sedimentary deposits containing the erosional remnants derived from primary impactites represent a different type of impact deposit, as they continue to form as a crater erodes over time, and thus preserve long-term archives of terrestrial impact cratering processes. Detrital shocked minerals are those which originated in target rocks (igneous, metamorphic, sedimentary), and then were shock-deformed during impact, and subsequently eroded and transported as sand grains. Examples of local (mostly within or proximal to source crater) sedimentary reworking of shocked target rocks, minerals, and impact glass by glacial and fluvial processes were reviewed by Buchner and Schmieder (2009). Distally-transported detrital shocked minerals in modern and ancient sedimentary deposits have since been reported from several confirmed impact structures. Along with shocked quartz, accessory minerals such as zircon, monazite, and xenotime, are known to form shock deformation microstructures, and have proven to be particularly useful in detrital shocked mineral studies given their refractory character and use as U-Pb geochronometers. Detrital shocked quartz, monazite, xenotime, and zircon eroded from the Vredefort Dome have been reported within the structure (Cavosie et al., 2010, 2021), and at distances up to nearly ~2000 km downstream from the impact structure in modern alluvium from the Vaal and Orange rivers (Erickson et al., 2013; Montalvo et al., 2017). Detrital shocked minerals have also been reported in mid-Pleistocene (~1.7–1.3 Ma) fluvial terraces of the Vaal River up to ~750 km downstream from the Vredefort Dome (Cavosie et al., 2018a), and in Permian glacial deposits (diamictite and tillite) of the ca. 300 Ma Dwyka Group in a southwest (down-ice) direction from the Vredefort structure (Pincus et al., 2015). Detrital shocked quartz and zircon were also been reported from the Sudbury impact structure, in both modern alluvium and Holocene glacio-fluvial outwash delta deposits and eskers (Thomson et al., 2014). Detrital shocked minerals have also been used to better resolve the distribution of shocked bedrock at craters that are poorly preserved or have otherwise been deformed and/or deeply eroded (e.g., Montalvo et al., 2018).

Table 6
Degree of erosion of terrestrial craters.

	Dence (1972)	This study	Examples
1	ejecta blanket largely preserved	ejecta blanket, rim and crater-fill impactites* predominantly preserved	Barringer, Bosumtwi
2	ejecta blanket partly preserved	ejecta blanket and rim partly preserved; crater-fill impactites largely preserved	Boltysh, Haughton
3	ejecta blanket removed, rim partly preserved	ejecta blanket eroded; rim partly preserved; crater-fill impactites largely preserved	Kardla, Pantasma
4	rim largely eroded, breccias within crater preserved	ejecta blanket eroded; rim largely eroded; crater-fill impactites largely preserved	Obolon, Puchezh-Katunki
5	crater breccias and melt rocks partly preserved	ejecta blanket and rim eroded; crater-fill impactites partly preserved	Kara, Strangways
6	remnants only of breccias and melt rocks in crater floor	ejecta blanket and rim eroded; remnants of crater-fill impactites preserved	Connolly Basin, Lappajärvi
7	crater floor removed, substructure exposed	ejecta blanket, rim and crater-fill impactites eroded; substructure exposed; only allochthonous impactites possible are injected impactite dykes	Lawn Hill, Tunnunik

* See Section 10.

6. Preservation state of the terrestrial record

As noted at the outset, the power and utility of the impact cratering record on Earth is the ability to conduct fieldwork, drilling, geophysical surveys, and to collect samples from known locations, which are all lacking in the remote observations of craters on other planetary bodies. An obvious drawback, which is also true for some other planetary bodies with active erosion (e.g., Mars, Titan), is that all craters on Earth are eroded to some degree. This makes comparative studies with other terrestrial craters, on other planetary bodies, fraught with uncertainty, and also makes the determination of age (Section 7), size (Section 8), and original morphology (Section 9) difficult or impractical in some cases. However, the erosional state of terrestrial craters is also a positive attribute depending what aspect of the cratering process one is interested in, as it allows for direct observations of their subsurface nature. For example, more deeply eroded craters provide an excellent opportunity to study the structural geology of complex impact craters once the overlying allochthonous ejecta and crater-fill deposits are removed.

A useful concept introduced by Dence (1972) is the degree of erosion (Table 6), which is essentially a measure of the preservation state of a particular crater. In compiling the *Impact Earth* database, we have determined the degree of erosion for all impact craters and hypervelocity impact craters, which has resulted in some suggested clarifications and minor changes to the original classification (Table 6). It is clear, with certain exceptions (e.g., Pantasma, erosion level 3), that the majority of craters discovered in the past couple of decades are deeply eroded.

It is hoped that providing the degree of erosion will enable future studies of the terrestrial impact record by making it easier to "select" craters for study. For example, if the goal is to study impact ejecta emplacement, then only craters with degree of erosion 1 or 2 should be considered. The degree of erosion also provides a certain first-order qualitative measure of reliability of certain other attributes, particularly for attributes such as crater size (see Section 8), which generally speaking becomes harder to determine the more eroded a crater becomes.

7. Crater ages

7.1. Approaches and challenges in dating terrestrial impact structures

Establishing accurate and precise ages for impact craters can: link impacts to mass extinctions and other effects on the geo- and biosphere (Schulte et al., 2010; Swisher et al., 1992) and the other way around (Holm-Alwmark et al., 2021); reveal trends in impact flux through time and allow evaluation of periodicity (e.g., Bland, 2005; Deutsch and Schärer, 1994); help to calibrate the geological time scale via ejecta in sedimentary records and sedimentary deposits within the crater for palaeoclimate studies (e.g., Jolley et al., 2013; Parnell et al., 2010); link distal ejecta deposits with source craters (e.g., Deutsch and Koeberl, 2006; Renne et al., 2018); constrain duration of crater cooling and hydrothermal activity (e.g., Kenny et al., 2019; Schmieder and Jourdan, 2013); and constrain the overall continental cratering rate which helps to inform the present day likelihood of impact on Earth (Kelley and Sherlock, 2013).

The two main ways of establishing impact structure chronology are stratigraphic and isotopic dating techniques (e.g., Kelley and Sherlock, 2013; Schmieder and Kring, 2020). A summary of the main techniques used for impact geochronology and referred to in the *Impact Earth Database* can be found in Table 7. Stratigraphy can be used to establish an age bracket for an impact event, but with a very small number of exceptions (e.g., Mjolnir; Smelror et al., 2001) this does not produce precise ages. A higher degree of precision is often required in order to establish exact timing of an impact event, for which we turn to isotopic dating (Table 7) (Deutsch and Schärer, 1994; Jourdan et al., 2009; Schmieder and Kring, 2020).

It is notable that many impact structures have only poor to non-existent age constraints. Indeed, only 37 (out of 188) hypervelocity impact structures in the *Impact Earth Database* have ages that are precise (± 2% at 2σ) (Table 4) (Fig. 9) (cf., Jourdan et al., 2009; Schmieder and Kring, 2020). To provide context, ± 2% precision is still poor relative to the objectives of the international EarthTime initiative (http://www.earth-time.org), established to sequence Earth history at a resolution of ±0.1% at 2σ. The most precise impact crater ages are Carancas and Sikhote Alin, as they were observed events on 15 September 2007 (Brown et al., 2008) and 12 February 1947 (Krinov, 1971), respectively. The most precise age determined for a hypervelocity impact crater is Sudbury at 1849.53 ± 0.21 (2σ, 0.011%, $^{207}Pb/^{206}Pb$ melt-grown zircon; Davis, 2008). Because impact craters are smaller than hypervelocity impact craters, they are harder to prove as unambiguously impact-generated, tend to be younger when found (older ones are more easily erased), and produce fewer datable phases, making them a significant challenge to determine precise and accurate ages. As a result, only 3 out of 13 impact craters in the *Impact Earth Database* have age precisions <2%, and two of those were observed events. Despite the challenges, there is hope for the dating of the terrestrial impact cratering record, due to recent improvements in geochronology, particularly in the accuracy and precision of the $^{40}Ar/^{39}Ar$ and U-Pb systems (e.g., Kenny et al., 2019; Renne et al., 2013; Renne et al., 2010; Schoene, 2014; Sprain et al., 2018). Indeed, age constraints on impact structures can achieve precision on the scale of thousands of years, but only if suitable phases exist that can be clearly associated with the impact event.

The *Impact Earth Database* allows a re-evaluation of the precision of impact structures with ages updated according to the recommendations of Jourdan et al. (2009), Schmieder and Kring (2020) and publications released since, and shows the following: total number of hypervelocity impact structures = 188; total not successfully dated (those reported with ~, <, or >, or age ranges rather than uncertainties) = 123 (65%), with only 37 (19%) dated at "high-precision" better than ±2% (Figs. 9, 10). The number of "high-precision" ages in this re-evaluation is substantially higher than the 15 reported by Jourdan et al. (2009), due to recent improvements to the ages of several (28) new/revised ages since 2009. Jourdan et al. (2009) also point out that in the case of many

Table 7
Summary of dating techniques referred to in the *Impact Earth Database*. Columns summarize key aspects of each technique: lithologies and minerals from impact structures which are suitable; the age range to which each technique is applicable; the criteria for resetting the system (for most isotopic systems this is the closure temperature); advantages, limitations, and cautions about using this technique; the number of craters for which the best (currently accepted) age is determined by the technique; and some references for more details about each technique.

Technique	Material	Age range	Resetting criteria	Advantages, limitations, and cautions	#	References
U-Pb	Impact melt rocks, intensely shocked minerals or newly grown in the melt (zircon, baddeleyite, monazite, titanite, apatite, xenotime, thorite, allanite, perovskite, rutile)	100 s kyrs to ~4.6 Gyrs	~450–550 °C (apatite, rutile) ~500–700 °C (titanite) ~900–1200 °C (zircon)	• *In situ* analyses (via. SIMS) preserve textural context, but has only moderate precision • High precision and internal reliability checks (data quality, statistical relevance) achieved through TIMS but completely dissolves the sample • Resistant to reheating so unlikely to be disturbed, however may also result in incomplete resetting during impact • Need to be cautious of overprinting history and inherited minerals from target rock	17	(Corfu, 2013; Schoene, 2014)
$^{40}Ar/^{39}Ar$	Impact melt rocks (whole rock or glass), melted/heated or newly grown K-bearing phases (e.g., feldspar, biotite, hornblende, pyroxene, alunite, jarosite, glauconite)	~500 yrs. to ~4.6 Gyrs	~200–400 °C (K-rich feldspar) ~250–350 °C (biotite) ~300–400 °C (muscovite) ~500–600 °C (hornblende)	• *In situ* analyses (via UV-laser) preserve textural context, but has only moderate precision and lacks internal reproducibility checks • High precision and internal reliability checks (data quality, statistical relevance) achieved through step-heating, but sample entirely melted during analysis • All isotopes measured in one experiment, reduces problems associated with heterogeneous samples • Small amount of sample material needed • Ar loss/redistribution and alteration result in younger apparent ages • Extraneous $^{40}Ar^{*}$ (inherited from target rock or incorporated via fluid) results in older apparent ages • Disturbed spectra can sometimes be mitigated by examining isotope correlation plots (inverse isochrons) • 40Ar* from high-Ca inherited clasts is decoupled from melt rocks during step heating enabling robust allowing plateau ages	45	(Holm-Alwmark et al., 2021; Kelley, 2002; Kuiper, 2002; McDougall and Harrison, 1999; Renne et al., 2009)
K-Ar	Same as $^{40}Ar/^{39}Ar$	10s kyrs to ~4.6 Gyrs	Same as $^{40}Ar/^{39}Ar$	• ^{40}K and ^{40}Ar isotopes must be measured on different parts of a sample, so heterogeneous samples result in inaccurate ages • Relatively low precision • Largely replaced by $^{40}Ar/^{39}Ar$ in modern age determinations	7	(McDougall and Harrison, 1999)
Stratigraphy	Various Best: target with well-constrained age, crater that is quickly filled by micro-fossil rich sediment that can be dated	Any	N/A	• Frequently the only option, (i.e., craters with no melt rocks available or those that have been highly altered) • Age bracket only (i.e., by determining the age of the target rocks and the age of the first overlying sediment) • Usually imprecise (ranges of hundreds of millions of years or constrained to ">" or "<" ages) • Precise age constraints can be provided in cases with minimal erosion, magneto-stratigraphy, and/or swiftly evolving fossil species • "Absolute" ages of structures with stratigraphic constraints must be periodically updated as the absolute ages of those boundaries in the chronostratigraphic timescale are updated • Perceived stratigraphic alignment can disagree with isotopic ages	98	(Kelley and Sherlock, 2013)
Paleo-magnetism	Impact melt rocks, slowly cooling breccias	No technical limit, but practically	Melted/heated rocks as they cool through 500–900 °C; or magnetic grains grow	• Best estimate provided they agree with local geologic constraints • Require careful cross-checking with other techniques	3	(Tauxe et al., 2018)

(*continued on next page*)

Table 7 (*continued*)

Technique	Material	Age range	Resetting criteria	Advantages, limitations, and cautions	#	References
		<100 Ma to be precise	during chemical reactions	• Need an estimate of the approximate crater age to start with • Magnetostratigraphic pattern in samples needs to match polarity time scale with few zones ignored in either section or scale • Ideally measurements matched from multiple sites in the section of interest.		
Luminescence	Quartz, feldspar	10s yrs. to 100 s kyrs	~30 °C to ~90 °C	• Relatively low precision • Date the most recent exposure of a mineral grain to daylight or heating • Multiple techniques: Thermoluminescence (TL), optically stimulated luminescence (OSL), infrared stimulated luminescence (IRSL)	2	(Ault et al., 2019; Liritzis et al., 2013; Wintle, 2008)
Cosmogenic nuclide exposure ages (^{10}Be, ^{26}Al, ^{36}Cl)	Material excavated by impact, the meteorite; (quartz, calcite, feldspar, garnet, hornblende, magnetite, olivine, pyroxene)	<~4 Myrs	N/A	• Production stops when rock/mineral is sufficiently shielded from cosmic radiation (buried under 10s of meters on Earth) • Ages based on terrestrial age of meteorite (time since atmospheric shielding started) or exposure age of material excavated by impact (previously shielded from cosmic rays)	2	(Dunai, 2010)
Fission track	Zircon, apatite, titanite, glasses have been dated, but tracks in glass less stable	~100 ka to ~1 Ga	~60–120 °C (apatite) ~250–350 °C (titanite) ~200–350 °C (zircon)	• Need to measure ~100 tracks for statistical significance • Need to account for track orientation relative to the crystal and the polished surface	3	(Ault et al., 2019; Dumitru, 2000; Malusà and Fitzgerald, 2019)
(U-Th)/He	Apatite, zircon, titanite,	100 kyrs to ~4.56 Ga	~30–120 °C (apatite ~20–200 °C (zircon) ~20–210 °C (titanite)	• Age dispersion within a single crystal can be very high • Age reproducibility between grains is key to demonstrating quality because inclusions with high U and Th are heterogeneously distributed • Usually requires sampling of high volume (3–10 kg) of rock in order to get mg quantities of appropriate minerals • Mineral size and morphology requirements for proper age determination (e.g., > ~ 75 μm and euhedral apatite)	3	(Ault et al., 2019; Ehlers and Farley, 2003)
^{14}C (radio-carbon)	Organic matter associated with the impact (e.g., charcoal)	<50,000 yrs	N/A	• Particularly useful on young craters, but only when organic matter has been preserved and is clearly associated with the impact. The age estimation needs to take into account "an old wood problem" • Proper age determination requires multiple samples related to the same impact event; a) from multiple structures within the same strewn field, b) from multiple geomorphological settings within a single crater (e.g., the deepest organic-rich layer within crater compared with the age of paleosoil), c) the best ages are delivered by dating multiple charcoals from proximal ejecta blanket.	3	(Hajdas, 2008, 2009; Losiak et al., 2016, 2018, 2020)
Rb-Sr	Melt rocks, biotite, muscovite, k-rich feldspar	>10s Myrs	~300–500 °C (biotite and muscovite)	• Rb and Sr both highly mobile so susceptible to dispersion due to alteration or inherited components • Assumes at rock formation all phases share same Sr isotope composition, therefore the impact must have completely melted and homogenized to give good data • Problems with heterogeneous samples • Requires at least two phases (minerals or whole rocks) with different Rb-Sr ratios	0	(Dickin, 2018; Rink and Thompson, 2015)
Geo-morphology	Various	N/A	N/A	• Based on apparent erosional state (definition of rim, central uplift, preservation of deposits, etc.) and comparison with preservation of craters of known age	4	

(*continued on next page*)

Table 7 (*continued*)

Technique	Material	Age range	Resetting criteria	Advantages, limitations, and cautions	#	References
				• Only provides very broad (imprecise) age range • Potentially highly inaccurate depending on what is known of geological history of the area		

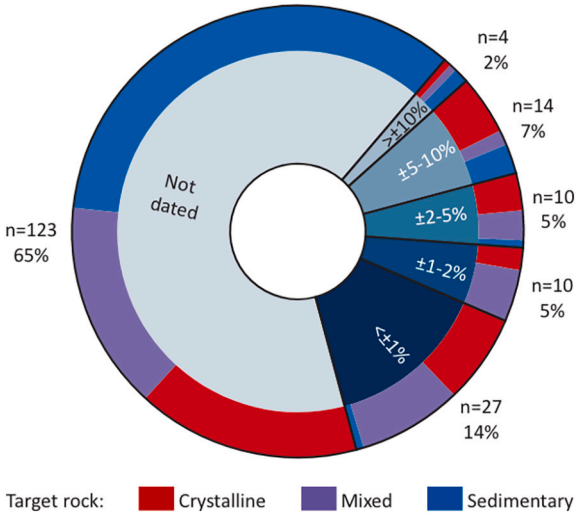

Fig. 9. Pie chart showing precision of hypervelocity impact crater ages. The 123 "Not dated" craters are those reported with only approximate age constraints. Also shown are the target rock types associated with each category. This highlights the challenges of determining precise ages for sedimentary targets. There is only one crater in a sedimentary target with an age precision <±2% (Kamensk), and only two total < ±5% (Kamensk and Montagnais), despite purely sedimentary targets making up ~40% of the target rock types.

impact structures, little can be done to improve the chronology using current technology, dating schemes, and approaches, as many impact structures lack datable lithologies (i.e., lithologies, such as impact melt rocks, in which the isotope systematics were demonstrably reset by the impact).

Difficulties with dating impact structures arise from the availability of samples appropriate for geochronology (e.g., sedimentary targets often lack minerals suitable for radiosotopic age determination) and the textural and chemical complexity of impactites. Such complexities include variable degrees of melting and isotopic resetting (90% of target rocks are not completely reset by impact events (Deutsch and Schärer, 1994)), inclusion of unmelted clasts in impact melt rocks and glasses (Deutsch and Schärer, 1994; Jourdan et al., 2009), the complex effects of shock metamorphism (Winslow III et al., 2004), and post-impact hydrothermal alteration of materials.

7.2. Case studies

Due to improvements in the isotopic techniques, as well as refinements in the ages of stratigraphic boundaries, the accepted ages of impact structures have been known to change, sometimes substantially, over time. For example, the Haughton impact structure has had its age determined at least seven times between 1987 (Omar et al., 1987) and 2021 (Erickson et al., 2021) by numerous techniques including apatite fission track (Omar et al., 1987), $^{40}Ar/^{39}Ar$ (Erickson et al., 2021; Jessberger, 1988; Sherlock et al., 2005; Stephan and Jessberger, 1992), zircon and monazite U-Pb (Erickson et al., 2021; Schärer and Deutsch, 1990) and zircon (U-Th)/He (Young et al., 2013). With ages ranging from 22.4 ± 1 Ma (Omar et al., 1987) to ~39 Ma (Sherlock et al., 2005), Haughton embodies many of the difficulties with achieving precise and accurate ages for impact structures because it formed in ~1880 m of sedimentary rocks overlying a high-grade metamorphic basement, and has impact melt rocks originating from carbonates and not silicate lithologies; this limits the amount of phases available for radioisotopic studies. However, Erickson et al. (2021) conducted a combined study of the age of Haughton using U-Pb of zircon and monazite with $^{40}Ar/^{39}Ar$ of impact-melted K-rich feldspar derived from clasts of impact breccia (interestingly, from the same samples used by Schärer and Deutsch (1990) and Stephan and Jessberger (1992)). Critically Erickson et al. (2021) coupled their isotopic measurements with detailed microanalysis to inform interpretation of age data. They found that the U-Pb and $^{40}Ar/^{39}Ar$ ages agreed within uncertainty but recommend use of the $^{40}Ar/^{39}Ar$ age because it is more precise at 31.04 ± 0.38 Ma. Like many recent studies that have ended up "unchaining" apparent crater clusters, this work also moves Haughton out of age uncertainty with Wanapitei and Mistastin Lake (as was suggested by (Sherlock et al., 2005)), and makes it clear that Haughton was not part of the Oligocene impact spike

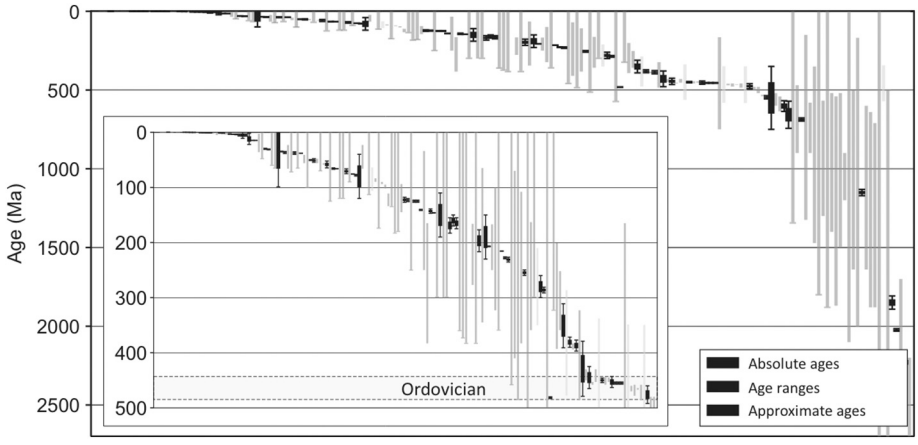

Fig. 10. Age versus rank plot of the ages of all terrestrial hypervelocity impact structures, ranked by age (for those with absolute age) or 'mean age' for those reported with only approximate age constraints. Inset shows an expanded version of the chart with ages <500 Ma. Chart highlights the large number of imprecisely dated structures and emphasizes the better results in the past 500 Myrs. Also highlighted is the Ordovician Period, highlighting the 22 impacts formed between ~485 and ~ 443 Ma. Other than this one cluster, there are not enough robust and precise data to identify any other groupings at this time.

or the possible Eocene "spike" of Popigai and Chesapeake Bay.

Another major debate of impact synchronicity has involved the apparent crater doublet of East and West Clearwater Lakes. Since 1963 at least 9 attempts have been made to determine precise and accurate ages for these structures using fission track, Rb-Sr, K-Ar, $^{40}Ar/^{39}Ar$, and (U-Th)/He. East Clearwater has proven notoriously difficult to date due to the presence of extraneous ^{40}Ar in impact melt rocks (for detailed discussion of the effects of extraneous argon see e.g., Jourdan et al. (2007), Kelley (2002), and Pickersgill et al. (2020). The possibility that Clearwater East and West formed by impact of a binary asteroid rested largely on a Rb-Sr mineral isochron age of 287 ± 26 Ma for East Clearwater (Reimold et al., 1981, recalculated and reanalysed by Schmieder et al. (2015) to 293 ± 110 Ma). This age agreed with previous ages for Clearwater West of ~300 Ma (using K-Ar, Rb-Sr, and fission track). However, statistical analysis of the Clearwater East age by Schmieder et al. (2015) demonstrated that the Rb-Sr age was disturbed, and likely not representative of the true age of the crater. Schmieder et al. (2015) then conducted $^{40}Ar/^{39}Ar$ analysis on samples of melt rock from both Clearwater East and West and determined an age for West of 286.2 ± 2.6 Ma, in agreement with previous age estimates; and a best estimate age for East of ~460–470 Ma, in agreement with the maximum age estimate of Bottomley et al. (1990). Both Bottomley et al. (1990) and Schmieder et al. (2015) encountered characteristic signs of extraneous ^{40}Ar in the age spectra plots from Clearwater East, which is why despite having used a robust isotopic system the age is still is still regarded as a "best estimate" at ~460–470 Ma. A subsequent (U-Th)/He study (Biren et al., 2016) on both East and West yielded results in agreement with Schmieder et al. (2015) of an age for Clearwater West of 280 ± 27 Ma (compare to 286.2 ± 2.6 Ma from Schmieder et al., 2015) and 450 ± 56 Ma for East Clearwater (compare to 460–470 Ma from Schmieder et al., 2015). These combined results confirm that East and West Clearwater did not form at the same time, as further supported by palaeomagnetic studies (the two craters have different remanent magnetisation as measured by Scott et al. (1997) and discussed in Schmieder et al., 2015), stratigraphic considerations (Ordovician clasts have been found in West, but not in East (Schmieder et al., 2015, and references therein), and no meteoritic signature has been detected in Clearwater West, while Clearwater East shows a clear chondritic signature (Palme et al., 1978).

7.3. Ages of terrestrial impact structures through time

The *Impact Earth* database (Appendix A) reveals that the oldest preserved hypervelocity impact structure on Earth is the Yarrabubba impact structure in Australia, which is dated at 2229 ± 5 (Ma (2σ, 0.2%) as determined by U-Pb of monazite and zircon in impact melt rocks (Erickson et al., 2020). Thus, there are no impact structures from the first two-and-a-half billion years of Earth's existence (Fig. 10). The youngest hypervelocity impact structures are the Wabar craters in Saudi Arabia at 290 ± 38 years (luminescence), and suggested to be linked to a fireball in 1863 (Prescott et al., 2004). The youngest impact crater is Carancas, Peru, which was observed to form on 15 September 2007 (0.000014 Ma). The youngest with age determined by isotopic methods is Whitecourt, Canada (<0.0011 Ma (<1.1 ka), determined by ^{14}C of charcoal by Herd et al., 2008).

As mentioned previously, the main reasons to be interested in impact crater ages is to tie them to events in Earth's (and the Solar System's) history. However, there is clear bias in the record of terrestrial impact structures as evidenced by the rather small number found on Earth compared to other planetary bodies. In addition to the challenge of highly precise and accurate geochronology, we are faced with the challenge of Earth being a less-than-ideal laboratory for impact crater preservation due to plate tectonics, water coverage, and burial. This causes substantial difficulties in recognising periodicity or clusters of craters, as well as in associating craters with past events in Earth's climate, biological, and geological evolution.

It is always tempting to think that when craters are spatially related (i.e., formed close together) that they are temporally related as well; however, as discussed above in the case of ~28 km apart Clearwater East and Clearwater West structures such assumptions are frequently unfounded. Similarly, the Suvasvesi North and South structures, which are located ~7 km from each other, formed at least 630 Myrs apart (Schmieder et al., 2016). The Lockne and Målingen impacts on the other hand (~16 km apart) appear to have a strong case for being a doublet both having formed in the same biostratigraphic zone and with neither preserving ejecta from the other (Ormö et al., 2014). Discussions of the merits of several potential crater doublets (two craters formed by impact of a binary asteroid) is discussed in Miljković et al. (2013) and Schmieder et al. (2015).

Going beyond the possibility of crater doublets (two forming simultaneously), we can look at more spread out clusters, potentially related to multiple impacts over several million years by a family of asteroids. The most prominent such clustering are the 22 impact structures which formed during the Ordovician (~485 to ~443 Ma) (Fig. 10). Also associated with such a spike are the fossil meteorites found in Sweden (Schmitz et al., 2001), and an impact breccia in Estonia (Alwmark et al., 2010), many of which have yielded an impactor signature associated with an L-chondrite source. This cluster of impacts and meteorites has been explained as being due to the impact disruption of the L chondrite parent body resulting in an enhanced flux of asteroids to Earth during the following 30 Myr (Schmitz et al., 2001). Lagain et al. (2022) recently challenged this idea and instead ascribe this as a preservation bias in the rock record. A late Eocene (~38 to ~35 Ma) cluster of four impact structures coupled with extraterrestrial geochemical signatures at the Eocene-Oligocene boundary supports a clustered bombardment of Earth at that time also (Schmieder and Kring (2020) and references therein). Conversely, improved geochronology has recently "unchained" several impacts (Lake Saint Martin, Manicouagan, Obolon, Red Wing, and Rochechouart; Appendix A) once suggested to represent an impact spike in the late Triassic (~214 Ma; Spray et al., 1998).

Another significant discussion over the past ~40 years is the possibility of periodicity in the impact cratering record. Raup and Sepkoski (1984) first suggested the possibility after observing a periodic pattern of mass extinctions in during the Phanerozoic with a mean interval of 26 Myrs. Subsequent research found similar repetitive pattern of large impacts, and hypothesized that the extinctions and the impacts may be linked (e.g., Alvarez and Muller, 1984; Rampino et al., 2002; Rampino and Caldeira, 2015). However those results were based largely on crater ages that have since been refined, and other researchers have questioned the validity of the periodicity hypothesis (e.g., Bailer-Jones, 2011; Baksi, 1990; Grieve et al., 1985, 1988; Heisler and Tremaine, 1989; MacLeod, 1998). Most recently, Meier and Holm-Alwmark (2017) conducted a circular spectral analysis of terrestrial hypervelocity impact craters over the last 260 Myrs, and, in contrast to the findings of Rampino and Caldeira (2015), found no evidence for periodicity in the impact record. The main difference between the two studies is the accuracy and precision of ages used. The former used only those with precision <2%, while the latter used those with precision <10%, further emphasizing the need for improvement in the precision and accuracy of impact-related ages.

Thus far, the only convincing case of hypervelocity impact as a driver of mass extinction remains the Chicxulub impact structure, which has been linked to the end-Cretaceous mass extinction by $^{40}Ar/^{39}Ar$ and U-Pb geochronology, stratigraphy, micro-paleaontology, and geochemistry (e.g., Hildebrand et al., 1991; Schulte et al., 2010; Swisher et al., 1992).

In summary, there is an urgent need to improve the precision and accuracy of impact crater ages, which has been substantially addressed over the last decade (~80 new/refined ages for impact structures in the last 10 years), but most ages still remain poorly refined and too imprecise to confidently correlate with other events in Earth's past. Based on the current record, synchronous multiple impacts on Earth are rare, with no robust evidence for a large multiple impact event; although Miljković et al. (2013) point out that impacts by doublet asteroids might be

disguised as apparent single circular craters or elongate craters, rather than two separate structures. Excitingly, geochronology has now reached a precision level capable of resolving crater cooling history (e.g., Kenny et al., 2019; Timms et al., 2020), opening the door to empirical measurements of duration of hydrothermal activity and crater temperature-time curves.

8. Crater diameter

One of the most fundamental parameters of a crater is its diameter. Unfortunately, this is one of the more difficult metrics to determine for craters on Earth, due to variations in their preservation state (see Section 6). On other planetary bodies, the question is much simpler, as the result of their better state of preservation. In the planetary case, the diameter of a crater can be defined and determined by measuring of the diameter of the topographic rim that rises above the pre-impact target surface. This metric is referred to as the "rim diameter" or "final crater diameter" (Turtle et al., 2005) (Figs. 3a,b). As noted earlier, in simple craters, this topographic rim represents a modified version of the original transient cavity rim. In complex craters, however, the inward collapse of the transient cavity walls during the modification stage of crater formation results in a crater structure significantly larger than the original transient cavity (Kenkmann et al., 2012; Melosh and Ivanov, 1999). In this case, the topographic rim typically corresponds to one of the largest fault scarps in the terraced crater rim region (Fig. 4b). For non-elliptical craters, the fastest and preferred method is to use a software package that allows the user to draw a best-fit circle aligned with the crater rim. Studies have shown that this provides estimates with less than ~10% variation from person-to-person (Robbins and Hynek, 2013; Tornabene et al., 2018). It is this diameter that is typically quoted in numerical modeling studies.

On Earth, such pristine craters are rare (see Section 6). In their detailed study of the eroded Brent crater, Canada, Grieve and Cintala (1981), referred to the rim or final crater diameter as the "pre-erosional rim crest diameter". These authors, together with Grieve et al. (1981) also introduced the term "apparent diameter", where this is "the final crater is that produced after all impact-related modification has ceased" and is "measured at or from the original ground surface". The Brent crater is the most intensively drilled simple terrestrial impact crater and, thus, represents an excellent case study for determining diameter. Grieve and Cintala (1981) record the present diameter as 3.0 km, the pre-erosional rim crest diameter as 3.8 km, and the pre-erosional diameter at the original ground surface as 3.4 km. It is the latter that the authors originally defined as the apparent crater diameter. Turtle et al. (2005) defined "apparent crater diameter" of complex craters as "the diameter of the outermost ring of (semi-) continuous concentric normal faults, measured with respect to the pre-impact surface (i.e., accounting for the amount of erosion that has occurred)." In practice, it is very difficult, and likely close to impossible, to accurately estimate the amount of erosion due to local variations in climatical and geological properties at a crater. Even if regional estimates are well known, a precise and accurate age for the impact is required – which is often not the case (see Section 6) – and differential erosion of topographically high crater rims may be significantly different that regional estimates. Indeed, in practice, the apparent crater diameter for complex craters has morphed into the diameter measured at the present day surface.

In this study, we, thus, define *apparent crater diameter* as the *diameter of the outermost ring of (semi-) continuous concentric normal faults at the present-day erosional surface*. For most complex impact structures in the *Impact Earth Database*, this is the only value known. This requires detailed field mapping and/or reflection seismic surveys to delineate faults. For an example of a well-constrained apparent crater diameter and a robust estimate for the rim diameter, the Haughton impact structure, Canada, provides an excellent case study. Due to its relatively young age, it is well-preserved, and, additionally, it is well exposed due to the prevailing polar desert environment. This made it possible to conduct a detailed field mapping campaign that resulted in the production of a detailed 1:25,000 scale geological map that represents the most detailed, complete geological map of a crater of this size (Osinski, 2005); other detailed maps are available but typically only for central uplifts (e.g., Kenkmann et al., 2017; Scherler et al., 2006; Wilshire et al., 1972; Wilson and Stearns, 1968). This mapping documented concentric faults with strike lengths of several kilometers out to a radial distance of 12 km in the north, west, and south, and 11 km in the east of the structure, resulting in the value of 23 km for the apparent crater diameter for Haughton (Osinski and Spray, 2005). The presence of concentric faults out to 12 km is also confirmed in the single seismic reflection profile through the northwest of the structure (Scott and Hajnal, 1988). This agreement between field mapping and seismic investigations provides a reasonable level of certainty for determining apparent crater diameter for craters, where only the latter is available.

What about the rim diameter for Haughton? While the original morphology of the rim region has largely been lost, there is a topographic depression with a diameter of ~16 km, which represents one of the earliest estimates for the diameter of Haughton (Frisch and Thorsteinsson, 1978). Importantly, detailed mapping revealed that the outer limit of this depression at ~8 km radius is marked by a semi-continuous line of concentric listric normal faults that record large-scale (up to 400 m) displacements of slump blocks in towards the crater center (Osinski and Spray, 2005). While normal faults are present further out, as noted above, displacements are rarely >50 m such that, in the newly formed Haughton crater, the outermost concentric faults would likely have been concealed by ejecta. Thus, drawing comparisons to fresh complex craters on other planetary bodies, this semi-continuous line of large-displacement concentric listric normal faults provides a robust estimate of the rim diameter of Haughton at 16 km (Osinski et al., 2005a). Thus, the rim diameter is significantly smaller than the apparent crater diameter of 23 km.

Unfortunately, for most complex craters on Earth, such detailed field maps and/or seismic surveys are not available and so it is not possible to determine the location of the outermost ring of (semi-) continuous concentric normal faults. Mapping faults in the field is also inherently much harder in craters formed in crystalline bedrock that lacks stratigraphic markers. In some cases, the mapping of fractures and lineaments from satellite images has proven to be an effective approach for estimating apparent crater diameter, particularly in glaciated terrains (Mader et al., 2013; Smith et al., 1999).

An alternative approach to determine the apparent diameter of a crater based on shatter cone distributions was provided by Osinski and Ferrière (2016), who defined the relationship $D_{sc} = 0.4\ D_a$, where D_{sc} is the maximum spatial extent of *in situ* shatter cones and D_a is apparent crater diameter. This relationship was derived from the detailed outcrop-scale mapping of the Haughton and Tunnunik impact structures, where both D_{sc} and D_a were determined to within a few hundred metres. As central uplifts, which contain shatter cones *in situ*, are typically the last structural feature left remaining/exposed, this relationship is useful for placing a constraint – typically a minimum value – on the diameter of deeply eroded craters of similar size (i.e., 10s km diameter). Indeed, using this knowledge, Osinski and Ferrière (2016) were able to provide revised estimates for the diameters of several eroded craters, which is reflected in the *Impact Earth Database* (Appendix A): Charlevoix (70 km), Gosses Bluff (32 km), Keurusselkä (36 km), Luizi (15 km), Presqu'ile (15 km), Rochechouart (32 km), Sierra Madera (20 km), and Siljan (75 km) impact structures. It should be noted that this approach is only likely appropriate for structures similar in morphology and morphometry to Haughton and Tunnunik.

Finally, it should be noted that the above discussion about crater diameter is applicable only for impacts on land. As Dypvik and Jansa (2003) note, the lack of a continuous elevated rim – due to the return or "resurge" of water into the newly formed crater – is a conspicuous feature of shallow and deeper marine impacts. In addition, many hypervelocity impact craters in the marine environment display a

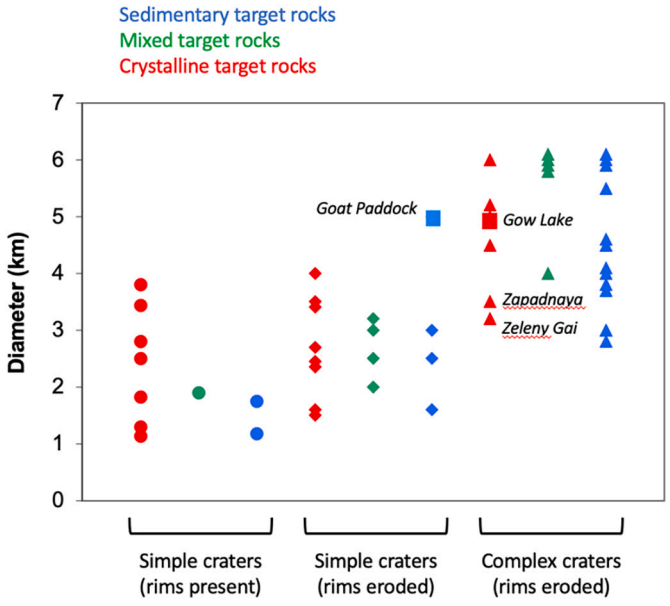

Fig. 11. Comparing the sizes of simple and complex craters in sedimentary versus crystalline targets.

morphology (see Section 9 below) that is commonly referred to as an "inverted sombrero" (Powars and Bruce, 1999). Both of these attributes makes the determination of crater diameter difficult for hypervelocity marine hypervelocity impact craters.

9. Crater morphology and morphometry

On the Moon, and since confirmed on other terrestrial planetary bodies, there is a well-known progression in morphology with increasing crater size, from simple bowl-shaped craters, modified so-called transitional craters, to complex craters with central uplifts whose morphology also changes with increasing diameter (Fig. 3) (see Section 3). It is typically assumed that this same progression in morphology and morphometry with increasing diameter should occur on Earth. In this section, we explore the terrestrial impact record to ascertain whether this is the case.

9.1. Revisiting the simple-to-complex transition on Earth

It is widely cited that the transition from simple to complex craters on Earth occurs at a smaller diameter in sedimentary (2 km) than in crystalline targets (4 km). This dates back to the work of Dence (1972), who based this observation on a compilation of the 50 known impact structures at that time. The greater number of craters available with the *Impact Earth Database*, makes it clear that the situation is more complex. Fig. 11 provides a plot of all craters in our database between 1 and 6 km in diameter ($n = 50$), grouped into simple craters with rims preserved (i.e., preservation state 1–3), eroded simple craters (i.e., preservation state 4–7), and complex craters, all of which are eroded to some degree.

Based on Fig. 11, it is apparent that the simple-to-complex transition for craters developed in crystalline, sedimentary, and mixed sedimentary-crystalline targets is less clear-cut than reported by Dence (1972) and that this transition occurs over a range of diameters. For crystalline targets, complex structures are observed at sizes of 3.2 km and greater, a smaller transitional diameter than earlier suggested by Dence (1972). However, it should be noted that the two smallest reported complex craters in crystalline targets in Fig. 10 are the Zapadnayav (d = 3.2 km) and Zeleny Gai (d = 3.5 km), both of which are buried and with poorly constrained diameters. The original morphology of these two structures is also difficult to judge from the literature. Furthermore, it is important to note that the present-day morphology of craters can be very deceiving due to erosion. The 5-km diameter Gow Lake impact structure, Canada, is an excellent example (Fig. 12b). This structure is often cited as a prototypical central peak crater; however, the first detailed field mapping of this structure (Osinski et al., 2012b) following its initial description (Thomas and Innes, 1977) reveals that the central island in Gow Lake is capped by, and comprised predominantly of, allochthonous impact melt rocks and breccias such that in its pristine state, no emergent central peak would have been visible. The island, thus, represents inverted topography whereby the coherent impact melt rocks were more resistant to erosion via glacial and fluvial activity than the surrounding fracture target rocks and less coherent impact breccias. The best explanation for Gow Lake is, thus, that it represents a transitional impact structure.

For sedimentary targets, complex structures start to appear at diameters greater than 2.8 km, i.e., larger than reported by Dence (1972). However, the three smallest structures (B.P. Structure, Goyder, and Ouarkziz), are all deeply eroded impact structures (level 5 or 6), such that estimates for their diameters should be treated with caution. If anything, these diameters could be larger than reported. A notable outlier in Fig. 10 for simplex craters in sedimentary targets is the Goat Paddock impact structure, Australia. Early papers suggested that this structure was a simple impact crater (Harms et al., 1980). More recent work by Milton and Macdonald (2005) confirms the lack of a central uplift, but also noted the modification of the crater walls by slumping and the scalloped outline of the crater rim. These authors suggest that Goat Paddock "bridges the two traditional classes of impact crater: simple and complex". In other words, like Gow Lake, Goat Paddock may be a transitional impact structure. In summary, the transition from simple to complex craters is more complicated than previously recognized, with the transition diameter for craters developed in different target rocks being less pronounced than previously reported.

9.2. Nature of complex impact structures on Earth

As discussed in Section 3, fresh complex impact craters on the Moon comprise a centrally uplifted topographic high, surrounded by a low-lying annular region infilled with allochthonous impact breccias and melt rocks (i.e., crater-fill impactites) and, finally, a faulted terraced crater rim (Figs. 3b,c, 4b). In the smallest complex craters on the Moon, the central uplift takes the form of a peak, or closely-spaced cluster of peaks (Fig. 3b). With increasing diameter, a ring appears, forming structures referred to as protobasins or central-peak basins; the disappearance of the peak then signifies the transition to a peak-ring basin (Fig. 3c). It is generally assumed that this same progression occurs for craters on Earth (e.g., Grieve and Pesonen, 1992; Pike, 1985). For example, Grieve and Pesonen (1992) cite examples of central peak craters (Steinheim; Flynn Creek), central-peak basins (Red Wing Creek; Mistastin), and peak-ring basins (West Clearwater; Puchezh-Katunki). However, an analysis of the *Impact Earth* database suggests that the tacit assumption that fresh terrestrial complex craters would have looked like lunar complex craters is complicated at best, and, potentially, incorrect. We outline the rationale for this statement below.

The first observation is that all complex craters on Earth are eroded to some degree and so that current topography may differ from the original morphology. The presence of lakes can be particularly misleading (Fig. 12), as there is a natural tendency to equate the flat surface of a lake to the relatively flat crater floors of lunar craters (Fig. 3), which represents the top of the allochthonous crater-fill impactites. As discussed in the previous section, the Gow impact structure appears at first glance to have a central peak morphology (Fig. 12b) but it is more likely an example of a transitional impact crater. Another example is the West Clearwater Lake impact structure (Fig. 12c). This crater has often been referred to as a peak-ring structure but field mapping reveals that the topographic high points on the ring of islands is predominantly allochthonous impact melt rock and breccia. Thus, while

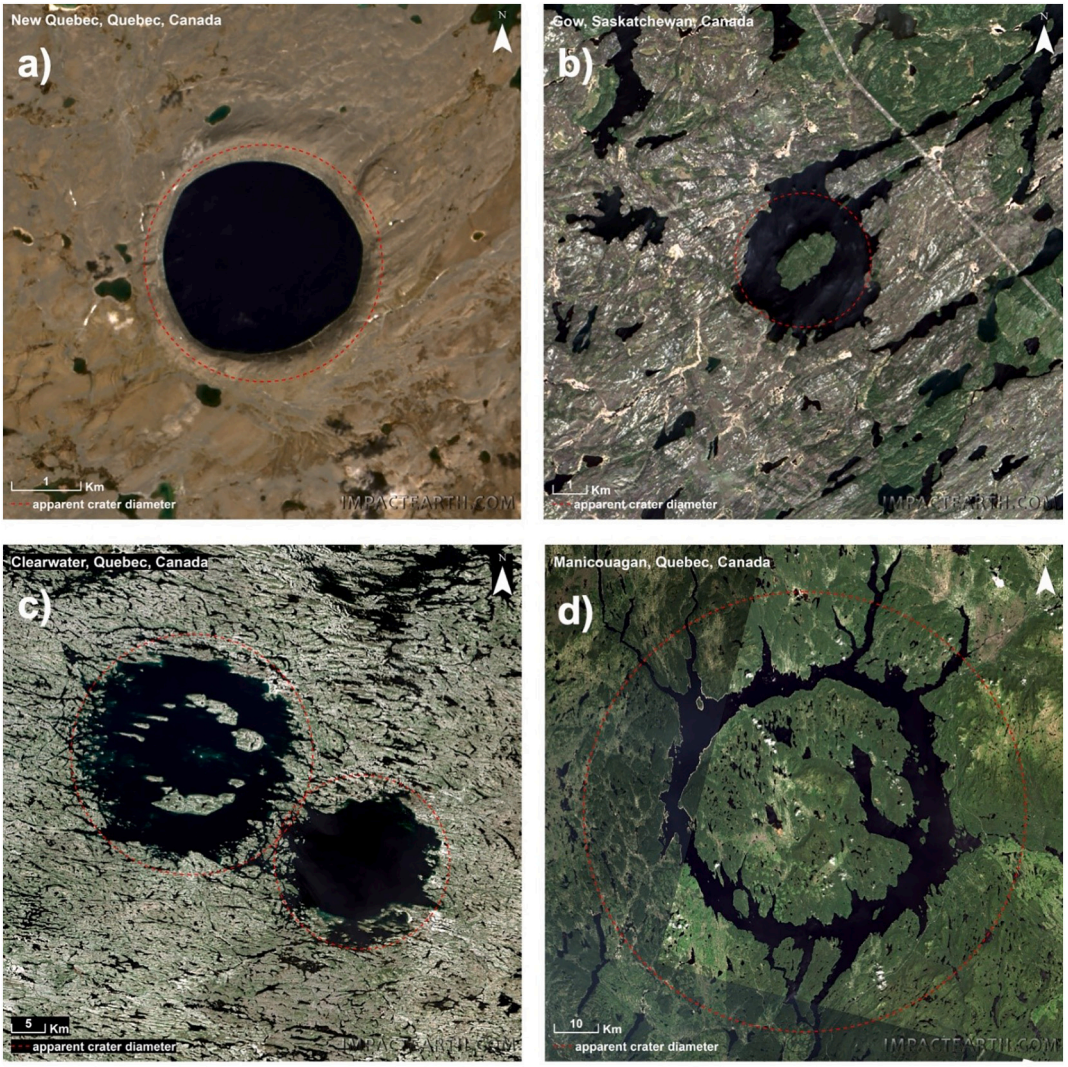

Fig. 12. Satellite images of the Pingualuit (originally called New Quebec) (a), Gow Lake (b), East and West Clearwater Lakes (c), and Manicouagan (d) impact structures. Landsat-8 images courtesy of the U.S. Geological Survey.

there is uplifted bedrock on these islands, it is, or was, typically entirely overlain by allochthonous impact melt rocks and breccias such that a topographic peak-ring emergent through the crater-fill deposits the likes of Schrödinger crater on the Moon (Fig. 3c) would likely not have been present at the time of formation.

This begs the question as to what do fresh complex craters on Earth look like? With this question in mind, in Table 8 we provide details on the nature of the central uplift in all well-preserved (erosion level 1–3) small- to mid-size <30 km diameter non-marine craters (as marine impacts have added complications) for which we could glean enough information from the literature. Several things are apparent from Table 8. First, central uplifts that are unequivocally central peaks are rare. The smallest crater with the most well constrained central peak is the 10.7 km diameter Bosumtwi impact crater in Ghana (Ferrière et al., 2008), which is arguably the best-preserved complex impact structure in crystalline rocks known on Earth, which can be ascribed to its young age of 1.13 ± 0.10 Ma. In the 13 to 18 km in diameter size range, neither the Zhamanshin, Ames, nor Logoisk structures appear to possess central peaks. There are conflicting interpretations for El'gygytgyn, with the potential of a small central peak (Table 8).

In the mid-20 km size range, there are some well-known and well-studied craters that provide important constraints. Based on detailed field mapping and/or geophysical and drill core data it is clear that the 23 km diameter Haughton, 24 km diameter Ries, and 25 km diameter Steen River structures do not possess central peaks. In contrast, the 24 km diameter Boltysh structure and, potentially, the Mistastin Lake structure both do. Erosion does not seem to be a factor as all of these structures are relatively young and well-preserved. The most obvious difference between these craters is the nature of the target rocks. The Haughton, Ries and Steen River structures formed in mixed targets, with ~1.9, 0.5–0.8, and 1.2 km of sedimentary rocks, respectively, overlying crystalline basement; whereas the Boltysh and Mistastin Lake structures formed entirely in crystalline rocks. Thus, a simple explanation is that the presence of sedimentary rocks in the target is responsible for the lack of a central peak. Grieve and Therriault (2004) reached a similar conclusion suggesting "it would appear that the lack of central peaks at Haughton, Ries, and Zhamanshin is most likely an effect of target material" but that the ultimate reason "is a more complex (but yet unknown) function of target and impact characteristics".

Based on a critical review of the *Impact Earth* database, we offer the following explanation: central peaks form in all complex craters during the early part of the modification stage. This is consistent with data, albeit with uncertainty due to erosion, that central peaks are present at the Steinheim and Flynn Creek (not included in Table 8 as erosion level 4) impact craters, which formed entirely in sedimentary targets and that are both ~4 km in diameter (Table 8). In craters formed in sedimentary

Table 8
Nature of the central uplift for relatively well-preserved (erosion level 1–4) non-marine craters <50 km diameter and for which enough information is available in the literature*.

Name	D (km)	T	EL	CP?	Central uplift notes
Steinheim	*3.8*	S	3	Y	The asymmetrical central uplift is ~600–800 m wide and 50 m high (Buchner and Schmieder, 2010; Ernstson, 1984). Jurassic and Triassic strata were uplifted at least 350 m, and possibly as much as 400 m (Buchner and Schmieder, 2010). Unclear as to how much erosion has affected the crater-fill impactites and central uplift.
Kursk	6	M		N	Drilling and geophysical data indicate the presence of a central uplift ~1–2 km in diameter that rises 200 m above the crater floor; it is completely covered by ~200 m of allochthonous crater-fill impactites (Masaitis, 1999).
Beyenchime-Salaatin	*8*	S	3	N	The crater interior comprises a "flat depression" with "isolated hills" of allochthonous crater-fill impactites (Masaitis, 1999). There is no evidence for a central uplift.
Bosumtwi	*10.5*	C	2	Y	Central peak ~1.8 km diameter and a maximum height of 120 m above the top of the allochthonous crater-fill impactites imaged in seismic reflection data (Karp et al., 2002; Scholz et al., 2002). Central uplift not exposed but drill core data indicates at that one location ~25 m of lithic and melt-bearing breccias drape over the central peak (Koeberl et al., 2007).
Zhamanshin	*13*	M	3	N	Geophysical data suggests the presence of a central uplift ~1 km across and ~ 250 m above the crater floor that is completely overlain by allochthonous crater-fill impactites (Masaitis, 1999).
Ames	16	M	2	N	Data from drill cores and geophysics indicates the presence of a 5 km diameter central uplift that is described as "collapsed" or "eroded" (Koeberl et al., 2001); this rises ~60 m above the floor of the annular depression.
Logoisk	17	M	3/4	N	Drilling indicates the presence of a central uplift comprising brecciated Precambrian gneisses. From the cross section in Veretennikov (2010) the central uplift appears to be completely covered by allochthonous crater-fill impactites and so does not appear to be emergent. In contrast, a cross-section in Masaitis (1999) suggests the presence of a small central peak.
El'gygytgyn	*18*	C	3	N	Conflicting evidence for presence of a small central peak. Based on gravity measurements, Dabizha and Feldman (1982) proposed the presence of an ~2 km wide central peak buried beneath post-impact sediments. Other workers suggest instead that the central uplift comprises a "ring structure" 7–7.5 km diameter composed of parautochthonous bedrock, which is brecciated in places and entirely covered by ~100 m of allochthonous crater-fill breccias, which thicken to ~400 m in the surrounding basin (Gebhardt et al., 2006).
Haughton	23	M	2	N	No evidence for a central peak. Field mapping indicates that the central uplift was originally completely covered with allochthonous crater-fill impactites and comprises 3 distinct zones (Osinski and Spray, 2005): a ~ 2 km diameter central region of isolated, differentially uplifted, megablocks of variable orientation; a surrounding region pf several large km-size fault-bounded blocks with gentle dips; a zone of (sub-) vertical and/or overturned strata at a radial distance of ~5.0–6.5 km.
Boltysh	24	C	2	Y	Geophysics and drill cores indicate a topographic central peak emerges from the surrounding allochthonous crater-fill breccias (Grieve et al., 1987). The central uplift is ~3.8 km wide and emerges by ~100–200 m above the top of the allochthonous crater-fill impactites (Gurov et al., 2006); impact melt-bearing breccias drape part of the central peak.
Steen River	25	M	3	N	Geophysics and drill cores indicate that the central uplift is ~8 km wide at the base. Precambrian basement is uplifted by up to 1.7 km above regional levels (MacLagan et al., 2018). The central uplift is completely covered by crater-fill impactites.
Mistastin	28	C	3	Y	Horseshoe Island in the centre of Mistastin Lake appears to have very little erosion consistent with an estimate of 10 to 100 m erosion of melt rocks in the inner rim region of the structure (Marion, 2009). This suggests that the island is an original topographic high. Most of the island is shocked target rocks with one small outcrop of impact melt rocks, interpreted as a veneer (Singleton et al., 2011).
Ries	*24*	M	2	N	The centre of the structure comprises a flat-floored central basin (depth ~ 0.6–0.7 km) due to uplifted crystalline basement bordered by an inner ring of uplifted basement and sedimentary megablocks (radius 6 km) (Pohl et al., 1977).

* Abbreviations: T: target lithology(C-crystalline, S-sedimentary, M-mixed); E: erosion level; CP: central peak. For diameters italicized entries = rim diameter.

rocks or mixed targets with thick sedimentary sequences, as diameter increases, these central peaks are inherently unstable and rapidly collapse downwards and outwards during the final phase of the modification stage. Support for this comes from field mapping at the Haughton impact structure, where there is evidence for the outwards collapse of the central uplift following the initial inward and upwards tectonic deformation (Osinski and Spray, 2005), and numerical models (Collins et al., 2008). In craters formed in crystalline rocks, these central peaks are more stable because of the greater strength of the target rocks and, more importantly, the absence of layering, which provides pre-existing planes of weakness that aids outwards collapse.

At larger diameters, the cratering record is so incomplete that less can be said about morphology. At some point, however, a transition to

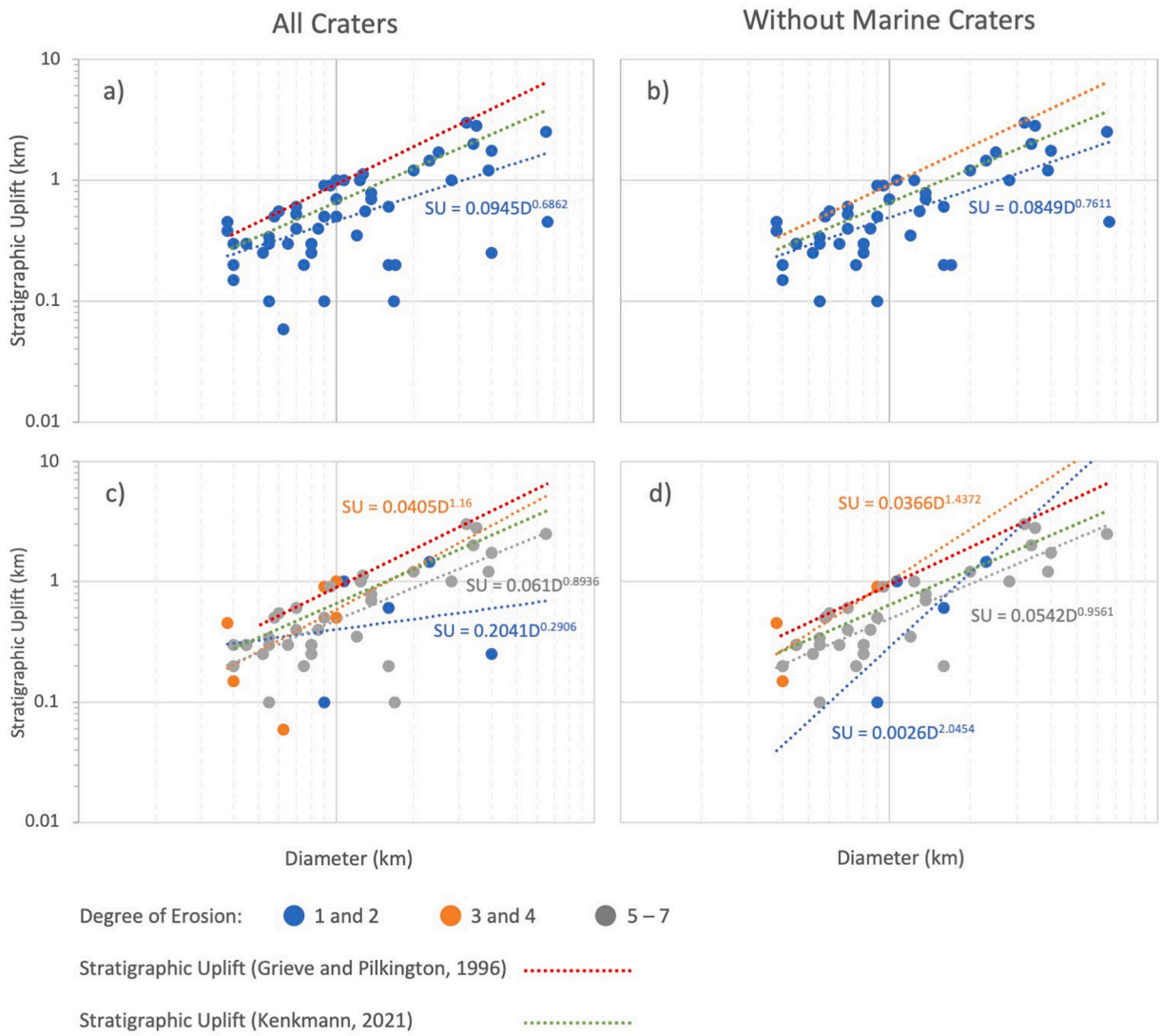

Fig. 13. Plots of stratigraphic uplift (SU) versus apparent crater diameter. a) Plot with all craters and a comparison to previous estimates of SU by Grieve and Pilkington (1996) (red dotted line) and Kenkmann (2021) (green dotted line). b) Plot with marine craters removed. c) Plot with all craters divided into 3 groups based on degree of erosion. d) A similar plot as c) but with marine craters removed. (For interpretation of the references to colour in this figure legend, the reader is referred to the web version of this article.)

the peak-ring morphology should theoretically occur. A recently published synthesis suggests that the 80 km-diameter Puchezh-Katunki structure possesses neither a central peak or a peak-ring (Masaitis et al., 2020). At the 100 km-diameter Popigai structure, the exposure is very poor in the crater interior. Based on the compilation map of Whitehead et al. (2002), there are a series of outcrops of uplifted basement rocks in the northeast quadrant that, if they continue around the crater under the Quaternary cover, would suggest that Popigai possesses a peak-ring with a diameter of ~45 km. However, these outcrops are juxtaposed with impact melt rocks and impact melt-bearing breccias and, in places, overlain by patches of these same impactites, such that this would likely not have been a very prominent topographic peak-ring if it was, in fact, produced.

If we consider the three largest hypervelocity impact craters on Earth (Chicxulub, Sudbury, and Vredefort), the Chicxulub structure is the best preserved one and preserves an unambiguous peak-ring (Morgan et al., 2016). It is, however, notable that although the peak-ring in the Schrödinger Crater on the Moon (Fig. 2c) rises up to 2.5 km above the basin floor (Kring et al., 2016), seismic reflection data indicates that Chicxulub's peak ring had as little as ~0.2 km,and a maximum of ~0.6 km, of relief before being buried by post-impact sedimentary rocks (Gulick et al., 2008; Morgan et al., 2000). There is substantial evidence that Sudbury also possesses a peak-ring (Grieve and Osinski, 2020), although little can be said about its original morphology and morphometry due to substantial post-impact deformation and erosion. The nature of the central area at the Vredefort impact structure is unknown, because of the substantial (~10 km) of erosion of the structure.

In summary, it appears that the lunar record may be misleading when it comes to reconstructing the morphology of fresh complex craters on Earth. The central uplifts of terrestrial complex impact craters are on the whole, more subdued in their morphology and morphometry. One reason for this difference appears to be the nature of target rocks. As discussed above, mid-sized complex craters in sedimentary or mixed sedimentary–crystalline target rocks (e.g., Haughton, Ries, Steen River) lack central peaks, in contrast to craters in crystalline targets that do (e.g., Boltysh, Mistastin Lake). However, even those craters in crystalline target rocks on Earth that did form central peaks, it is notable that the peaks do not reach the multi-km heights above crater-fill deposits that their lunar counterparts do. In other words, the central peaks, even in the instances where they did form on Earth, were never as high in the first place. The same is true for peak-ring structures as discussed above. We suggest that this is due to two main factors: higher gravity on Earth,

Table 9
Summary of the different types of impactites and their setting in terrestrial impact structures.

	Setting						Impactite type			
	Rim	Floor	Uplift	Crater-fill	Dykes	Ejecta	Shocked rocks	Lithic impact breccias	Impact melt-bearing breccias	Impact melt rocks
Autochthonous impactites	X	X					X			
Parautochthonous impactites		X	X				X	X		
Allochthonous impactites				X	X	X	X	X	X	X

which means that less vertical topography is possible, and the fact that topography is more likely to be "hidden" by crater-fill allochthonous impactites, due to differential scaling and less cratering efficiency for a given size (Grieve and Cintala, 1992). The added complication is that immediately upon formation, terrestrial craters are subject to endogenic erosion processes that can modify topography, not only reducing relief, but also accenting it, particularly in glaciated terrains, as glaciation does not necessarily strive to form an "equipotential" topographic surface (e.g., observe the Gow Lake, East and West Clearwater, and Manicouagan impact structures in Figs. 12b–d).

9.3. Stratigraphic uplift in complex impact structures

Notwithstanding the discussion in the previous section regarding ambiguities surrounding the original morphology of complex craters on Earth, it is clear that rocks in the centre of such craters are uplifted above their pre-impact stratigraphic level. This was recognized early on in the study of terrestrial craters and led to the definition of stratigraphic uplift (SU) "as the observed amount of uplift undergone by the deepest marker horizon now exposed in the center of a complex structure" (Grieve et al., 1981). A prediction of SU for craters of a certain diameter is an incredibly useful metric as it can potentially provide important information about the subsurface of planetary bodies where the only available information comes from satellite observations; although the effect of differences in gravity has yet to be determined. Based on data from 15 complex impact structures at the time, Grieve et al. (1981) defined the relationship $SU = 0.06D^{1.1}$. This was later updated to $SU = 0.086D^{1.03}$ in Grieve and Pilkington (1996), based on data from 24 structures. Kenkmann (2021) recently provided the relationship $SU = 0.069D^{0.96}$, which is slightly lower than the previous values.

Our analysis of the *Impact Earth Database* is presented in Fig. 13 and yields a $SU = 0.0945D^{0.6862}$ (Fig. 13a) based on 53 complex impact structures. This is lower still than the three previous estimates cited above; however, it is clear that there is considerable scatter (Fig. 13a). We considered several possible explanations for this result. First, it has been discussed elsewhere (e.g., Sections 8, 10.3.) that craters formed in marine environments undergo rapid modification by seawater that can immediately change their morphology. This might be expected to affect SU significantly, but Fig. 13b shows that removing marine craters does not have a pronounced effect.

A second major aspect that previous equations for SU did not take into account is the level of erosion. As noted above, SU is defined as the amount of uplift undergone by the deepest marker horizon exposed at the present-day (Grieve et al., 1981). Given our understanding of central uplifts – which is that, overall, the most deep-seated rocks are present in the very centre in a fresh crater (Kenkmann et al., 2014) – it stands to reason that erosion should have the effect of lowering SU through time. Given this, it would be expected that a plot of SU versus diameter with craters grouped based on degree of erosion (see Section 6, Table 6) would yield the highest value of SU for fresh relatively uneroded craters. However, Fig. 13c and d show that this is not the case. Considering only the best-preserved craters (i.e., degree of erosion 1 and 2), the estimate of SU is even lower, with two well-preserved craters (Mjolnir and Ragozinka) displaying anomalously low values of SU; however, there are only 5 datapoints. Curiously, the equation for SU based on the *Impact Earth Database* that is most similar to previous estimates comes from plotting the 7 craters with degree of erosion 3 and 4.

In summary, if all craters for which a value of SU from the literature is provided are considered – as was done in previous studies – then the *Impact Earth Database* yields a $SU = 0.0945D^{0.6862}$ (Fig. 13a) based on 53 complex impact structures. This is lower than the previous estimates of Grieve et al. (1981), Grieve and Pilkington (1996), and Kenkmann (2021). However, given the dependency of SU on both an accurate estimate of diameter – which is difficult for most complex impact structures (see Section 8) – and the determination of which rocks are exposed in the centre of a structure – which requires a good understanding of the pre-impact target stratigraphy and accurate geological mapping – we urge caution in the application of the above equation for determining SU. It is also notable that numerical models of terrestrial craters consistently overestimate the amount of SU (e.g., Collins et al., 2008). Clearly, this is a topic that deserves further research.

10. Impactites

One of the most distinctive features of terrestrial hypervelocity impact craters is the diverse array of rocks, termed *impactites*, which are produced. The term *impactite* was first suggested by Dr. H. B. Stenzel, as reported in Barnes (1940), and was originally applied solely to tektites. Nininger (1954) recognized that products other than silica glass are produced during hypervelocity impact and so broadened its use. The current definition of impactite is "all rocks affected by one or more hypervelocity impact(s) resulting from collision(s) of planetary bodies" (Stöffler and Grieve, 2007). Impactites can be classified based on two main approaches: (1) their textural characteristics, irrespective of setting, as *shocked rocks*, *impact breccias* or *impact melt rocks* (Stöffler and Grieve, 2007) (Table 9); and (2) the extent to which they have been moved from their original pre-impact location, as *autochthonous*, *parautochthonous* or *allochthonous* impactites, which can be further subdivided based on the setting in which they occur (Table 9). Unfortunately, there is no consistent terminology for impactites and the report by Stöffler and Grieve (2007) remains a "recommendation". Many workers have also pointed out issues with this existing terminology, particularly for melt-bearing impactites (Grieve and Therriault, 2012; Osinski et al., 2016), and further complications arise for impact craters formed in marine environments, where impactites can be rapidly eroded by resurgent waters and redeposited, resulting in mixtures of sedimentary and impact-related material (King et al., 2006; Ormö et al., 2006). Below we provide a synthesis of the main characteristics of impactites and their spatial distribution in terrestrial hypervelocity impact craters based on the *Impact Earth* database. Impactites in marine craters are discussed separately in Section 10.3.

10.1. Impactites based on textural characteristics

10.1.1. Shocked rocks

Shocked rocks are defined "as non-brecciated rocks, which show unequivocal effects of shock metamorphism, exclusive of whole rock melting" (Stöffler and Grieve, 2007). Unequivocal effects of shock metamorphism are discussed in Section 4.2. and presented in Table 2. They are subclassified according to the progressive stages, or Shock

Fig. 14. Field photographs of impact breccias. (a) Mostly monomict lithic impact breccia from the crater-fill deposits of the West Clearwater Lake impact structure. 35 cm long rock hammer for scale. (b) Polymict impact breccia that ranges from lithic to melt-poor. This represents the continuous ejecta blanket at the Mistastin Lake impact structure. Apple Pencil for scale. (c) Impact melt-poor impact breccias from the continuous ejecta blanket of Meteor Crater. Swiss army knife for scale. (d) Impact melt-bearing breccia in proximal ejecta from the Ries impact structure, Germany. Finger for scale. (e) Impact melt-bearing breccia in a dyke intruded into the crater floor of the Mistastin Lake impact structure. 7 cm wide lens cap for scale. (f) Impact melt-bearing breccia underlying the crater-fill impact melt sheet at the West Clearwater Lake impact structure. Image is 35 cm across.

Stages, of recorded shock metamorphism depending on their lithology (Stöffler et al., 2018). However, this definition for shocked rocks is actually at odds with the definition of impactites – which includes all rocks "affected by one or more hypervelocity impact(s)" – and the definition for Shock Stage 0 – which is "unshocked (no unequivocal shock effects)" (Stöffler and Grieve, 2007). This becomes important for rocks shocked to low shock levels, such as crater rims, where shock pressures were not sufficient to produce any unequivocal shock effects. Shocked rocks may occur *in situ* in the crater floor and rims of simple impact structures and as clasts in impact breccias (Fig. 14) and impact melt rocks (Fig. 15) (Table 9).

10.1.2. Impact breccias

Impact breccias are typically classified as either *lithic* (also referred to in the literature as fragmental or clastic) or *melt-bearing* (Stöffler and Grieve, 2007), with the latter also commonly being referred to as "suevite". Impact breccias can also be polymict or monomict and have clast sizes ranging from 100 s m to millimetres (Fig. 14). *Lithic impact breccias* contain lithic and mineral clasts, in a matrix comprised of the same, but finer-grained material (Fig. 14a). These melt-free impact breccias are the most abundant, occurring in 131 of the 188 hypervelocity impact craters on Earth; this includes most marine craters, where the impactites are also sometimes referred to as resurge breccias (Dypvik and Jansa, 2003). *Impact melt-bearing breccias* contain angular to amoeboid bodies of impact melt – quenched to glass – as clasts and in the matrix, in addition to lithic and mineral clasts (Grieve and Therriault, 2012) (Figs. 14b–f). (Because the glass can often be altered to secondary phases, such as clays, the term "melt-bearing breccia" is preferred, even though the melt is no longer molten.) These impactites occur in 79 hypervelocity impact structures (Appendix A). Impact melt-bearing breccias have been the subject of debate for many years (see Osinski et al., 2016, and references therein). Since their discovery, impact melt-bearing breccias have, in many cases, been referred to as "suevites" – based on the local name for such a rock at the Ries impact structure, Germany (Engelhardt, 1997) – and also "suevitic breccias" or "suevitic impact breccias" (e.g., Stöffler et al., 2018) and this blanket term has

Fig. 15. Field photographs of impact melt rocks. (a) Clast-rich impact melt rocks at the base of the crater-fill deposits at the West Clearwater Lake impact structure. 35 cm long rock hammer for scale (lower left). (b) Clast-rich impact melt rocks at the Haughton impact structure. 35 cm long rock hammer for scale. (c) Vesicular impact melt rocks at the Mistastin Lake impact structure. GPS for scale. (d) Coarse-grained impact melt rocks from the Sudbury Igneous Complex. Pencil for scale. (e) Columnar-jointed impact melt rocks in the proximal ejecta of the Mistastin Lake impact structure. The vertical section of the cliff is ~80 m high. (f) Dyke of impact melt (green) intruded into the crater floor of the Sudbury impact structure. White scale card in centre of image. (For interpretation of the references to colour in this figure legend, the reader is referred to the web version of this article.)

been applied to diverse impactites in different settings at a large number of impact structures (Dressler and Reimold, 2001; Masaitis, 1999). As lithological classification usually implies rocks with the same origin, this has hampered the understanding and classification of melt-bearing breccias, in general and specific occurrences, in particular (Grieve et al., 1977; Grieve and Therriault, 2012). It has, therefore, been recommended that the term "suevite" be reserved for the original "type" occurrence at the Ries impact structure (Grieve and Therriault, 2012; Osinski et al., 2016, 2020a). An additional complication to the understanding of melt-bearing breccias is that there is likely a continuum from melt-free lithic impact breccia to impact melt rock (see next section) endmembers, with impact melt-bearing breccias representing much of continuum. Current classification schemes do not currently account for this.

10.1.3. Impact melt rocks

Impact melt rocks form by adiabatic decompression from a high shocked compressed state, resulting in superheated conditions and can contain abundant rock and mineral clasts (Dence, 1971; Osinski et al., 2018). This is in contrast to endogenic igneous rocks, which form by flux melting or adiabatic decompression from depth, producing partial melting under liquidus temperature conditions, in specific geodynamical environments and without rock and mineral clasts (Osinski et al., 2018). Impact melt rocks can be subdivided into clast-rich (e.g., Figs. 14a,b), clast-poor (Fig. 14c), or clast-free (Fig. 14d) (Stöffler and Grieve, 2007). They can be further sub-classified based on the degree of crystallinity as glassy, hypocrystalline, or holocrystalline, and according to the groundmass texture as aphanitic, phaneritic, vesicular or particulate (Osinski et al., 2008a). Impact melt rocks have been documented in approximately one-third (57) of terrestrial hypervelocity impact craters (Appendix A).

Impact melt rocks share many textural similarities with volcanic rocks, both in outcrop and under the microscope (Fig. 15), with characteristic features such as columnar joints (Fig. 15e) and vesicles (Fig. 15d) being common. Such similarities offer a partial explanation for the original interpretation of many complex impact structures as

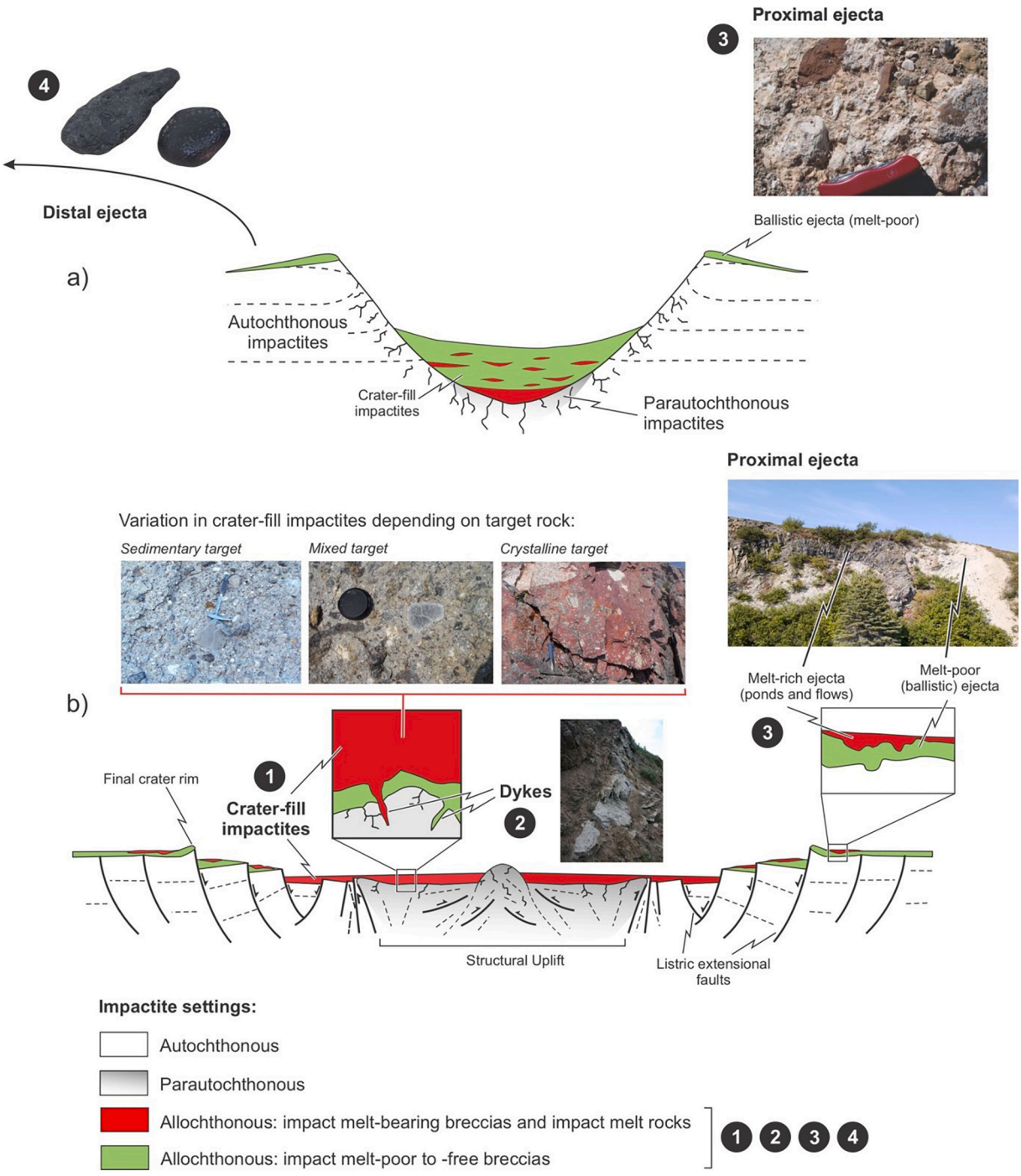

Fig. 16. Schematic cross sections of simple (a) and complex (b) craters showing the 3 different settings of impactites. Autochthonous impactites make up the crater rim and part of the crater floor of both simple and complex craters. Parautochthonous impactites are restricted to a small region in the centre of the crater floor in simple impact craters, whereas in complex craters they constitute the central uplift. Allochthonous impactites are present in four main settings in both simple and complex craters: 1) crater-fill impactites; 2) dykes; 3) proximal ejecta; and 4) distal ejecta (tektites shown).

cryptovolcanic structures (see Section 4.1). As with melt-bearing breccias, lithological terms defined at specific impact craters, such as dellenite, kärnäite, and tagamite, and more general terms, such "impact melt breccia" – which is more accurately "clast-rich impact melt rock" – have been used to describe terrestrial impact melt rocks in the literature. These terms should be avoided as they are impractical and have led to misuse and confusion in the literature (Osinski et al., 2008a; Reimold and Gibson, 2005).

Once thought to be absent in impact structures formed in predominantly sedimentary targets, it is now clear that impact melt-bearing breccias (Section 10.1.2) and impact melt rocks are generated during such impacts (Osinski et al., 2008b). What is clear, however, is that the products are different in their appearance and characteristics, with impact melt rocks in sedimentary target rocks being typically more clast-rich and unusual in colour (Fig. 15b). The demonstration that melt is produced irrespective of target lithology is consistent with thermodynamic numerical models that indicate that as much, or more, melt should be produced in sedimentary compared to crystalline target rocks (Kieffer and Simonds, 1980; Wünnemann et al., 2008).

10.2. Impactites based on setting

10.2.1. Autochthonous impactites

Autochthonous (also referred to as authigenic in the literature) impactites refer to impactites formed in their present location and that have undergone no transport during crater excavation. They comprise crater rims, in both simple and complex impact structures (Fig. 16) (Table 9), can be faulted and fractured, but they retain their pre-impact stratigraphic relations to surrounding rocks (Grieve and Therriault, 2012). As noted above, there are some contradictions in the literature about the definition of impactites, but autochthonous impactites comprise *shocked rocks* but that lack any unequivocal shock effects.

10.2.2. Parautochthonous impactites

Impactites that have been transported by the cratering flow field but that appear to be "in place" are termed *parautochthonous* (Stöffler and Grieve, 2007). They are intermediate between *autochthonous* (see above) and *allochthonous* (see next section) impactites. Parautochthonous impactites comprise the floors of simple and complex impact craters (Figs. 16a, b), and the central uplifts of complex craters (Fig. 16b) (Table 9) (Grieve and Therriault, 2012). Indeed, despite significant displacement during the modification stage of crater formation, reaching many km in large complex impact craters, parautochthonous impactites in central uplifts retain their broad pre-impact stratigraphic relationships to surrounding rocks (Kenkmann et al., 2014). Notwithstanding the above noted issues in terminology, parautochthonous impactites comprise *shocked rocks* or poorly sorted monomict *impact breccias* with angular clasts (Grieve and Therriault, 2012). The *Impact Earth* Database shows that shock effects are common in parautochthonous impactites (Appendix A), in particular central uplifts, with shatter cones and PDFs in quartz being common (e.g., Fig. 5b).

10.2.3. Allochthonous impactites

Allochthonous (also referred to as allogenic in the literature) impactites are those formed elsewhere and subsequently transported to their current location. They are by far the most variable and varied impactites in terms of both lithological character and setting. They can be found in four settings in both simple and complex craters (Fig. 16) (Table 9): (1) as crater-fill deposits in the crater interior, (2) as injection dykes in the crater floor, (3) as proximal ejecta deposits, and (4) as distal ejecta deposits.

Crater-fill impactites: Approximately three quarters of hypervelocity impact craters on Earth preserve some portion of their crater-fill impactites (Appendix A). Crater-fill impactites cover up to half of the rim to floor depth in simple craters (Melosh, 1989) (Fig. 16). In complex craters, their thickness increases with the size of the crater (Fig. 15), ranging up to an ~5 km thick sequence of impactites at the ~200 km diameter Sudbury impact structure (Dreuse et al., 2010; Therriault et al., 2002). Lithic impact breccias are the most widely documented, occurring in 128 craters, followed by impact melt-bearing breccias (78), and then impact melt rocks (57). Only 35 structures preserve all three of these impactite types. At these sites, there is a general progression upwards from lithic impact breccias, to impact melt-bearing breccias, to impact melt rocks (cf., Dressler and Reimold, 2001; Grieve et al., 1977; Osinski and Grieve, 2012). There are two important points that warrant discussion with respect to impact melt rocks. First, the term "impact melt sheet" is often applied to crater-fill impact melt rocks, with the implication that there is a continuous "sheet" of impact melt rock in the crater interior (cf., fresh lunar craters, e.g., Figs. 3b–d). However, it is apparent from the *Impact Earth* database that only the West Clearwater, Manicouagan, and Sudbury impact structures preserve unambiguous impact melt "sheets". In many craters where a melt sheet would be expected given their size, there is either insufficient data at present to make a conclusive determination (e.g., Chicxulub), or the impact melt rocks occur as lenses intercalated with impact melt-bearing and lithic impact breccias (e.g., Popigai). This leads on to the second important point, which is that impact melt rocks are either lacking entirely, or are volumetrically minor, in craters formed in mixed sedimentary – crystalline targets (e.g., Ries, Steen River). Instead, the crater-fill impactites are dominated by impact melt-bearing breccias. This has been previously noted and is ascribed as being due to the presence of sedimentary rocks in the target rocks (Osinski et al., 2008a); although the exact reason for this remains poorly understood.

Dykes: Dykes of impact melt rocks, impact melt-bearing breccias, lithic impact breccias, and pseudotachylite occur in the crater floor and central uplifts of many hypervelocity impact craters (Fig. 16) (Appendix A). Insight into impact dykes have benefited from studies of partly to deeply eroded impact structures, where, as noted above, they are often the only impactites left preserved. In general, impact dykes are typically less than a few m wide and a few m long (Dressler and Reimold, 2004; Osinski et al., 2018). While various mechanisms have been proposed for the origin and emplacement of dykes in hypervelocity impact craters, they generally fall into two main categories. Most impact melt rocks, impact melt-bearing breccias, and lithic impact breccias are interpreted to have been injected into fracture systems – either caused by the impact or pre-existing weaknesses – although there is considerable debate at which point in the cratering process this occurs (Dressler and Reimold, 2004). Pseudotachylite on the other hand is generally thought to represent melt generated *in situ* (e.g., O'Callaghan et al., 2016; Reimold, 1995; Thompson and Spray, 1996), although again there is considerable debate as to when in the cratering process this occurs.

Dykes at a much greater scale, up to 10s of metres wide and several kilometres long, have been observed at the two largest hypervelocity impact craters on Earth: Sudbury (e.g., Pilles et al., 2018; Wood and Spray, 1998) and Vredefort (e.g., Lieger and Riller, 2012; Reimold and Gibson, 2006). These so-called Offset Dykes at the Sudbury impact structure are connected to the Sudbury Igneous Complex (SIC), the up to ~5 km-thick impact melt sheet. While most authors agree that the Offset Dykes represent impact melt injected into fractures in the crater floor, the timing of emplacement of these dykes is still unclear. Some authors have proposed that the dykes formed from an injection during the excavation stage before differentiation occurred in the Sudbury Igneous Complex (Tuchscherer and Spray, 2002), others have suggested multiple injection events during the excavation and modification stages (Lightfoot and Farrow, 2002; Murphy and Spray, 2002; Rickard and Watkinson, 2001). More recent studies have supported a single injection event following the modification stage for the Foy Offset Dyke (Pilles et al., 2018).

Proximal ejecta deposits: Proximal ejecta deposits are defined as material that has been transported beyond the rim of the transient cavity, within five crater radii of the source crater (Grieve and Therriault, 2004; Stöffler and Grieve, 2007). Impact ejecta deposits are the first impactite type to be eroded and few proximal ejecta deposits are preserved around hypervelocity impact craters on Earth, with only 15 possible examples (Appendix A). In contrast, due to their young age, all impact craters preserve some portion of their ejecta deposits (Appendix A). Like their planetary counterparts, all terrestrial hypervelocity impact craters possess a continuous ejecta deposit commonly referred to as an "ejecta blanket" (Melosh, 1989) (Fig. 15). These continuous ejecta blankets comprise melt-free lithic impact breccias to melt-poor impact melt-bearing breccias (Osinski et al., 2012a) and form via ballistic sedimentation and radial flow during the excavation stage of crater formation (Hörz et al., 1977; Oberbeck, 1975). Most complex hypervelocity impact craters on Earth also preserve a second patchy layer of impact melt-bearing breccias and/or impact melt rock overlying the continuous ejecta blanket (Osinski et al., 2011) (Fig. 16). The presence of a second layer of melt-rich material is also common to the other rocky planets, the Moon, and large asteroids and has been explained by a second major pulse of impact ejecta emplacement during the final modification stage of crater formation (Osinski et al., 2011).

In smaller simple craters, impact melt has also been documented as isolated glass fragments not contained in a breccia ("melt beads") (e.g.,

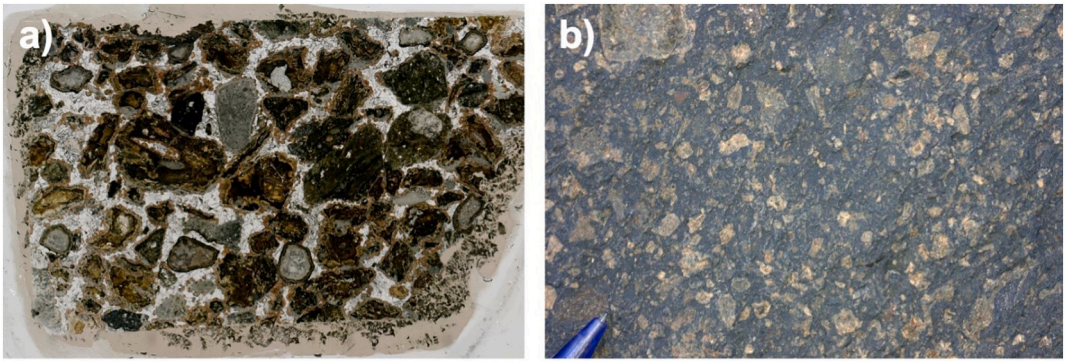

Fig. 17. Impactites formed through the explosive interaction of impact melt and seawater during marine impacts. (a) Thin section scan of melt-rich breccias from the Chicxulub impact structure. Image is 4 cm across. b) Field image of the Onaping Formation of the Sudbury impact structure. Pencil tip for scale.

at the Aouelloul, Barringer, Henbury, Kamil, Odessa, and Wabar craters). In marine and submarine impact structures, resurge deposits, which contain reworked impact material, can fill completely the cavity, and extend beyond the rims, for example at the Lockne (Sjöqvist et al., 2016) and Chesapeake Bay (Poag et al., 2004) impact structures. It is worth noting that these deposits do not constitute primary ejecta deposits.

Distal ejecta deposits: Distal ejecta deposits form beyond 5 crater radii of the source crater, up to a global dispersion (Fig. 16). The majority of distal ejecta deposits comprise tektites and spherules, described in Sections 5.4.1. and 5.4.2., respectively.

Finally, as noted at the outset of this contribution, in the past couple of decades it has been recognized that the majority of craters on Earth above a few km in diameter have generated local hydrothermal systems (e.g., Kirsimäe and Osinski, 2012; Naumov, 2005; Osinski et al., 2013). Such systems are important for astrobiology (Osinski et al., 2020c) and economic geology (Grieve, 2012), and result in alteration of impactites, complicating our understanding of impact cratering processes and products. The description of hydrothermal alteration products in terrestrial craters, however, is outside the scope of this contribution and the reader is referred to reviews by Naumov (2005), Kirsimäe and Osinski (2012), Osinski et al. (2013) and references, therein.

10.3. Impactites in marine impacts

When an impact event occurs in a marine environment, seawater is rapidly expelled radially from the cavity, while ejecta deposits are forming. Water then rushes back into the structure, eroding the recently ejected material and converging at the center of the crater, which results in a central water plume that subsequently collapses and produces an outward flow, followed by oscillating impact-triggered tsunami waves (Dypvik and Jansa, 2003; Ormö et al., 2007). As a result, the products of marine impacts contain reworked impact-generated and sedimentary material, and usually display an upward fining and a transition into post-impact sedimentary conditions. In smaller marine craters (e.g., the 14 km diameter Lockne impact structure), the resurge of seawater into the crater cavity immediately after the impact resulted in the primary impactites being immediately reworked, such that in their place is a series of sedimentary rocks containing primary impact material (Sturkell, 1998). This eroded, transported, and redeposited material does not strictly conform the current definition of impactites.

Similar to impacts into sedimentary rocks, it was thought that impact melt was not produced in marine impacts in any significant quantity; however, as pointed out by Dypvik and Jansa (2003), this is not the case and impact melt rocks and impact melt-bearing breccias are present in a number of marine impact craters (see Appendix A). As with subaerial impacts, the volumes of impact melt rocks and impact melt-bearing breccias increases with crater size for marine impact craters. In the past decade it has also been recognized that for large marine impacts, as exemplified by Chicxulub and Sudbury, the presence of such large volumes of impact melt results in explosive molten-fuel-coolant interaction (MFCI), analogous to what occurs during phreatomagmatic volcanic eruptions (Grieve et al., 2010; Osinski et al., 2020c). This process fractures and disperses the melt to form a series of well sorted glass-rich deposits (Fig. 17) that bear little resemblance to the products of impacts in continental setting. These lithologies are not accounted for in current classification schemes for impactites and may not actually conform to the definition of an impactite.

11. Concluding remarks

It can be reasoned that the impact of extraterrestrial objects with planetary bodies is one of the most fundamental and ubiquitous geological processes in the Solar System, with implications for the origin and evolution of planets and of life itself. One of the main approaches to understanding the impact cratering process and its products and effects is the geological record on Earth. In this contribution, we have conducted a comprehensive review of the terrestrial impact record. In addition to being presented here, this database is provided via the *Impact Earth* website (http://www.impactearth.com) that will be continually updated in order to provide a living resource for those who wish to track what has changed over time. In addition, given the shear breadth of the literature on terrestrial impacts, we acknowledge that there will be omissions and even errors in this database and we welcome input from the community to ensure that the *Impact Earth* database is kept as accurate and up-to-date as possible.

We hope that the definitions and criteria for how *impact craters*, *hypervelocity impact craters*, and *impact deposits* on Earth can be confirmed will be useful for experienced and new impact researchers alike. It is our goal that by publishing this database, that it will enable and encourage renewed interest and research on the impact record of Earth, in particular in the field investigation of craters and in the laboratory analysis of samples, which has diminished in recent years. We have barely scratched the surface of what this database can tell us about impact cratering processes and products, yet even our high-level examination presented here has yielded important new information, for example, on the simple-to-complex crater transition diameter and the nature of complex craters on Earth.

With the ongoing robotic exploration of two impact craters on Mars (Gale and Jezero) and the imminent prospect of humans conducting fieldwork once again on the heavily cratered lunar surface, it is our hope that as happened during Apollo, that the exploration of the Moon, Mars and other Solar System bodies will occur hand in hand with the exploration of the impact record here on Earth.

Declaration of Competing Interest

None.

Acknowledgments

This work was supported by numerous different grants to GRO, primarily from the Natural Sciences and Engineering Research Council of Canada's (NSERC) Discovery Grant, Discovery Accelerator, and Industrial Research Chair (IRC) programs. IRC partner's MDA, the Canadian Space Agency, and the Centre for Excellence in Mining Innovation (CEMI) are also thanked for their funding and support. Anna Losiak is funded by the National Science Centre, Poland grant UMO-2020/39/D/ST10/02675. In addition to the co-authors, the following students and postdoctoral fellows are thanked for their contributions to the *Impact Earth Database* over the past several years: Chimira Andres, Sharini Kanni Suresh Babu, Christy Caudill, Paige Cincio, Neeraja Chinchalkar, Rajit Das, Leah Davis-Purcell, Anthony Dicecca, Nico Garroni, Kayle Hansen, Jack Hostrawser, Adrienne Iannicca, Clodagh Kells, Keelan Kells, Marcel Kim, Joshua Laughton, Marc Mechem, Gabriela Ospina, Nikol Posnov, Nandini Shahi, Racel Sopoco, Andrew Siwabessy, Lauren Stone, Matthew Svensson, and Gavin Tolometti. Many of these students received support for this work from the NSERC Undergraduate Student Research Awards (USRA) program, the MITACS Globalink program, Western's Undergraduate Summer Research Internships (USRI) and Work Study programs, and the Institute for Earth and Space Exploration's Summer Exploration Internship programs. Drs. Sanna Alwmark and David King are thanked for their constructive reviews. The authors would like to dedicate this contribution to H. Jay Melosh who sadly passed away in September 2020. As somebody who literally wrote the book on *Impact Cratering – A Geologic Process*, we hope that he would have enjoyed reading this review.

Appendix A. Supplementary data

Supplementary data to this article can be found online at https://doi.org/10.1016/j.earscirev.2022.104112.

References

Aaloe, A.O., Tiirmaa, R.T., 1982. Meteorite matter in small Kaali craters and their vicinity. Meteoritika 41, 120–125.
Ahrens, T.J., O'Keefe, J.D., 1972. Shock melting and vaporization of Lunar rocks and minerals. Moon 4, 214–249.
Ahrens, T.J., O'Keefe, J.D., 1977. Equations of state and impact-induced shock wave attenuation on the moon. In: Merrill, R.B., Pepin, R.D.J., Pepin, R.O. (Eds.), Impact and Explosion Cratering. Pergamon Press, New York, pp. 639–656.
Alderman, A.R., 1932. The meteorite craters at Henbury, Central Australia. Mineral. Mag. 23, 19–32.
Alvarez, W., Muller, R.A., 1984. Evidence from crater ages for periodic impacts on the Earth. Nature 308, 718–720. https://doi.org/10.1038/308718a0.
Alvarez, L.W., Alvarez, W., Asaro, F., Michel, H.V., 1980. Extraterrestrial cause for the Cretaceous/Tertiary extinction. Science. 208, 1095–1108.
Alwmark, C., Schmitz, B., 2007. Extraterrestrial chromite in the resurge deposits of the early Late Ordovician Lockne Crater, central Sweden. In: Earth and Planetary Science Letters. Elsevier, Amsterdam, pp. 291–303. https://doi.org/10.1016/j.epsl.2006.10.034.
Alwmark, C., Schmitz, B., Kirsimae, K., 2010. The Mid-Ordovician Osmussaar Breccia in Estonia linked to the disruption of the L-chondrite parent body in the asteroid belt. Geol. Soc. Am. Bull. 122, 1039–1046. https://doi.org/10.1130/B30040.1.
Alwmark, C., Ferrière, L., Holm-Alwmark, S., Ormö, J., Leroux, H., Sturkell, E., 2015. Impact origin for the Hummeln structure (Sweden) and its link to the Ordovician disruption of the L chondrite parent body. Geology 43, 279–282. https://doi.org/10.1130/G36429.1.
American Meteor Society, 2022, Website:. https://www.amsmeteors.org. (Accessed 15 June 2022).
Amor, K., Hesselbo, S.P., Porcelli, D., Thackrey, S., Parnell, J., 2008. A Precambrian proximal ejecta blanket from Scotland. Geology 36, 303–306.
Artemieva, N., Shuvalov, V., 2019. Atmospheric shock waves after impacts of cosmic bodies up to 1000 m in diameter. Meteorit. Planet. Sci. 54, 592–608. https://doi.org/10.1111/maps.13229.
Artemieva, N., Pierazzo, E., Stoffler, D., 2002. Numerical modeling of tektite origin in oblique impacts: Implication to Ries-Moldavites strewn field. Bull. Czech Geol. Surv. 77, 303–311.
Ault, A.K., Gautheron, C., King, G.E., 2019. Innovations in (U–Th)/He, Fission Track, and Trapped Charge Thermochronometry with Applications to Earthquakes, Weathering, Surface-Mantle Connections, and the Growth and Decay of Mountains. Tectonics 38, 3705–3739. https://doi.org/10.1029/2018TC005312.
Bailer-Jones, C.A.L., 2011. Bayesian time series analysis of terrestrial impact cratering. Mon. Not. R. Astron. Soc. 416, 1163–1180. https://doi.org/10.1111/j.1365-2966.2011.19112.x.
Baksi, A.K., 1990. Search for periodicity in global events in the geologic record: Quo vadimus? Geology 18, 983–986. https://doi.org/10.1130/0091-7613(1990)018<0983:SFPIGE>2.3.CO;2.
Baratoux, D., Reimold, W.U., 2016. The current state of knowledge about shatter cones: Introduction to the special issue. Meteorit. Planet. Sci. 51, 1389–1434. https://doi.org/10.1111/maps.12678.
Barnes, V.E., 1940. (University of Texas Publications), Contributions to Geology, 1939, Part 2, 3945. In: North American Tektites, pp. 475–582.
Barringer, D.M., 1905. Coon Mountain and its crater. Proc. Acad. Nat. Sci. Philadelphia 57, 861–886.
Barringer, D.M.J., 1928. A New Meteor Crater. Proc. Acad. Nat. Sci. Philadelphia 80, 307–311.
Beals, C.S., 1958. A survey of terrestrial craters. Nature 181, 559.
Beals, C.S., 1965. The identification of ancient craters. Ann. N. Y. Acad. Sci. 123, 904–914. https://doi.org/10.1111/j.1749-6632.1965.tb20409.x.
Beals, C.S., Innes, M.J.S., Rottenberg, J.A., 1960. The search for fossil meteorite craters. Ottawa Dom. Obs. Contrib. 4, 1–31.
Beals, C.S., Dence, M.R., Cohen, A.J., 1967. Evidence for the impact origin of Lac Couture. Publ. Dom. Obs. Ottawa 31, 409–426.
Beere, G.M., 1983. The Piccaninny structure – a cryptoexplosive feature in the Ord Basin, East Kimberly. In: Geological Survey of Western Australia Record, p. 8.
Begemann, F., Li, Z., Schmitt-Strecker, S., Weber, H.W., Xu, Z., 1985. Noble gases and the history of Jilin meteorite. Earth Planet. Sci. Lett. 72, 247–262. https://doi.org/10.1016/0012-821X(85)90010-X.
Bendeliani, N.A., Popova, S.V., Vereshchagin, L.F., 1966. New modification of titanium dioxide obtained at high pressures. Geochem. Int. 3, 387–390.
Beran, A., Koeberl, C., 1997. Water in tektites and impact glasses by fourier-transformed infrared spectrometry. Meteorit. Planet. Sci. 32, 211–216.
Bevan, A.W.R., Shoemaker, E.M., Shoemaker, C.S., 1995. Metallography and thermo-mechanical treatment of the Veevers (IIAB) crater-forming iron meteorite. Rec. West. Aust. Museum 17, 51–59.
Biren, M.B., van Soest, M.C., Wartho, J.-A., Hodges, K.V., Spray, J.G., 2016. Diachroneity of the Clearwater West and Clearwater East impact structures indicated by the (U–Th)/He dating method. Earth Planet. Sci. Lett. 453, 56–66. https://doi.org/10.1016/j.epsl.2016.07.053.
Bland, P.A., 2005. The impact rate on Earth. Philos. Trans. R. Soc. A Math. Phys. Eng. Sci. 363, 2793 LP – 2810. https://doi.org/10.1098/rsta.2005.1674.
Bland, P.A., Artemieva, N.A., 2006. The rate of small impacts on Earth. Meteorit. Planet. Sci. 41, 607–631.
Boon, J.D., Albritton, C.C., 1936. Meteorite craters and their possible relationship to "cryptovolcanic structures.". F. Lab. 5, 1–9.
Boslough, M.B.E., Crawford, D.A., 2008. Low-altitude airbursts and the impact threat. Int. J. Impact Eng. 35, 1441–1448.
Bostock, H.H., 1969. The Clearwater Complex. New Quebec, Geolological Survey of Canada Bulletin, p. 178.
Bottke, W.F., Norman, M.D., 2017. The Late Heavy Bombardment. Annu. Rev. Earth Planet. Sci. 45, 619–647. https://doi.org/10.1146/annurev-earth-063016-020131.
Bottomley, R.J., York, D., Grieve, R.A.F., 1990. Argon-40-Argon-39 dating of impact craters. Proc. Lunar Planet. Sci. Conf. 20, 421–431.
Branco, W., Fraas, E., 1905. Das Kryptovulkanische Becken von Steinheim. In: Abhandlungen Der Königlich Preußischen Akademie Der Wissenschaften, pp. 1–64.
Bronikowska, M., Artemieva, N.A., Wünnemann, K., 2017. Reconstruction of the Morasko meteoroid impact—insight from numerical modeling. Meteorit. Planet. Sci. 52, 1704–1721. https://doi.org/10.1111/maps.12882.
Brown, P., Spalding, R.E., ReVelle, D.O., Tagliaferri, E., Worden, S.P., 2002. The flux of small near-Earth objects colliding with the Earth. Nature 420, 294–296.
Brown, P., ReVelle, D.O., Silber, E.A., Edwards, W.N., Arrowsmith, S., Jackson Jr., L.E., Tancredi, G., Eaton, D., 2008. Analysis of a crater-forming meteorite impact in Peru. J. Geophys. Res. Earth Planets 113. https://doi.org/10.1029/2008JE003105.
Brown, P.G., Assink, J.D., Astiz, L., Blaauw, R., Boslough, M.B., Borovicka, J., Brachet, N., Brown, D., Campbell-Brown, M., Ceranna, L., Cooke, W., de Groot-Hedlin, C., Drob, D.P., Edwards, W., Evers, L.G., Garces, M., Gill, J., Hedlin, M., Kingery, A., Laske, G., Le Pichon, A., Mialle, P., Moser, D.E., Saffer, A., Silber, E., Smets, P., Spalding, R.E., Spurny, P., Tagliaferri, E., Uren, D., Weryk, R.J., Whitaker, R., Krzeminski, Z., 2013. A 500-kiloton airburst over Chelyabinsk and an enhanced hazard from small impactors. Nature 503, 238–241.
Bucher, W.H., 1936. Cryptovolcanic structures in the United States. In: Report of the XVI International Geological Congress, Vol. II, pp. 1055–1084.
Buchner, E., Kenkmann, T., 2008. Upheaval Dome, Utah, USA: impact origin confirmed. Geology 36, 227–230.
Buchner, E., Schmieder, M., 2009. Multiple fluvial reworking of impact ejecta—A case study from the Ries crater, southern Germany. Meteorit. Planet. Sci. 44, 1051–1060. https://doi.org/10.1111/j.1945-5100.2009.tb00787.x.
Buchner, Schmieder, M., 2010. Steinheim suevite—a first report of melt-bearing impactites from the Steinheim Basin (SW Germany). Meteorit. Planet. Sci. 45, 1093–1107. https://doi.org/10.1111/j.1945-5100.2010.01073.x.
Bunch, T.E., Quaide, W.L., 1968. Shatter cones in the Danny Boy nuclear crater. In: French, B.M., Short, N.M. (Eds.), Shock Metamorphism of Natural Materials. Mono Book Corp, Baltimore, pp. 285–286.
Bunch, T.E., Cassidy, W.A., 1968. Impact-induced deformation in the Campo del Cielo meteorite. In: French, B.M., Short, N.M. (Eds.), Shock Metamorphism of Natural Materials. Mono Book Corp, Baltimore, pp. 601–612.

Bunch, T.E., Cohen, A.J., Dence, M.R., 1967. Natural terrestrial maskelynite. Am. Mineral. 52, 244–253.
Canup, R.M., 2012. Forming a Moon with an Earth-like Composition via a Giant Impact. Science 338, 1052–1055. https://doi.org/10.1126/science.1226073.
Carter, N.L., 1965. Basal quartz deformation lamellae; a criterion for recognition of impactites. Am. J. Sci. 263, 786–806.
Carter, N., 1968. Dynamic deformation of quartz. In: French, B.M., Short, N.M. (Eds.), Shock Metamorphism of Natural Materials. Mono Book Corporation, Baltimore, pp. 453–474.
Cavosie, A.J., Koeberl, C., 2019. Overestimation of threat from 100 Mt–class airbursts? High-pressure evidence from zircon in Libyan Desert Glass. Geology 47, 609–612. https://doi.org/10.1130/G45974.1.
Cavosie, A.J., Quintero, R.R., Radovan, H.A., Moser, D.E., 2010. A record of ancient cataclysm in modern sand; shock microstructures in detrital minerals from the Vaal River, Vredefort Dome, South Africa. Geol. Soc. Am. Bull. 122, 1968–1980. https://doi.org/10.1130/B30187.1.
Cavosie, A.J., Timms, N.E., Erickson, T.M., Hagerty, J.J., Hörz, F., 2016. Transformations to granular zircon revealed: Twinning, reidite, and ZrO2 in shocked zircon from Meteor Crater (Arizona, USA). Geology 44, 703–706. https://doi.org/10.1130/G38043.1.
Cassidy, W.A., Renard, M.L., 1996. Discovering research value in the Campo del Cielo, Argentina, meteorite craters. Meteorit. Planet. Sci. 31, 433–448. https://doi.org/10.1111/j.1945-5100.1996.tb02087.x.
Cavosie, A.J., Erickson, T.M., Montalvo, P.E., Prado, D.C., Cintron, N.O., Gibbon, R.J., 2018a. The Rietputs Formation in South Africa. Microstruct. Geochronol., Geophysical Monograph Series. https://doi.org/10.1002/9781119227250.ch9.
Cavosie, A.J., Timms, N.E., Erickson, T.M., Koeberl, C., 2018b. New clues from Earth's most elusive impact crater: Evidence of reidite in Australasian tektites from Thailand. Geology 46, 203–206. https://doi.org/10.1130/G39711.1.
Cavosie, A.J., Timms, N.E., Ferrière, L., Rochette, P., 2018c. FRIGN zircon—The only terrestrial mineral diagnostic of high-pressure and high-temperature shock deformation. Geology 46, 891–894. https://doi.org/10.1130/G45079.1.
Cavosie, A.J., Kirkland, C.L., Reddy, S.M., Timms, N.E., Talavera, C., Pincus, M.R., 2021. Extreme plastic deformation and subsequent Pb loss in shocked xenotime from the Vredefort Dome, South Africa. Large Meteor. Impacts Planet. Evol. VI. https://doi.org/10.1130/2021.2550(20).
Chao, E.C.T., 1967. Shock effects in certain rock-forming minerals. Science 156, 192–202.
Chao, E.C.T., Shoemaker, E.M., Madsen, B.M., 1960. First natural occurrence of coesite. Science 132, 220–222. https://doi.org/10.1126/science.132.3421.220.
Chao, E.C.T., Fahey, J.J., Littler, J., Milton, D.J., 1962. Stishovite, SiO2, a very high pressure new mineral from Meteor Crater, Arizona. J. Geophys. Res. 67, 419–421.
Chen, M., Yin, F., Li, X., Xie, X., Xiao, W., Tan, D., 2013. Natural occurrence of reidite in the Xiuyan crater of China. Meteorit. Planet. Sci. 48, 796–805. https://doi.org/10.1111/maps.12106.
Chyba, C.F., 1993. The violent environment of the origin of life: Progress and uncertainties. Geochim. Cosmochim. Acta 57, 3351–3358.
Collins, G.S., Melosh, H.J., Marcus, R.A., 2005. Earth Impact Effects Program: a web-based computer program for calculating the regional environmental consequences of a meteoroid impact on Earth. Meteorit. Planet. Sci. 40, 817–840.
Classen, J., 1978. The meteorite craters of Morasko in Poland. Meteoritics 13, 245–255. https://doi.org/10.1111/j.1945-5100.1978.tb00814.x.
Collins, G.S., Kenkmann, T., Osinski, G.R., Wunnemann, K., 2008. Mid-sized complex crater formation in mixed crystalline-sedimentary targets: Insight from modeling and observation. Meteorit. Planet. Sci. 43, 1955–1977.
Compston, W., Taylor, S.R., 1969. Rb/Sr study of impact glass and country rocks from the Henbury meteorite crater field. Geochim. Cosmochim. Acta 33, 1037–1043.
Corfu, F., 2013. A century of U-Pb geochronology: The long quest towards concordance. GSA Bull. 125, 33–47. https://doi.org/10.1130/B30698.1.
Cox, M.A., Erickson, T.M., Schmieder, M., Christoffersen, R., Ross, D.K., Cavosie, A.J., Bland, P.A., Kring, D.A., Scientists, I.E. 364, 2020. High-resolution microstructural and compositional analyses of shock deformed apatite from the peak ring of the Chicxulub impact crater. Meteorit. Planet. Sci. 55, 1715–1733. https://doi.org/10.1111/maps.13541.
Cressman, E.R., 1981. Surface geology of the Jeptha Knob cryptoexplosion structure, Shelby County, Kentucky, ed. USGS Professional Paper, p. 1151-B. https://doi.org/10.3133/pp1151B.
Ćuk, M., Stewart, S.T., 2012. Making the Moon from a Fast-Spinning Earth: A Giant Impact Followed by Resonant Despinning. Science 338, 1047–1052. https://doi.org/10.1126/science.1225542.
Currie, K.L., 1971. Geology of the resurgent cryptoexplosion crater at Mistastin Lake, Labrador, Bulletin of the Geological Survey of Canada 207. Geological Survey of Canada, Ottawa.
Currie, K.L., 1972. Geology and petrology of the Manicouagan resurgent caldera, Quebec, Geol. Surv. Can. Bull.
Dabizha, A.I., Feldman, V.I., 1982. Geophysical characteristics of some astroblemes of USSR. Meteoritika 40, 91–101.
Daly, R.T., Schultz, P.H., 2018. The delivery of water by impacts from planetary accretion to present. Sci. Adv. 4 https://doi.org/10.1126/sciadv.aar2632.
Davis, D.W., 2008. Sub-million-year age resolution of Precambrian igneous events by thermal extraction–thermal ionization mass spectrometer Pb dating of zircon: application to crystallization of the Sudbury impact melt sheet. Geology 36, 383–386. https://doi.org/10.1130/G24502A.1.
Dence, M.R., 1965. The extraterrestrial origin of Canadian craters. Ann. N. Y. Acad. Sci. 123, 941–969.
Dence, M.R., 1968. Shock zoning at Canadian Craters: Petrography and structural implications. In: French, B.M., Short, N.M. (Eds.), Shock Metamorphism of Natural Materials. Mono Book Corp, Baltimore, pp. 169–184.
Dence, M.R., 1971. Impact melts. J. Geophys. Res. 76, 5552–5565.
Dence, M.R., 1972. The nature and significance of terrestrial impact structures. Int. Geol. Congr. Proc. 24th, 77–89.
Dence, M.R., Popelar, J., 1972. Evidence for an impact origin for Lake Wanapitei, Ontario. Geol. Assoc. Can. Spec. Pap. 10, 117–124.
Dence, M.R., Innes, M.J.S., Robertson, P.B., French, B.M., Short, N.M., 1968. Recent geological and geophysical studies of Canadian craters. In: French, B.M., Short, N.M. (Eds.), Shock Metamorphism of Natural Materials. Mono Book Corporation, Baltimore, pp. 339–362.
Deutsch, A., Koeberl, C., 2006. Establishing the link between the Chesapeake Bay impact structure and the North American tektite strewn field: the Sr-Nd isotopic evidence. Meteorit. Planet. Sci. 41, 689–703.
Deutsch, A., Schärer, U., 1994. Dating terrestrial impact events. Meteoritics 29, 301–322. https://doi.org/10.1111/j.1945-5100.1994.tb00595.x.
Deutsch, A., Ostermann, M., Masaitis, V.L., 1997. Geochemistry and neodymium-strontium isotope signature of tektite-like objects from Siberia (urengoites, South-Ural glass). Meteorit. Planet. Sci. 32, 679–686.
Dewing, K., Pratt, B.R., Hadlari, T., Brent, T., Bedard, J., Rainbird, R.H., 2013. Newly identified "Tunnunik" impact structure, Prince Albert Peninsula, northwestern Victoria Island, Arctic Canada. Meteorit. Planet. Sci. 48, 211–223. https://doi.org/10.1111/maps.12052.
Dickin, A.P., 2018. Radiogenic Isotope Geology. Cambridge University Press, Cambridge.
Dietz, R.S., 1946. Geological structures possibly related to lunar craters. Pop. Astron. 54, 465–467.
Dietz, R.S., 1947. Meteorite impact suggested by the orientation of shatter-cones at the Kentland, Indiana disturbance. Science 42–43.
Dietz, R.S., 1968. Shatter cones in cryptoexplosion craters. In: French, B.M., Short, N.M. (Eds.), Shock Metamorphism of Natural Materials. Mono Book Corp, Baltimore, pp. 267–285.
Dressler, B.O., Reimold, W.U., 2001. Terrestrial impact melt rocks and glasses. Earth Sci. Rev. 56, 205–284.
Dressler, B.O., Reimold, W.U., 2004. Order or chaos? Origin and mode of emplacement of breccias in floors of large impact structures. Earth Sci. Rev. 67, 1–54.
Dreuse, R., Doman, D., Santimano, T., Riller, U., 2010. Crater floor topography and impact melt sheet geometry of the Sudbury impact structure, Canada. Terra Nova 22, 463–469.
Dumitru, T.A., 2000. Fission-Track Geochronology. Quat. Geochronol., AGU Reference Shelf. https://doi.org/10.1029/RF004p0131.
Dunai, T.J., 2010. Cosmogenic Nuclides: Principles, Concepts and Applications in the Earth Surface Sciences. Cambridge University Press, Cambridge.
Dypvik, H., Jansa, L.F., 2003. Sedimentary signatures and processes during marine bolide impacts: a review. Sediment. Geol. 161, 309–337.
Dypvik, H., Gudlaugsson, S.T., Tsikalas, F., Attrep Jr., M., Ferrell Jr., R.E., Krinsley, D.H., Mørk, A., Faleide, J.I., Nagy, J., 1996. Mjølnir structure: an impact crater in the Barents Sea. Geology 24, 779–782. https://doi.org/10.1130/0091-7613(1996)024<0779:MLSAIC>2.3.CO;2.
Ehlers, T.A., Farley, K.A., 2003. Apatite (U–Th)/He thermochronometry: methods and applications to problems in tectonic and surface processes. Earth Planet. Sci. Lett. 206, 1–14. https://doi.org/10.1016/S0012-821X(02)01069-5.
Elkins-Tanton, L.T., 2012. Magma oceans in the inner solar system. Annu. Rev. Earth Planet. Sci. 40, 113–139.
Elkins-Tanton, L.T., Hager, B.H., Grove, T.L., 2004. Magmatic effects of the lunar late heavy bombardment. Earth Planet. Sci. Lett. 222, 17–27.
Engelhardt, W.V., 1997. Suevite breccia of the Ries impact crater, Germany: petrography, chemistry and shock metamorphism of crystalline rock clasts. Meteorit. Planet. Sci. 32, 545–554.
Engelhardt, W.V., Bertsch, W., 1969. Shock induced planar deformation structures in quartz from the Ries crater, Germany. Contrib. Mineral. Petrol. 20, 203–234.
Erickson, T.M., Cavosie, A.J., Moser, D.E., Barker, I.R., Radovan, H.A., Wooden, J., 2013. Identification and provenance determination of distally transported, Vredefort-derived shocked minerals in the Vaal River, South Africa using SEM and SHRIMP-RG techniques. Geochim. Cosmochim. Acta 107, 170–188. https://doi.org/10.1016/j.gca.2012.12.008.
Erickson, T.M., Kirkland, C.L., Timms, N.E., Cavosie, A.J., Davison, T.M., 2020. Precise radiometric age establishes Yarrabubba, Western Australia, as Earth's oldest recognised meteorite impact structure. Nat. Commun. 11, 300. https://doi.org/10.1038/s41467-019-13985-7.
Erickson, T.M., Kirkland, C.L., Jourdan, F., Schmieder, M., Hartnady, I.H., Cox, M.A., Timms, N.E., 2021. Resolving the age of the Haughton impact structure using coupled 40Ar/39Ar and U-Pb geochronology. Geochim. Cosmochim. Acta 304, 68–82. https://doi.org/10.1016/j.gca.2021.04.008.
Erickson, T.M., Timms, N.E., Pearce, M.A., Cayron, C., Deutsch, A., Keller, L.P., Kring, D.A., 2019. Shock-produced high-pressure (La, Ce, Th)PO4 polymorph revealed by microstructural phase heritage of monazite. Geology 47, 504–508. https://doi.org/10.1130/G46008.1.
Ernstson, K., 1984. A gravity-derived model for the Steinheim impact crater. Geol. Rundsch. 73, 483–498. https://doi.org/10.1007/BF01824969.
Fagereng, Å., Biggs, J., 2019. New perspectives on 'geological strain rates' calculated from both naturally deformed and actively deforming rocks. J. Struct. Geol. 125, 100–110. https://doi.org/10.1016/j.jsg.2018.10.004.
Ferrière, L., Osinski, G.R., 2012. Shock Metamorphism, Impact Cratering: Processes and Products. https://doi.org/10.1002/9781118447307.ch8.

Ferrière, L., Koeberl, C., Ivanov, B.A., Reimold, W.U., 2008. Shock metamorphism of Bosumtwi impact crater rocks, shock attenuation, and uplift formation. Science 322, 1678–1681. https://doi.org/10.1126/science.1166283.
Ferrière, L., Barrat, J.A., Giuli, G., Koeberl, C., Schulz, T., Topa, D., Wagner, W., 2017. A new tektite strewn field discovered in Uruguay (abstract). Meteorit. Planet. Sci. 52, A89.
Ferrière, L., Crósta, A.P., Wegner, W., Libowitzky, E., Iwashita, F., Koeberl, C., 2021. Distinguishing volcanic from impact glasses—the case of the Cali glass (Colombia). Geology 49, 1421–1425. https://doi.org/10.1130/G48925.1.
Fiske, P.S., Nellis, W.J., Sinha, A.K., 1994. Shock-induced phase transitions of ZrSiO4, reversion kinetics, and implications for terrestrial impact craters (abstract). EOS Trans. Am. Geophys. Union 75, 416–417.
Foote, A.E., 1891. A new locality for meteoric iron, with a preliminary notice of discovery of diamonds in the iron. Nature 45, 178–180.
Fox, M.E., 2014. An Assessment of Shock Metamorphism for Jeptha Knob, A Suspected Impact Crater in North-Central Kentucky. Ohio University.
Fredriksson, K., Wickman, F.E., 1963. Meteoriter. In: Svensk Naturvetenskap. Statens Naturvetenskapliga Forskningsråd, Stockholm, Sweden, pp. 121–157.
French, B.M., 1998. Traces of Catastrophe: A handbook of Shock-Metamorphic Effects in Terrestrial Meteorite Impact Structures, LPI Contribution No. 954. Lunar and Planetary Institute, Houston.
French, B.M., 2004. The importance of being cratered: The new role of meteorite impact as a normal geological process. Meteorit. Planet. Sci. 39, 169–197.
French, B.M., Cordua, W.S., 1999. Intense fracturing of quartz at the Rock Elm (Wisconsin) "cryptoexplosion" structure: evidence for meteorite impact. Lunar Planet. Sci. Conf. 30, 1123 (pdf).
French, B.M., Koeberl, C., 2010. The convincing identification of terrestrial meteorite impact structures: what works, what doesn't, and why. Earth-Science Rev. 98, 123–170.
French, B.M., Short, N.M., 1968. Shock Metamorphism of Natural Materials. Mono Book Corp, Baltimore.
French, B.M., McKay, R.M., Liu, H.P., Briggs, D.E.G., Witzke, B.J., 2018. The Decorah structure, northeastern Iowa: geology and evidence for formation by meteorite impact. GSA Bull. 130, 2062–2086. https://doi.org/10.1130/B31925.1.
Frisch, T., Thorsteinsson, R., 1978. Haughton Astrobleme: A Mid-Cenozoic impact crater, Devon Island, Canadian Arctic Archipelago. Arctic 31, 108–124.
Fritz, J., Assis Fernandes, V., Greshake, A., Holzwarth, A., Böttger, U., 2019. On the formation of diaplectic glass: Shock and thermal experiments with plagioclase of different chemical compositions. Meteorit. Planet. Sci. 54, 1533–1547. https://doi.org/10.1111/maps.13289.
Gault, D.E., Sonett, C.P., 1982. Laboratory simulation of pelagic asteroidal impact: Atmospheric injection, benthic topography, and the surface wave radiation field. In: Silver, L.T., Schultz, P.H. (Eds.), Geological Implications of Impacts of Large Asteroids and Comets on the Earth. Geological Society of America. https://doi.org/10.1130/SPE190-p69, p. 0.
Gault, D.E., Quaide, W.L., Oberbeck, V.R., 1968. Impact cratering mechanics and structures. In: French, B.M., Short, N.M. (Eds.), Shock Metamorphism of Natural Materials. Mono Book Corp, Baltimore, pp. 87–99.
Gebhardt, A.C., Niessen, F., Kopsch, C., 2006. Central ring structure identified in one of the world's best-preserved impact craters. Geology 34, 145–148. https://doi.org/10.1130/G22278.1.
Gibbons, R.V., Horz, F., Thompson, T.D., Brownless, D.E., 1976. Metal spherules in Wabar, Monturaqui, and Henbury impactites. Proc. Lunar Planet. Sci. Conf. 7, 863–880.
Gilbert, G.K., 1893. The Moon's face; a study of the origin of its features. Bull. Philisophical Soc. Washingt. 12, 241–292.
Gilbert, G.K., 1896. The origin of hypotheses, illustrated by the discussion of a topographic problem. Science 3, 1–13.
Glass, B.P., 1990. Tektites and microtektites: Key facts and inferences. Tectonophysics 171, 393–404.
Glass, B.P., Liu, S., 2001. Discovery of high-pressure ZrSiO4 polymorph in naturally occurring shock-metamorphosed zircons. Geology 29, 371–373. https://doi.org/10.1130/0091-7613(2001)029<0371:DOHPZP>2.0.CO;2.
Glass, B.P., Liu, S., Leavens, P.B., 2002. Reidite: An impact-produced high-pressure polymorph of zircon found in marine sediments. Am. Mineral. 87, 562–565. https://doi.org/10.2138/am-2002-0420.
Glass, B.P., Simonson, B.M., 2012. Distal impact ejecta layers: spherules and more. Elements 8, 43–48.
Gnos, E., Hofmann, B.A., Halawani, M.A., Tarabulsi, Y., Hakeem, M., Al Shanti, M., Greber, N.D., Holm, S., Alwmark, C., Greenwood, R.C., Ramseyer, K., 2013. The Wabar impact craters, Saudi Arabia, revisited. Meteorit. Planet. Sci. 48, 2000–2014. https://doi.org/10.1111/maps.12218.
Goderis, S., Paquay, F., Claeys, P., 2012. Impactor identification in terrestrial impact structures and ejecta material. In: Osinski, G.R., Pierazzo, E. (Eds.), Impact Cratering: Processes and Products. Wiley-Blackwell, Chichester, pp. 223–239.
Golabek, G.J., Keller, T., Gerya, T.V., Zhu, G., Tackley, P.J., Connolly, J.A.D., 2011. Origin of the martian dichotomy and Tharsis from a giant impact causing massive magmatism. Icarus 215, 346–357. https://doi.org/10.1016/j.icarus.2011.06.012.
Gold, D., Tanner, J., Halliday, D., 1978. The Lac La Moinerie crater: A probable impact site in New Quebec. Abstr. Programs - Geol. Soc. Am. 44.
Gomes, R., Levison, H.F., Tsiganis, K., Morbidelli, A., 2005. Origin of the cataclysmic Late Heavy Bombardment period of the terrestrial planets. Nature 435, 466–469.
Gorter, J.D., Glikson, A.Y., 2012. Talundilly, Western Queensland, Australia: geophysical and petrological evidence for an 84 km-large impact structure and an Early Cretaceous impact cluster. Aust. J. Earth Sci. 59, 51–73.
Grieve, R.A.F., 1991. Terrestrial impact: the record in the rocks. Meteoritics 26, 175–194.
Grieve, R.A.F., 2012. Economic deposits at terrestrial impact structures. In: Osinski, G.R., Pierazzo, E. (Eds.), Impact Cratering: Processes and Products. Wiley-Blackwell, pp. 177–193.
Grieve, R.A.F., Cintala, M.J., 1981. A method for estimating the initial impact conditions of terrestrial cratering events, exemplified by its application to Brent crater, Ontario. Proc. Lunar Planet. Sci. Conf. 12B, 1607–1621.
Grieve, R.A.F., Cintala, M.J., 1992. An analysis of differential impact melt-crater scaling and implications for the terrestrial impact record. Meteoritics 27, 526–538.
Grieve, R.A.F., Osinski, G.R., 2020. The Upper Contact Unit of the Sudbury Igneous Complex in the Garson region: constraints on the depth of origin of a peak ring at the Sudbury impact structure. Meteorit. Planet. Sci. 55 https://doi.org/10.1111/maps.13542.
Grieve, R.A.F., Pesonen, L.J., 1992. The terrestrial impact cratering record. Tectonophysics 216, 1–30.
Grieve, R.A.F., Pilkington, M., 1996. The signature of terrestrial impacts. J. Aust. Geol. Geophys. 16, 399–420.
Grieve, R.A.F., Shoemaker, E.M., 1994. The record of past impacts on Earth. In: Gehrels, T. (Ed.), Hazards Due to Comets and Asteroids. University of Arizona Press, Tucson, pp. 417–462.
Grieve, R.A.F., Therriault, A., 2004. Observations at terrestrial impact structures: their utility in constraining crater formation. Meteorit. Planet. Sci. 39, 199–216.
Grieve, R.A.F., Therriault, A.M., 2012. Impactites: Their characteristics and spatial distribution. In: Osinski, G.R., Pierazzo, E. (Eds.), Impact Cratering: Processes and Products. Wiley-Blackwell, Oxford, United Kingdom (GBR), pp. 90–105.
Grieve, R.A.F., Dence, M.R., Robertson, P.B., 1977. Cratering processes: As interpreted from the occurrences of impact melts. In: Roddy, D.J., Pepin, R.O., Merrill, R.B. (Eds.), Impact and Explosion Cratering. Pergamon Press, New York, pp. 791–814.
Grieve, R.A.F., Robertson, P.B., Dence, M.R., 1981. Constraints on the formation of ring impact structures, based on terrestrial data. In: Schultz, P.H., Merrill, R.B. (Eds.), Proceedings of the Conference on Multi-Ring Basins: Formation and Evolution. Pergamon Press, New York, pp. 37–57.
Grieve, R.A.F., Sharpton, V.L., Goodacre, A.K., Garvin, J.B., 1985. A perspective on the evidence for periodic cometary impacts on Earth. Earth Planet. Sci. Lett. 76, 1–9. https://doi.org/10.1016/0012-821X(85)90143-8.
Grieve, R.A.F., Reny, G., Gurov, E.P., Ryabenko, V.A., 1987. The melt rocks of the Boltysh impact crater, Ukraine. USSR. Contrib. Mineral. Petrol. 96, 56–62.
Grieve, R.A.F., Sharpton, V.L., Rupert, J., Goodacre, A.K., 1988. Detecting a periodic signal in the terrestrial cratering record. Proc, Lunar Planet. Sci. Conf. 18, 375–382.
Grieve, R.A.F., Langenhorst, F., Stöffler, D., 1996. Shock metamorphism of quartz in nature and experiment: II. Significance in geoscience. Meteorit. Planet. Sci. 31, 6–35.
Grieve, R.A.F., Cintala, M.J., Therriault, A.M., 2006. Large-scale impacts and the evolution of the Earth's crust: The early years. In: Reimold, W.U., Gibson, R.L. (Eds.), Geological Society of America Special Paper 405: Processes on the Early Earth. Geological Society of America, Boulder, Colorado, pp. 23–31.
Grieve, R.A.F., Ames, D.E., Morgan, J.V., Artemieva, N., 2010. The evolution of the Onaping Formation at the Sudbury impact structure. Meteorit. Planet. Sci. 45, 759–782. https://doi.org/10.1111/j.1945-5100.2010.01057.x.
Gucsik, A., Koeberl, C., Brandstatter, F., Libowitzky, E., Reimold, W.U., 2004. Cathodoluminescence, electron microscopy, and raman spectroscopy of experimentally shock metamorphosed zircon crystals and naturally shocked zircon from the ries impact crater. In: Dypvik, H., Burchell, M., Claeys, P. (Eds.), Cratering in Marine Environments and On Ice. Impact Studies. Springer, Heidelberg-Berlin, pp. 281–322.
Gudlaugsson, S.T., 1993. Large impact crater in the Barents Sea. Geology 21, 291–294. https://doi.org/10.1130/0091-7613(1993)021<0291:LICITB>2.3.CO;2.
Gudmundsson, A., 2014. Elastic energy release in great earthquakes and eruptions. Front. Earth Sci. https://doi.org/10.3389/feart.2014.00010.
Güldemeister, N., Wünnemann, K., Durr, N., Hiermaier, S., 2013. Propagation of impact-induced shock waves in porous sandstone using mesoscale modeling. Meteorit. Planet. Sci. 48, 115–133. https://doi.org/10.1111/j.1945-5100.2012.01430.x.
Gulick, S.P.S., Barton, P.J., Christeson, G.L., Morgan, J.V., McDonald, M., Mendoza-Cervantes, K., Pearson, Z.F., Surendra, A., Urrutia-Fucugauchi, J., Vermeesch, P.M., Warner, M.R., 2008. Importance of pre-impact crustal structure for the asymmetry of the Chicxulub impact crater. Nat. Geosci. 1, 131–135. https://doi.org/10.1038/ngeo103.
Gurov, E.P., Gurova, E.P., 1998. The group of Macha craters in western Yakutia. Planet. Space Sci. 46, 323–328.
Gurov, E.P., Gurova, E.P., Kovalyuch, N.N., 1987. The group of young Macha craters in Western Yakutiya. Dokl. Acad. Nauk USSR 296, 185–188.
Gurov, E.P., Kelley, S.P., Koeberl, Christian, Dykan, N.I., 2006. Sediments and impact rocks filling the Boltysh impact crater. In: Cockell, C.S., Koeberl, C., Gilmour, I. (Eds.), Biological Processes Associated with Impact Events. Springer-Verlag, Berlin, pp. 335–358.
Haines, R.A., 1997. Comparison of Sylvan Structure residual maps of the Ames Feature, using control as of December 1990 and December 1994. Circ. - Oklahoma Geol. Surv. 100, 374.
Haines, P.W., 2005. Impact cratering and distal ejecta: the Australian record. Aust. J. Earth Sci. 52, 481–507.
Haines, P.W., Therriault, A.M., Kelly, S.P., 1999. Evidence for Mid-Cenozoic(?) Low-Angle Multiple Impacts in South Australia. Annu. Meteorit. Soc. Meet. 62, 5148 (pdf).
Haines, P.W., Jenkins, R.J.F., Kelley, S.P., 2001. Pleistocene glass in the Australian desert: the case for an impact origin. Geology 29, 899–902.
Hajdas, I., 2008. Radiocarbon dating and its applications in Quaternary studies. E&G Quat. Sci. J. 57, 2–24. https://doi.org/10.3285/eg.57.1-2.1.
Hajdas, I., 2009. Applications of radiocarbon dating method. Radiocarbon 51, 79–90.

Harms, J.E., Milton, D.J., Ferguson, J., Gilbert, D.J., Harris, W.K., Goleby, B., 1980. Goat Paddock cryptoexplosion crater, Western Australia. Nat. 286, 704–706.
Hart, R.J., Cloete, M.C., McDonald, I., Andreoli, M.C., 2002. Siderophile-rich inclusions from the Morokweng impact melt sheet, South Africa: possible fragments of a chondritic meteorite. Earth Planet. Sci. Lett. 198, 49–62.
Hartmann, W.K., Kuiper, G.P., 1962. Concentric structures surrounding lunar basins. Commun. Lunar Planet. Lab. 1, 51–66.
Hawke, B.R., Head, J.W., 1977. Impact melt on lunar crater rims. In: Roddy, D.J., Pepin, R.O., Merrill, R.B. (Eds.), Impact and Explosion Cratering. Pergamon Press, New York, pp. 815–841.
Hayward, P.J., Cecchetto, E.V., 1982. Scientific Basis for Nuclear Waste Management. Lutze, W., Ed 319.
Heide, K., Heide, G., Kloess, G., 2001. Glass chemistry of tektites. Planet. Space Sci. 49, 839–844.
Heisler, J., Tremaine, S., 1989. How dating uncertainties affect the detection of periodicity in extinctions and craters. Icarus 77, 213–219. https://doi.org/10.1016/0019-1035(89)90017-1.
Herd, C.D.K., Froese, D.G., Walton, E.L., Kofman, R.S., Herd, E.P.K., Duke, M.J.M., 2008. Anatomy of a young impact event in central Alberta, Canada: prospects for the missing Holocene impact record. Geology 36, 955–958. https://doi.org/10.1130/g25236a.1.
Hergarten, S., Kenkmann, T., 2015. The number of impact craters on Earth: any room for further discoveries? Earth Planet. Sci. Lett. 425, 187–192. https://doi.org/10.1016/j.epsl.2015.06.009.
Herwartz, D., Pack, A., Friedrichs, B., Bischoff, A., 2014. Identification of the giant impactor Theia in lunar rocks. Science 344, 1146–1150. https://doi.org/10.1126/science.1251117.
Hildebrand, A.R., Penfield, G.T., Kring, D.A., Pilkington, M., Camargo, A.Z., Jacobsen, S.B., Boynton, W.V., 1991. Chicxulub Crater: a possible Cretaceous/Tertiary boundary impact crater on the Yucatan Peninsula, Mexico. Geology 19, 867–871.
Holm-Alwmark, S., Jourdan, F., Ferrière, L., Alwmark, C., Koeberl, C., 2021. Resolving the age of the Puchezh-Katunki impact structure (Russia) against alteration and inherited 40Ar* – No link with extinctions. Geochim. Cosmochim. Acta 301, 116–140. https://doi.org/10.1016/j.gca.2021.03.001.
Hörz, F., Hartung, J.B., Gault, D.E., 1971. Micrometeorite craters on lunar rock surfaces. J. Geophys. Res. 76, 5770–5798. https://doi.org/10.1029/JB076i023p05770.
Hörz, F., Gall, H., Huttner, R., Oberbeck, V.R., Roddy, D.J., Pepin, R.O., Merrill, R.B., 1977. Shallow drilling in the "Bunte Breccia" impact deposits, Ries Crater, Germany. In: Impact and Explosion Cratering. Pergamon Press, New York, pp. 425–448.
Huber, M.S., Plado, J., Ferrière, L., 2013. Oldest impact structures on Earth - The case study of the Suavjärvi structure (Russia). Large Meteor. Impacts Planet. Evol. 5, 3073 pdf.
Innes, M.J.S., 1964. Recent advances in meteorite crater research at the Dominion Observatory, Ottawa, Canada. Meteoritics 2, 219–241.
Jarosewich, E., 1990. Chemical analyses of meteorites: A compilation of stony and iron meteorite analyses. Meteoritics 25, 323–337. https://doi.org/10.1111/j.1945-5100.1990.tb00717.x.
Jessberger, E.K., 1988. 40Ar-39Ar dating of the Haughton impact structure. Meteoritics 23, 233–234. https://doi.org/10.1111/j.1945-5100.1988.tb01285.x.
Johnson, B.C., Melosh, H.J., 2012. Formation of spherules in impact produced vapor plumes. Icarus 217, 416–430.
Jolley, D.W., Daly, R., Gilmour, I., Kelley, S.P., 2013. Climatic oscillations stall vegetation recovery from K/Pg event devastation. J. Geol. Soc. Lond. 170, 477–482. https://doi.org/10.1144/jgs2012-088.
Jourdan, F., Renne, P.R., Reimold, W.U., 2007. The problem of inherited 40Ar* in dating impact glass by the 40Ar/39Ar method: evidence from the Tswaing impact crater (South Africa). Geochim. Cosmochim. Acta 71, 1214–1231.
Jourdan, F., Renne, P.R., Reimold, W.U., 2009. An appraisal of the ages of terrestrial impact structures. Earth Planet. Sci. Lett. 286, 1–13.
Jull, A.J.T., 2001. In: Peucker-Ehrenbrink, B., Schmitz, B. (Eds.), Terrestrial Ages of Meteorites BT - Accretion of Extraterrestrial Matter Throughout Earth's History. Springer US, Boston, MA, pp. 241–266. https://doi.org/10.1007/978-1-4419-8694-8_14.
Jull, A.J., Cheng, S., Gooding, J.L., Velbel, M.A., 1988. Rapid growth of magnesium-carbonate weathering products in a stony meteorite from antarctica. Science 242, 417–419. https://doi.org/10.1126/science.242.4877.417.
Karp, T., Milkereit, B., Janle, P., Danuor, S.K., Pohl, J., Berckhemer, H., Scholz, C.A., 2002. Seismic investigation of the Lake Bosumtwi impact crater: preliminary results. Planet. Space Sci. 50, 735–743. https://doi.org/10.1016/S0032-0633(02)00049-1.
Kegerreis, J.A., Teodoro, L.F.A., Eke, V.R., Massey, R.J., Catling, D.C., Fryer, C.L., Korycansky, D.G., Warren, M.S., Zahnle, K.J., 2018. Consequences of giant impacts on early uranus for rotation, internal structure, debris, and atmospheric erosion. Astrophys. J. 861, 52. https://doi.org/10.3847/1538-4357/aac725.
Kelley, S., 2002. Excess argon in K-Ar and Ar-Ar geochronology. Chem. Geol. 188, 1–22. https://doi.org/10.1016/S0009-2541(02)00064-5.
Kelley, S.P., Sherlock, S.C., 2013. The geochronology of impact craters. In: Osinski, G.R., Pierazzo, E. (Eds.), Impact Cratering: Processes and Products. Wiley-Blackwell, pp. 240–253.
Kenkmann, T., 2021. The terrestrial impact crater record: a statistical analysis of morphologies, structures, ages, lithologies, and more. Meteorit. Planet. Sci. 56, 1024–1070. https://doi.org/10.1111/maps.13657.
Kenkmann, T., von Dalwigk, I., 2000. Radial transpression ridges: a new structural feature of complex impact craters. Meteorit. Planet. Sci. 35, 1189–1201.
Kenkmann, T., Artemieva (Artem'yeva), N.A., Wuennemann, K., Poelchau, M.H., Elbeshausen, D., Nunez del Prado, H., 2009. The Carancas Meteorite impact crater, Peru; geologic surveying and modeling of crater formation and atmospheric passage. Meteorit. Planet. Sci. 44, 985–1000. https://doi.org/10.1111/j.1945-5100.2009.tb00783.x.
Kenkmann, T., Collins, G.S., Wünnemann, K., 2012. The modification stage of crater formation. In: Osinski, G.R., Pierazzo, E. (Eds.), Impact Cratering: Processes and Products. Wiley-Blackwell, Chichester, pp. 60–75.
Kenkmann, T., Poelchau, M., Wulf, G., 2014. Structural geology of impact craters. J. Struct. Geol. 62, 156–182. https://doi.org/10.1016/j.jsg.2014.01.015.
Kenkmann, T., Sturm, S., Krüger, T., Salameh, E., Al-Raggad, M., Konsul, K., 2017. The structural inventory of a small complex impact crater: Jebel Waqf as Suwwan. Jordan. Meteorit. Planet. Sci. 52, 1351–1370. https://doi.org/10.1111/maps.12823.
Kenkmann, T., Sundell, K.A., Cook, D., 2018. Evidence for a large Paleozoic Impact Crater Strewn Field in the Rocky Mountains. Sci. Rep. 8, 13246. https://doi.org/10.1038/s41598-018-31655-4.
Kenny, G.G., Schmieder, M., Whitehouse, M.J., Nemchin, A.A., Morales, L.F.G., Buchner, E., Bellucci, J.J., Snape, J.F., 2019. A new U-Pb age for shock-recrystallised zircon from the Lappajärvi impact crater, Finland, and implications for the accurate dating of impact events. Geochim. Cosmochim. Acta 245, 479–494. https://doi.org/10.1016/j.gca.2018.11.021.
Khryanina, L.P., 1981. Sobolevskiy meteorite crater (Sikhote-Alin' Range). Int. Geol. Rev. 23, 1–10. https://doi.org/10.1080/00206818209467207.
Kieffer, S.W., 1971. Shock metamorphism of the Coconino sandstone at Meteor Crater, Arizona. J. Geophys. Res. 76, 5449–5473.
Kieffer, S.W., Simonds, C.H., 1980. The role of volatiles and lithology in the impact cratering process. Rev. Geophys. Sp. Phys. 18, 143–181.
Kieffer, S.W., Phakey, P.P., Christie, J.M., 1976. Shock processes in porous quartzite: Transmission electron microscope observations and theory. Contrib. Mineral. Petrol. 59, 41–93.
King, D.T., Ormö, J., Petruny, L.W., Neathery, T.L., 2006. Role of water in the formation of the Late Cretaceous Wetumpka impact structure, inner Gulf Coastal Plain of Alabama, USA. Meteorit. Planet. Sci. 41, 1625–1631.
Kirchoff, M.R., Marchi, S., Bottke, W.F., Chapman, C.R., Enke, B., 2021. Suggestion that recent ($\leq$ 3 Ga) flux of kilometer and larger impactors in the Earth-Moon system has not been constant. Icarus 355, 114110. https://doi.org/10.1016/j.icarus.2020.114110.
Kirsimäe, K., Osinski, Gordon R., 2012. Impact-Induced Hydrothermal Activity. In: Osinski, G.R., Pierazzo, E. (Eds.), Impact Cratering: Processes and Products. John Wiley & Sons, Ltd, Chichester, UK, pp. 76–89. https://doi.org/10.1002/9781118447307.ch6.
Kjær, K.H., Larsen, N.K., Binder, T., Bjørk, A.A., Eisen, O., Fahnestock, M.A., Funder, S., Garde, A.A., Haack, H., Helm, V., Houmark-Nielsen, M., Kjeldsen, K.K., Khan, S.A., Machguth, H., McDonald, I., Morlighem, M., Mouginot, J., Paden, J.D., Waight, T.E., Weikusat, C., Willerslev, E., Mac Gregor, J.A., 2018. A large impact crater beneath Hiawatha Glacier in northwest Greenland. Sci, Adv, p. 4.
Koeberl, C., 1994. Tektite origin by hypervelocity asteroidal or cometary impact: Target rocks, source craters, and mechanisms. In: Dressler, B.O., Grieve, R.A.F., Sharpton, V.L. (Eds.), Large Meteorite Impacts and Planetary Evolution, Geological Society of America Special Paper 293. Boulder, Colorado, pp. 133–152.
Koeberl, C., Ferrière, L., 2019. Libyan Desert Glass area in western Egypt: Shocked quartz in bedrock points to a possible deeply eroded impact structure in the region. Meteorit. Planet. Sci. 54, 2398–2408. https://doi.org/10.1111/maps.13250.
Koeberl, C., Reimold, W.U., Kelley, S.P., 2001. Petrography, geochemistry, and argon-40/argon-39 ages of impact-melt rocks and breccias from the Ames impact structure, Oklahoma: the Nicor Chestnut 18-4 drill core. Meteorit. Planet. Sci. 36, 651–669.
Koeberl, C., Milkereit, B., Overpeck, J.T., Scholz, C.A., Amoako, P.Y.O., Boamah, D., Danuor, S., Karp, T., Kueck, J., Hecky, R.E., King, J.W., Peck, J.A., 2007. An international and multidisciplinary drilling project into a young complex impact structure: the 2004 ICDP Bosumtwi Crater Drilling Project - an overview. Meteorit. Planet. Sci. 42, 483–511.
Kolesnikov, E.M., Lavrukhina, A.K., Fisenko, A.V., Levsky, L.K., 1972. Radiation ages of different fragments of the Sikhote-Alin meteorite fall. Geochim. Cosmochim. Acta 36, 573–576. https://doi.org/10.1016/0016-7037(72)90076-2.
Korpikiewicz, H., 1978. Meteoritic Shower Morasko. Meteoritics 13, 311–326.
Kovaleva, E., Kusiak, M.A., Kenny, G.G., Whitehouse, M.J., Habler, G., Schreiber, A., Wirth, R., 2021. Nano-scale investigation of granular neoblastic zircon, Vredefort impact structure, South Africa: Evidence for complete shock melting. Earth Planet. Sci. Lett. 565, 116948 https://doi.org/10.1016/j.epsl.2021.116948.
Kring, D.A., 2003. Environmental consequences of impact cratering events as a function of ambient conditions on Earth. Astrobiology 3, 133–152.
Kring, D.A., Kramer, G.Y., Collins, G.S., Potter, R.W.K., Chandnani, M., 2016. Peak-ring structure and kinematics from a multi-disciplinary study of the Schrödinger impact basin. Nat. Commun. 7, 13161.
Krinov, E.L., 1963. Meteorite craters on the Earth's surface. In: Middlehurst, B.M., Kuiper, G.P. (Eds.), The Moon, Meteorites and Comets. University of Chicago Press, Chicago, pp. 183–207.
Krinov, E.L., 1966. Giant Meteorites. Pergamon Press, New York.
Krinov, E.L., 1971. New studies of the Sikhote-Alin iron meteorite shower. Meteoritics 6, 127–138. https://doi.org/10.1111/j.1945-5100.1971.tb00104.x.
Krüger, T., Hergarten, S., Kenkmann, T., 2018. Deriving Morphometric Parameters and the Simple-to-Complex Transition Diameter From a High-Resolution, Global Database of Fresh Lunar Impact Craters $\geq \sim$ 3 km. J. Geophys. Res. 123, 2667–2690.
Kuiper, Y.D., 2002. The interpretation of inverse isochron diagrams in $^{40}Ar/^{39}Ar$ geochronology. Earth Planet. Sci. Lett. 203, 499–506. https://doi.org/10.1016/S0012-821X(02)00833-6.
Kurosaki, K., Inutsuka, S., 2018. The exchange of mass and angular momentum in the impact event of ice giant planets: implications for the origin of Uranus. Astron. J. 157 https://doi.org/10.3847/1538-3881/aaf165. doi:10.3847/1538-3881/aaf165.

Lagain, A., Kreslavsky, M., Baratoux, D., Liu, Y., Devillepoix, H., Bland, P., Benedix, G.K., Doucet, L.S., Servis, K., 2022. Has the impact flux of small and large asteroids varied through time on Mars, the Earth and the Moon? Earth Planet. Sci. Lett. 579, 117362 https://doi.org/10.1016/j.epsl.2021.117362.

Latypov, R., Chistyakova, S., Grieve, R., Huhma, H., 2019. Evidence for igneous differentiation in Sudbury Igneous Complex and impact-driven evolution of terrestrial planet proto-crusts. Nat. Commun. 10, 508. https://doi.org/10.1038/s41467-019-08467-9.

Lawson, D.E., 1973. Torridonian volcanic sediments. Scott. J. Geol. 8 https://doi.org/10.1144/sjg08040345, 345 LP – 362.

Leroux, H., Warme, J.E., Doukhan, J.-C., 1995. Shocked quartz in the Alamo breccia, southern Nevada: Evidence for a Devonian impact event. Geology 23, 1003–1006. https://doi.org/10.1130/0091-7613(1995)023<1003:SQITAB>2.3.CO;2.

Lieger, D., Riller, U., 2012. Emplacement history of Granophyre dikes in the Vredefort Impact Structure, South Africa, inferred from geochemical evidence. Icarus 219, 168–180. https://doi.org/10.1016/j.icarus.2012.02.026.

Lightfoot, P.C., Farrow, C.E.G., 2002. Geology, geochemistry, and mineralogy of the Worthington Offset Dike: a genetic model for Offset Dike mineralization in the Sudbury Igneous Complex. Econ. Geol. 97, 1419–1446.

Lindgren, P., Broman, C., Holm, N.G., Parnell, J., Bowden, S.A., Osinski, G.R., Lee, P., 2009. The RAMAN signature of shocked carbonates from the Haughton Impact Structure, Devon Island, Canada. Lunar Planet. Sci. Conf 39, 1258 pdf.

Liritzis, I., Singhvi, A.K., Feathers, J.K., Wagner, G.A., Kadereit, A., Zacharias, N., Li, S.-H., 2013. Luminescence Dating in Archaeology, Anthropology, and Geoarchaeology. Springer, Heidelberg.

Losiak, A., Wild, E.M., Geppert, W.D., Huber, M.S., Jõeleht, A., Kriiska, A., Kulkov, A., Paavel, K., Pirkovic, I., Plado, J., Steier, P., Välja, R., Wilk, J., Wisniowski, T., Zanetti, M., 2016. Dating a small impact crater: an age of Kaali crater (Estonia) based on charcoal emplaced within proximal ejecta. Meteorit. Planet. Sci. 51, 681–695. https://doi.org/10.1111/maps.12616.

Losiak, A., Jõeleht, A., Plado, J., Szyszka, M., Wild, E.M., Steier, P., 2018. Dating small impact craters on Earth and the "old wood problem". In: 81st Annual Meeting of The Meteoritical Society, p. 6219 pdf.

Losiak, A., Jõeleht, A., Plado, J., Szyszka, M., Kirsimäe, K., Wild, E.M., Steier, P., Belcher, C.M., Jazwa, A.M., Helde, R., 2020. Determining the age and possibility for an extraterrestrial impact formation mechanism of the Ilumetsa structures (Estonia). Meteorit. Planet. Sci. 55, 274–293. https://doi.org/10.1111/maps.13431.

Lowe, D.R., Byerly, G.R., Kyte, F.T., 2014. Recently discovered 3.42–3.23 Ga impact layers, Barberton Belt, South Africa: 3.8 Ga detrital zircons, Archean impact history, and tectonic implications. Geology 42, 747–750. https://doi.org/10.1130/G35743.1.

MacLagan, E.A., Walton, E.L., Herd, C.D.K., Dence, M., 2018. Investigation of impact melt in allochthonous crater-fill deposits of the Steen River impact structure, Alberta, Canada. Meteorit. Planet. Sci. 53, 2285–2305. https://doi.org/10.1111/maps.13122.

MacLeod, N., 1998. Impacts and marine invertebrate extinctions. Geol. Soc. London Spec. Publ. 140 https://doi.org/10.1144/GSL.SP.1998.140.01.16, 217 LP – 246.

Mader, M.M., Osinski, G.R., Tornabene, L.L., 2013. Structural geology of the Mistastin Lake impact structure, Labrador, Canada. Lunar Planet. Sci. Conf 44. Abstract #2517.

Maher, K.A., Stevenson, D.J., 1988. Impact frustration of the origin of life. Nature 331, 612–614.

Malusà, M.G., Fitzgerald, P.G., 2019. Fission-Track Thermochronology and its Application to Geology. Springer, Berlin.

Marinova, M.M., Aharonson, O., Asphaug, E., 2008. Mega-impact formation of the Mars hemispheric dichotomy. Nature 453, 1216–1219.

Marion, C.L., 2009. Geology, distribution and geochemistry of impact melt at the Mistastin Lake impact crater. Memorial University, Labrador.

Marvin, U.B., 2006. Meteorites in history: an overview from the Renaissance to the 20th century. Geol. Soc. London. Spec. Publ. 256, 15–71. https://doi.org/10.1144/GSL.SP.2006.256.01.02.

Masaitis, V.L., 1999. Impact structures of northeastern Eurasia: The territories of Russia and adjacent countries. Meteorit. Planet. Sci. 34, 691–711.

Masaitis, Victor L., Mashchak, M.S., Naumov, Mikhail V., Selivanovskaya, T.V., 2020. Mode of Occurrence and Composition of Impact-Generated and Impact-Modified Formations. In: Masaitis, V.L., Naumov, M.V. (Eds.), The Puchezh-Katunki Impact Crater: Geology and Origin. Springer International Publishing, Cham, pp. 35–99. https://doi.org/10.1007/978-3-030-32043-0_3.

Mashchak, M.S., Naumov, M.V., 2012. The Suavjarvi impact structure, NW Russia. Meteorit. Planet. Sci. 47, 1644–1658. https://doi.org/10.1111/j.1945-5100.2012.01428.x.

McCall, G.J.H., 1965. New material from, and a reconsideration of, the Dalgaranga meteorite and crater, Western Australia. Mineral. Mag. J. Mineral. Soc. 35, 476–487. https://doi.org/10.1180/minmag.1965.035.271.03.

McDougall, I., Harrison, T.M., 1999. Geochronology and Thermochronology by the $^{40}Ar/^{39}Ar$ Method, 2nd ed. Oxford University Press, Oxford.

McIntyre, D.B., 1962. Impact metamorphism at Clearwater Lake, Quebec. J. Geophys. Res. 67, 1647.

McIntyre, D.B., 1968. Impact metamorphism at Clearwater Lake, Quebec. In: French, B. M., Short, N.M. (Eds.), Shock Metamorphism of Natural Materials. Mono Book Corp, Baltimore, pp. 363–366.

Meen, V.B., 1957. Chubb Crater - a meteor crater. J. R. Astron. Soc. Can. 51, 137–154.

Meier, M.M.M., Holm-Alwmark, S., 2017. A tale of clusters: no resolvable periodicity in the terrestrial impact cratering record. Mon. Not. R. Astron. Soc. 467, 2545–2551. https://doi.org/10.1093/mnras/stx211.

Meisel, T., Koeberl, C., Ford, R.J., 1990. Geochemistry of Darwin impact glass and target rocks. Geochemica Cosmochim. Acta 54, 1463–1474.

Melosh, H.J., 1989. Impact Cratering: A Geologic Process. Oxford University Press, New York.

Melosh, H.J., Ivanov, B.A., 1999. Impact crater collapse. Annu. Rev. Earth Planet. Sci. 27, 385–415.

Miljković, K., Collins, G.S., Mannick, S., Bland, P.A., 2013. Morphology and population of binary asteroid impact craters. Earth Planet. Sci. Lett. 363, 121–132. https://doi.org/10.1016/j.epsl.2012.12.033.

Milton, D.J., 1977. Shatter cones - an outstanding problem in shock mechanics. In: Roddy, D.J., Pepin, R.O., Merrill, R.B. (Eds.), Impact and Explosion Cratering. Pergamon Press, New York, pp. 703–714.

Milton, D.J., Macdonald, F.A., 2005. Goat Paddock, Western Australia: an impact crater near the simple complex transition. Aust. J. Earth Sci. 52, 689–697.

Monod, T., 1965. Contribution à l'établissement d'une liste d'accidents circulaires d'origine météoritique (Reconnus, pos- sibles ou supposés). Cryptoexplosive I.F.A.N. DAKAR. cata- logue et documents n° 18.

Monson, C.C., Sweet, D., Segvic, B., Zanoni, G., Balling, K., Wittmer, J.M., Ganis, G.R., Cheng, G., 2019. The Late Ordovician (Sandbian) Glasford structure: a marine-target impact crater with a possible connection to the Ordovician meteorite event. Meteorit. Planet. Sci. 54, 2927–2950. https://doi.org/10.1111/maps.13401.

Montalvo, S.D., Cavosie, A.J., Erickson, T.M., Talavera, C., 2017. Fluvial transport of impact evidence from cratonic interior to passive margin: Vredefort-derived shocked zircon on the Atlantic coast of South Africa. Am. Mineral. 102, 813–823. https://doi.org/10.2138/am-2017-5857CCBYNCND.

Montalvo, P.E., Cavosie, A.J., Kirkland, C.L., Evans, N.J., McDonald, B.J., Talavera, C., Erickson, T.M., Lugo-Centeno, C., 2018. Detrital shocked zircon provides first radiometric age constraint (<1472 Ma) for the Santa Fe impact structure, New Mexico, USA. GSA Bull. 131, 845–863. https://doi.org/10.1130/B31761.1.

Morbidelli, A., Marchi, S., Bottke, W.F., Kring, D.A., 2012. A sawtooth-like timeline for the first billion years of lunar bombardment. Earth Planet. Sci. Lett. 355–356, 144–151. https://doi.org/10.1016/j.epsl.2012.07.037.

Morgan, J.V., Warner, M.R., Collins, G.S., Melosh, H.J., Christeson, G.L., 2000. Peak-ring formation in large impact craters; geophysical constraints from Chicxulub. Earth Planet. Sci. Lett. 183, 347–354.

Morgan, J.V., Gulick, S.P.S., Bralower, T., Chenot, E., Christeson, G., Claeys, P., Cockell, C., Collins, G.S., Coolen, M.J.L., Ferrière, L., Gebhardt, C., Goto, K., Jones, H., Kring, D.A., Le Ber, E., Lofi, J., Long, X., Lowery, C., Mellett, C., Ocampo-Torres, R., Osinski, G.R., Perez-Cruz, L., Pickersgill, A., Poelchau, M., Rae, A., Rasmussen, C., Rebolledo-Vieyra, M., Riller, U., Sato, H., Schmitt, D.R., Smit, J., Tikoo, S., Tomioka, N., Urrutia-Fucugauchi, J., Whalen, M., Wittmann, A., Yamaguchi, K.E., Zylberman, W., 2016. The formation of peak rings in large impact craters. Science 354, 878–882.

Movshovich, Y.V., Milyavskiy, A.Y., 1988. New data on the formation conditions and age of the Kamensk and Gusev astroblemes. Meteoritika 112–118.

Murphy, A.J., Spray, J.G., 2002. Geology, mineralization, and emplacement of the Whistle-Parkin Offset Dike, Sudbury. Econ. Geol. 97, 1399.

Muszynski, A., Kryza, R.L.K., Pilski, A.S., Muszynska, J., 2012. Morasko – the largest iron meteorite shower in Central Europe (ogucki Wydawnictwo Naukowe.

Naumov, M.V., 2005. Principal features of impact-generated hydrothermal circulation systems: mineralogical and geochemical evidence. Geofluids 5, 165–184.

Newman, J.D., Herd, C.D.K., 2015. Mineralogy, petrology, and distribution of meteorites at the Whitecourt crater, Alberta, Canada. Meteorit. Planet. Sci. 50, 305–317. https://doi.org/10.1111/maps.12422.

Newman, J.D., Osinski, G.R., 2017. Characterization of breccia dykes in the deeply eroded Tunnunik impact structure, Canada. Annu. Meet. Meteorit. Soc. 80, 6248 (pdf).

Nicolaysen, L.O., Ferguson, J., 1990. Cryptoexplosion structures, shock deformation and siderophile concentration related to explosive venting of fluids associated with alkaline ultramafic magmas. Tectonophysics 171, 303–335. https://doi.org/10.1016/0040-1951(90)90107-J.

Nininger, H.H., 1954. Impactite slag at Barringer Crater [Arizona]. Am. J. Sci. 252 https://doi.org/10.2475/ajs.252.5.277, 277 LP – 290.

Oberbeck, V.R., 1975. The role of ballistic erosion and sedimentation in lunar stratigraphy. Rev. Geophys. Sp. Phys. 13, 337–362.

O'Brien, D.P., Walsh, K.J., Morbidelli, A., Raymond, S.N., Mandell, A.M., 2014. Water delivery and giant impacts in the 'Grand Tack' scenario. Icarus 239, 74–84. https://doi.org/10.1016/j.icarus.2014.05.009.

O'Callaghan, J.W., Osinski, G.R., Lightfoot, P.C., Linnen, R.L., Weirich, J.R., 2016. Reconstructing the geochemical signature of Sudbury Breccia, Ontario, Canada: implications for its formation and trace metal content. Econ. Geol. 111, 1705–1729.

Omar, G., Johnson, K.R., Hickey, L.J., Robertson, P.B., Dawson, M.R., Barnosky, C.W., 1987. Fission-track dating of Haughton Astrobleme and included biota, Devon Island, Canada. Science 237, 1603–1605.

Oppenheimer, C., 2003. Climatic, environmental and human consequences of the largest known historic eruption: Tambora volcano (Indonesia) 1815. Prog. Phys. Geogr. Earth Environ. 27, 230–259. https://doi.org/10.1191/0309133303pp379ra.

Ormö, J., Lindström, M., Lepinette, A., Martinez-Frias, J., Diaz-Martinez, E., 2006. Cratering and modification of wet-target craters: Projectile impact experiments and field observations of the Lockne marine-target crater (Sweden). Meteorit. Planet. Sci. 41, 1605–1612.

Ormö, J., Sturkell, E., Lindström, M., 2007. Sedimentological analysis of resurge deposits at the Lockne and Tvären craters: clues to flow dynamics. Meteorit. Planet. Sci. 42, 1929–1943. https://doi.org/10.1111/j.1945-5100.2007.tb00551.x.

Ormö, J., Sturkell, E., Nõlvak, J., Melero-Asensio, I., Frisk, Å., Wikström, T., 2014. The geology of the Målingen structure: A probable doublet to the Lockne marine-target

impact crater, central Sweden. Meteorit. Planet. Sci. 49, 313–327. https://doi.org/10.1111/maps.12251.
Ormö, J., Nielsen, A.T., Alwmark, C., 2017. The Vakkejokk Breccia: an Early Cambrian proximal impact ejecta layer in the North-Swedish Caledonides. Meteorit. Planet. Sci. 52, 623–645. https://doi.org/10.1111/maps.12816.
Ormö, J., Gulick, S.P.S., Whalen, M.T., King, D.T., Sturkell, E., Morgan, J., 2021. Assessing event magnitude and target water depth for marine-target impacts: Ocean resurge deposits in the Chicxulub M0077A drill core compared. Earth Planet. Sci. Lett. 564, 116915 https://doi.org/10.1016/j.epsl.2021.116915.
Osinski, G.R., 2005. Geological map, Haughton impact structure, Devon Island, Nunavut, Canada. Meteorit. Planet. Sci. 40. Supplement.
Osinski, G.R., Ferrière, L., 2016. Shatter cones: (Mis)understood? Sci. Adv. 2, e1600616 https://doi.org/10.1126/sciadv.1600616.
Osinski, G.R., Grieve, R.A.F., 2012. Comparison of mid-size terrestrial complex impact structures: A case study. In: Osinski, G.R., Pierazzo, E. (Eds.), Impact Cratering: Processes and Products. Wiley-Blackwell, pp. 290–305.
Osinski, G.R., Grieve, R.A.F., 2019. Impact Earth: a new resource for outreach, teaching, and research. Elements 15, 70–71.
Osinski, G.R., Pierazzo, E., 2012. Impact Cratering: Processes and Products. Wiley-Blackwell.
Osinski, G.R., Spray, J.G., 2001. Impact-generated carbonate melts: Evidence from the Haughton Structure, Canada. Earth Planet. Sci. Lett. 194, 17–29.
Osinski, G.R., Spray, J.G., 2005. Tectonics of complex crater formation as revealed by the Haughton impact structure, Devon Island, Canadian High Arctic. Meteorit. Planet. Sci. 40, 1813–1834.
Osinski, G.R., Lee, P., Spray, J.G., Parnell, J., Lim, D.S.S., Bunch, T.E., Cockell, C.S., Glass, B.J., 2005a. Geological overview and cratering model for the Haughton impact structure, Devon Island, Canadian High Arctic. Meteorit. Planet. Sci. 40, 1759–1776.
Osinski, G.R., Spray, J.G., Lee, P., 2005b. Impactites of the Haughton impact structure, Devon Island, Canadian High Arctic. Meteorit. Planet. Sci. 40, 1789–1812.
Osinski, G.R., Schwarcz, H.P., Smith, J.R., Kleindienst, M.R., Haldemann, A.F.C., Churcher, C.S., 2007. Evidence for a ~200–100 ka meteorite impact in the Western Desert of Egypt. Earth Planet. Sci. Lett. 253, 378–388.
Osinski, G.R., Grieve, R.A.F., Collins, G.S., Marion, C., Sylvester, P., 2008a. The effect of target lithology on the products of impact melting. Meteorit. Planet. Sci. 43, 1939–1954.
Osinski, G.R., Grieve, R.A.F., Spray, J.G., 2008b. Impact melting in sedimentary target rocks: An assessment. In: Evans, K.R., Horton, W., King Jr., D.K., Morrow, J.R., Warme, J.E. (Eds.), The Sedimentary Record of Meteorite Impacts, Geological Society of America Special Publication 437. Geological Society of America, Boulder, pp. 1–18.
Osinski, G.R., Kieniewicz, J.M., Smith, J.R., Boslough, M.B., Eccleston, M., Schwarcz, H. P., Kleindienst, M.R., Haldemann, A.F.C., 2008c. The Dakhleh Glass: Product of an impact airburst or cratering event in the Western Desert of Egypt? Meteorit. Planet. Sci. 43, 2017–2089.
Osinski, G.R., Tornabene, L.L., Grieve, R.A.F., 2011. Impact ejecta emplacement on the terrestrial planets. Earth Planet. Sci. Lett. 310, 167–181.
Osinski, G.R., Grieve, R.A.F., Tornabene, L.L., 2012a. Excavation and impact ejecta emplacement. In: Osinski, G.R., Pierazzo, E. (Eds.), Impact Cratering: Processes and Products. Wiley-Blackwell, Chichester, pp. 43–59.
Osinski, G.R., Singleton, A.C., Ozaruk, A., Hansen, J.R., 2012b. New investigations of the Gow Lake impact structure, Saskatchewan, Canada: Impact melt rocks, astronaut training, and more. Lunar Planet. Sci. Conf. 43, 2367 pdf.
Osinski, G.R., Tornabene, L.L., Banerjee, N.R., Cockell, C.S., Flemming, R.L., Izawa, M.R. M., McCutcheon, J., Parnell, J., Preston, L.J., Pickersgill, A.E., Pontefract, A., Sapers, H.M., Southam, G., 2013. Impact-generated hydrothermal systems on Earth and Mars. Icarus 224, 347–363.
Osinski, G.R., Grieve, R.A.F., Chanou, A., Sapers, H.M., 2016. The "suevite" conundrum, Part 1: The Ries suevite and Sudbury Onaping Formation compared. Meteorit. Planet. Sci. 51, 2316–2333. https://doi.org/10.1111/maps.12728.
Osinski, G.R., Grieve, R.A.F., Bleacher, J.M., Neish, C.D., Pilles, E.A., Tornabene, L.L., 2018. Igneous rocks formed by hypervelocity impact. J. Volcanol. Geotherm. Res. 353, 25–54.
Osinski, G.R., Silber, E.A., Clayton, J., Grieve, R.A.F., Hansen, K., Johnson, C.L., Kalynn, J., Tornebene, L.L., 2019. Transitional impact craters on the Moon: insight into the effect of target lithology on the impact cratering process. Meteorit. Planet. Sci. 54, 573–591.
Osinski, G.R., Cockell, C.S., Pontefract, A., Sapers, H.M., 2020a. The role of meteorite impacts in the origin of life. Astrobiology 20, 1121–1149. https://doi.org/10.1089/ast.2019.2203.
Osinski, G.R., Ferrière, L., Hill, P.J.A., Prave, A.R., Preston, L.J., Singleton, A., Pickersgill, A.E., 2020b. The mesoproterozoic stac fada member, nw scotland: an impact origin confirmed but refined. J. Geol. Soc. Lond. 178 https://doi.org/10.1144/jgs2020-056.
Osinski, Gordon R., Grieve, R.A.F., Hill, P.J.A., Simpson, S.L., Cockell, C., Christeson, G. L., Ebert, M., Gulick, S., Melosh, H.J., Riller, U., Tikoo, S.M., Wittmann, A., 2020c. Explosive interaction of impact melt and seawater following the Chicxulub impact event. Geology 48, 108–112. https://doi.org/10.1130/G46783.1.
Palme, H., Janssens, M.J., Takahashi, H., Anders, E., Hertogen, J., 1978. Meteoritic material at five large impact craters. Geochim. Cosmochim. Acta 42, 313–323.
Paré, G., Trudel, M.-C., Jaana, M., Kitsiou, S., 2015. Synthesizing information systems knowledge: a typology of literature reviews. Inf. Manag. 52, 183–199. https://doi.org/10.1016/j.im.2014.08.008.
Parnell, J., Bowden, S., Lindgren, P., Burchell, M., Milner, D., Price, M., Baldwin, E.C., Crawford, I.A., 2010. The preservation of fossil biomarkers during meteorite impact events: Experimental evidence from biomarker-rich projectiles and target rocks. Meteorit. Planet. Sci. 45, 1340–1358. https://doi.org/10.1111/j.1945-5100.2010.01100.x.
Parnell, J., Mark, D., Fallick, A.E., Boyce, A., Thackrey, S., 2011. The age of the Mesoproterozoic Stoer Group sedimentary and impact deposits, NW Scotland. J. Geol. Soc. Lond. 168, 349–358. https://doi.org/10.1144/0016-76492010-099.
Peck, E., 1979. The fate of a Kansas meteorite crater. Sky Telescope 58, 126–128.
Petaev, M.I., 1992. Meteorite sterlitamak – a new crater forming fall. Meteoritics 27, 276.
Philby, H.S.J., 1933. Rub' al Khali: an account of exploration in the Great South Desert of Arabia under the auspices and patronage of his majesty 'Abdul 'aziz ibn Sa'ud, King of Hejaz and Nejd and its dependencies. Geogr. J. 81, 1–21.
Pickersgill, A.E., Mark, D.F., Lee, M.R., Osinski, G.R., 2020. 40Ar/39Ar systematics of melt lithologies and target rocks from the Gow Lake impact structure, Canada. Geochim. Cosmochim. Acta 274, 317–332. https://doi.org/10.1016/j.gca.2020.01.025.
Pierazzo, E., Artemieva, N., 2012. Local and global environmental effects of impacts on Earth. Elements 8, 55–60. https://doi.org/10.2113/gselements.8.1.55.
Pierazzo, E., Vickery, A.M., Melosh, H.J., 1997. A reevaluation of impact melt production. Icarus 127, 408–423.
Pike, R.J., 1977. Apparent depth/apparent diameter relation for lunar craters. Lunar Planet. Sci. Conf. 8, 3427–3436.
Pike, R.J., 1980. Control of crater morphology by gravity and target type - Mars, Earth, Moon. Proc. Lunar Planet. Sci. Conf. 11, 2159–2189.
Pike, R.J., 1985. Some morphologic systematics of complex impact structures. Meteoritics 20, 49–68. https://doi.org/10.1111/j.1945-5100.1985.tb00846.x.
Pike, R.J., Spudis, P.D., 1987. Basin-ring spacing on the Moon, Mercury, and Mars. Earth Moon Planet. 39, 129–194. https://doi.org/10.1007/BF00054060.
Pilles, E.A., Osinski, G.R., Grieve, R.A.F., Smith, D., Bailey, J., 2018. Formation of large-scale impact melt dikes: A case study of the Foy Offset Dike at the Sudbury impact structure, Canada. Earth Planet. Sci. Lett. 495, 224–233. https://doi.org/10.1016/j.epsl.2018.05.023.
Pincus, M.R., Cavosie, A.J., Gibbons, R., 2015. Preservation of detrital shocked minerals in Deep Time: Shocked grains in the 300 Myr Dwyka Group tillite, South Africa. Lunar Planet. Sci. Conf. 46, 1629 (pdf).
Poag, C.W., Koeberl, C., Reimold, W.U., 2004. The Chesapeaky Bay Crater. Springer.
Poelchau, M.H., Kenkmann, T., 2011. Feather features: a low-shock-pressure indicator in quartz. J. Geophys. Res. Solid Earth 116. https://doi.org/10.1029/2010JB007803.
Poelchau, M.H., Kenkmann, T., Thoma, K., Hoerth, T., Dufresne, A., SchÄFer, F., 2013. The MEMIN research unit: scaling impact cratering experiments in porous sandstones. Meteorit. Planet. Sci. 48, 8–22. https://doi.org/10.1111/maps.12016.
Pohl, J., Stoffler, D., Gall, H., Ernston, K., 1977. The Ries impact crater. In: Merrill, R.B., Pepin, R.D.J., Pepin, R.O. (Eds.), Impact and Explosion Cratering. Pergamom Press, New York, pp. 343–404.
Powars, D.S., Bruce, T.S., 1999. The effects of the Chesapeake Bay impact crater on the geological framework and correlation of hydrogeologic units of the lower York-James Peninsula, Virginia, U. S. Geological Survey Professional Paper 1612. U. S. Geological Survey, Reston, VA.
Prescott, J.R., Robertson, G.B., Shoemaker, C.S., Shoemaker, E.M., Wynn, J., 2004. Luminescence dating of the Wabar meteorite craters, Saudi Arabia. J. Geophys. Res. 109 (E01008), 2004. https://doi.org/10.1029/2003JE002136.
Rampino, M.R., Caldeira, K., 2015. Periodic impact cratering and extinction events over the last 260 million years. Mon. Not. R. Astron. Soc. 454, 3480–3484. https://doi.org/10.1093/mnras/stv2088.
Rampino, M., Koeberl, C., MacLeod, K.G., 2002. Role of the galaxy in periodic impacts and mass extinctions on the Earth. In: Catastropic Events and Mass Extinctions: Impacts and Beyond, Geological Society of America Special Paper 356. Geological Society of America, Boulder, Colorado, pp. 667–678.
Raup, D.M., Sepkoski, J.J., 1984. Periodicity of extinctions in the geologic past. Proc. Natl. Acad. Sci. 81 https://doi.org/10.1073/pnas.81.3.801, 801 LP – 805.
Reddy, S.M., Johnson, T.E., Fischer, S., Rickard, W.D.A., Taylor, R.J.M., 2015. Precambrian reidite discovered in shocked zircon from the Stac Fada impactite, Scotland. Geology 43, 899–902. https://doi.org/10.1130/G37066.1.
Reimold, W.U., 1995. Pseudotachylite in impact structures - generation by friction melting and shock brecciation?: a review and discussion. Earth Sci. Rev. 39, 247–265.
Reimold, W.U., Gibson, R.L., 2005. "Pseudotachylites" in large impact structures. In: Koeberl, C., Henkel, H. (Eds.), Impact Tectonics. Springer, pp. 1–55.
Reimold, W.U., Gibson, R.L., 2006. The melt rocks of the Vredefort impact structure - Vredefort Granophyre and pseudotachylitic breccias: implications for impact cratering and the evolution of the Witwatersrand Basin. Chemie der Erde - Geochemistry 66, 1–35.
Reimold, W.U., Grieve, R.A.F., Palme, H., 1981. Rb-Sr dating of the impact melt from East Clearwater, Quebec. Contrib. Mineral. Petrol. 76, 73–76.
Reimold, W.U., Koeberl, C., Gibson, R.L., Dressler, B.O., 2005. Economic mineral deposits in impact structures and their geological settings. In: Koeberl, C., Henkel, H. (Eds.), Impact Tectonics, Impact Studies Series, Vol. 6. Springer-Verlag, Berlin, pp. 479–552.
Reinwald, I.A., 1939. The Kaalijärvi meteor craters (Estonia). Publ. Geol. Inst. Univ. Tartu 55, 1–19.
Renne, P.R., Deino, A.L., Hames, W.E., Heizler, M.T., Hemming, S.R., Hodges, K.V., Koppers, A.A.P., Mark, D.F., Morgan, L.E., Phillips, D., Singer, B.S., Turrin, B.D., Villa, I.M., Villeneuve, M., Wijbrans, J.R., 2009. Data reporting norms for $^{40}Ar/^{39}Ar$ geochronology. Quat. Geochronol. 4, 346–352. https://doi.org/10.1016/j.quageo.2009.06.005.
Renne, P.R., Mundil, R., Balco, G., Min, K., Ludwig, K.R., 2010. Joint determination of 40K decay constants and 40Ar*/40K for the Fish Canyon sanidine standard, and

improved accuracy for 40Ar/39Ar geochronology. Geochim. Cosmochim. Acta 74, 5349–5367. https://doi.org/10.1016/j.gca.2010.06.017.
Renne, P.R., Deino, A.L., Hilgen, F.J., Kuiper, K.F., Mark, D.F., Mitchell, W.S.I., Morgan, L.E., Mundil, R., Smit, J., 2013. Time scales of critical events around the Cretaceous-Paleogene boundary. Science 339, 684–687. https://doi.org/10.1126/science.1230492.
Renne, P.R., Arenillas, I., Arz, J.A., Vajda, V., Gilabert, V., Bermúdez, H.D., 2018. Multi-proxy record of the Chicxulub impact at the Cretaceous- Paleogene boundary from Gorgonilla Island, Colombia. Geology 46, 547–550. https://doi.org/10.1130/G40224.1.
Rickard, J.H., Watkinson, D.H., 2001. Cu-Ni-PGE Mineralization within the Copper Cliff Offset Dike, Copper Cliff North Mine, Sudbury, Ontario: evidence for Multiple Stages of Emplacement. Explor. Min. Geol. 1–2, 111–124.
Rink, W.J., Thompson, J.W., 2015. Encyclopedia of Scientific Dating Methods. Springer Reference, Berlin.
Robbins, S.J., Hynek, B.M., 2013. Utility of laser altimeter and stereoscopic terrain models: Application to Martian craters. Planet. Space Sci. 86, 57–65. https://doi.org/10.1016/j.pss.2013.06.019.
Robertson, P.B., Greive, R.A.F., 1977. Shock attenuation at terrestrial impact structures. In: Merrill, R.B., Pepin, R.D.J., Pepin, R.O. (Eds.), Impact and Explosion Cratering. Pergamon Press, New York, pp. 687–702.
Robertson, P.B., Dence, M.R., Vos, M.A., 1968. Deformation in rock-forming minerals from Canadian craters. In: French, B.M., Short, N.M. (Eds.), Shock Metamorphism of Natural Materials. Mono Book Corp, Baltimore, pp. 433–452.
Rochette, P., Alaç, R., Beck, P., Brocard, G., Cavosie, A.J., Debaille, V., Devouard, B., Jourdan, F., Mougel, B., Moustard, F., Moynier, F., Nomade, S., Osinski, G.R., Reynard, B., Cornec, J., 2019. Pantasma: Evidence for a Pleistocene circa 14 km diameter impact crater in Nicaragua. Meteorit. Planet. Sci. 54 https://doi.org/10.1111/maps.13244.
Rochette, P., Beck, P., Bizzarro, M., Braucher, R., Cornec, J., Debaille, V., Devouard, B., Gattacceca, J., Jourdan, F., Moustard, F., Moynier, F., Nomade, S., Reynard, B., 2021. Impact glasses from Belize represent tektites from the Pleistocene Pantasma impact crater in Nicaragua. Commun. Earth Environ. 2, 94. https://doi.org/10.1038/s43247-021-00155-1.
Roperch, P., Gattacceca, J., Valenzuela, M., Devouard, B., Lorand, J.-P., Arriagada, C., Rochette, P., Latorre, C., Beck, P., 2017. Surface vitrification caused by natural fires in Late Pleistocene wetlands of the Atacama Desert. Earth Planet. Sci. Lett. 469, 15–26. https://doi.org/10.1016/j.epsl.2017.04.009.
Roperch, P., Gattacceca, J., Valenzuela, M., Devouard, B., Lorand, J.-P., Rochette, P., Latorre, C., Beck, P., 2022. Widespread glasses generated by cometary fireballs during the late Pleistocene in the Atacama Desert, Chile: COMMENT. Geology 50, e550. https://doi.org/10.1130/G49958C.1.
Sage, R.P., 1978. Diatremes and shock features in Precambrian rocks of the Slate Islands, northeastern Lake Superior. GSA Bull. 89, 1529–1540. https://doi.org/10.1130/0016-7606(1978)89<1529:DASFIP>2.0.CO;2.
Sandbakken, P.T., Langenhorst, F., Dypvik, H., 2005. Shock metamorphism of quartz at the submarine Mjolnir impact crater, Barents Sea. Meteorit. Planet. Sci. 40, 1363–1375.
Schärer, U., Deutsch, A., 1990. Isotope systematics and shock-wave metamorphism: II. U-Pb and Rb-Sr in naturally shocked rocks, the Haughton impact structure, Canada. Geochim. Cosmochim. Acta 54, 3435–3447.
Scherler, D., Kenkmann, T., Jahn, A., 2006. Structural record of an oblique impact. Earth Planet. Sci. Lett. 248, 43–53.
Schmieder, M., Jourdan, F., 2013. The Lappajärvi impact structure (Finland): Age, duration of hydrothermal crater cooling, and implications for life. Geochim. Cosmochim. Acta 112, 321–339. https://doi.org/10.1016/j.gca.2013.02.015.
Schmieder, M., Kring, D.A., 2020. Earth's impact events through geologic time: a list of recommended ages for terrestrial impact structures and deposits. Astrobiology 20, 91–141. https://doi.org/10.1089/ast.2019.2085.
Schmieder, M., Schwarz, W.H., Trieloff, M., Tohver, E., Buchner, E., Hopp, J., Osinski, G. R., 2015. New 40Ar/39Ar dating of the Clearwater Lake impact structures (Québec, Canada) – Not the binary asteroid impact it seems? Geochim. Cosmochim. Acta 148, 304–324. https://doi.org/10.1016/j.gca.2014.09.037.
Schmieder, M., Schwarz, W.H., Trieloff, M., Buchner, E., Hopp, J., Tohver, E., Pesonen, L. J., Lehtinen, M., Moilanen, J., Werner, S.C., Öhman, T., 2016. The two Suvasvesi impact structures, Finland: Argon isotopic evidence for a "false" impact crater doublet. Meteorit. Planet. Sci. 51, 966–980. https://doi.org/10.1111/maps.12636.
Schmitz, B., Tassinari, M., Peucker-Ehrenbrink, B., 2001. A rain of ordinary chondritic meteorites in the early Ordovician. Earth Planet. Sci. Lett. 194, 1–15.
Schoene, B., 2014. 4.10 - U–Th–Pb Geochronology. In: Holland, H.D., Turekian, K.K.B.T.-T., on G. (Second E. (Eds.), Treatise on Geochemistry (Second Edition). Elsevier, Oxford, pp. 341–378. https://doi.org/10.1016/B978-0-08-095975-7.00310-7.
Scholz, C.A., Karp, T., Brooks, K.M., Milkereit, B., Amoako, P.Y.O., Arko, J.A., 2002. Pronounced central uplift identified in the Bosumtwi impact structure, Ghana, using multichannel seismic reflection data. Geology 30, 939–942. https://doi.org/10.1130/0091-7613(2002)030<0939:PCUIIT>2.0.CO;2.
Schulte, P., Alegret, L., Arenillas, I., Arz, J.A., Barton, P.J., Bown, P.R., Bralower, T.J., Christeson, G.L., Claeys, P., Cockell, C.S., Collins, G.S., Deutsch, A., Goldin, T.J., Goto, K., Grajales-Nishimura, J.M., Grieve, R.A.F., Gulick, S.P.S., Johnson, K.R., Kiessling, W., Koeberl, C., Kring, D.A., MacLeod, K.G., Matsui, T., Melosh, J., Montanari, A., Morgan, J.V., Neal, C.R., Nichols, D.J., Norris, R.D., Pierazzo, E., Ravizza, G., Rebolledo-Vieyra, M., Reimold, W.U., Robin, E., Salge, T., Speijer, R.P., Sweet, A.R., Urrutia-Fucugauchi, J., Vajda, V., Whalen, M.T., Willumsen, P.S., 2010. The Chicxulub asteroid impact and mass extinction at the Cretaceous-Paleogene boundary. Science 327, 1214–1218. https://doi.org/10.1126/science.1177265.
Schultz, P.H., Zárate, M., Hames, B., Koeberl, C., Bunch, T., Storzer, D., Renne, P., Wittke, J., 2004. The Quaternary impact record from the Pampas, Argentina. Earth Planet. Sci. Lett. 219, 221–238.
Schultz, P.H., Harris, R.S., Clemett, S.J., Thomas-Keprta, K.L., Zárate, M., 2014. Preserved flora and organics in impact melt breccias. Geology 42, 515–518. https://doi.org/10.1130/G35343.1.
Schultz, P.H., Harris, R.S., Perroud, S., Blanco, N., Tomlinson, A.J., 2021. Widespread glasses generated by cometary fireballs during the late Pleistocene in the Atacama Desert, Chile. Geology. https://doi.org/10.1130/G49426.1.
Scott, E.R.D., 2020. Iron Meteorites: Composition, Age, and Origin. https://doi.org/10.1093/acrefore/9780190647926.013.206.
Scott, D., Hajnal, Z., 1988. Seismic signature of the Haughton structure. Meteoritics 23, 239–247.
Scott, R.G., Pilkington, M., Tanczyk, E.I., 1997. Magnetic investigations of the West Hawk, Deep Bay and Clearwater impact structures, Canada. Meteoritics 32, 293–308.
Seeger, C.R., 1968. Origin of the Jeptha Knob structure, Kentucky. Am. J. Sci. 266, 630–660. https://doi.org/10.2475/ajs.266.8.630.
Sherlock, S.C., Kelley, S.P., Parnell, J., Green, P., Lee, P., Osinski, G.R., Cockell, C.S., 2005. Re-evaluating the age of the Haughton impact event. Meteorit. Planet. Sci. 40, 1777–1787.
Shoemaker, E.M., Herkenhoff, K.E., 1983. Impact origin of Upheaval Dome, Utah (abstract). In: 36th Symposium on Southwestern Geology and Paleontology, Museum of Northern Arizona, Flagstaff, Arizona, p. 13.
Shoemaker, E.M., Gault, D.E., Lugn, R.V., 1961. Shatter cones formed by high speed impact in dolomite, 417, p. D365.
Shoemaker, E.M., Roddy, D.J., Shoemaker, C.S., Roddy, J.K., 1988. The Boxhole meteorite crater, Northern Territory, Australia. Lunar Planet. Sci. Conf. 19, 1081–1082.
Shoemaker, E.M., Shoemaker, C.S., 1985. Impact structures of Western Australia. Meteoritics 20, 754–756.
Simonson, B.M., Glass, B.J., 2004. Spherule layers - Records of ancient impacts. Annu. Rev. Earth Planet. Sci. 32, 329–361.
Singleton, A.C., Osinski, G.R., Grieve, R.A.F., Shaver, C., 2011. Characterization of impact melt-bearing impactite dykes from the central uplift of the Mistastin Lake impact structure, Labrador. 42nd Lunar Planet. Sci. Conf. Abstract #2250.
Sjöqvist, A.S.L., Lindgren, P., Sturkell, E.F.F., Hogmalm, K.J., Broman, C., Ivarsson, M., Lee, M.R., 2016. Shock metamorphism and hydrothermal alteration of mafic impact ejecta from the Lockne impact structure, Sweden. Gff 139, 119–128. https://doi.org/10.1080/11035897.2016.1227361.
Skála, R., Jakeš, P., 1999. Shock-induced effects in natural calcite-rich targets as revealed by X-ray powder diffraction. In: Dressler, B.O., Sharpton, V.L. (Eds.), Large Meteorite Impacts and Planetary Evolution II, Geological Society of America Special Paper 339. Geological Society of America, Boulder, pp. 205–214.
Sleep, N.H., Zahnle, K.J., Kasting, J.F., Morowitz, H.J., 1989. Annihilation of ecosystems by large asteroid impacts on the early Earth. Nature 342, 139–142.
Smelror, M., Kelly, S.R.A., Dypvik, H., Mork, A., Nagy, J., Tsikalas, F., 2001. Mjolnir (Barents Sea) meteorite impact ejecta offers a Volgian-Ryazanian boundary marker. Newsl. Stratigr. 38, 129–140.
Smith, S.K., Grieve, R.A.F., Harris, J.R., Singhroy, V., 1999. The utilization of RADARSAT-1 imagery for the characterization of terrestrial impact landforms. Can. J. Remote. Sens. 25, 218.
Spektor, K., Tran, D.T., Leinenweber, K., Häussermann, U., 2013. Transformation of rutile to TiO2-II in a high pressure hydrothermal environment. J. Solid State Chem. 206, 209–216. https://doi.org/10.1016/j.jssc.2013.08.018.
Spencer, L.J., 1933. Meteorite craters as topographical features on the Earth's surface. Geogr. J. 81, 227–243. https://doi.org/10.2307/1784038.
Sprain, C.J., Renne, P.R., Clemens, W.A., Wilson, G.P., 2018. Calibration of chron C29r: New high-precision geochronologic and paleomagnetic constraints from the Hell Creek region, Montana. GSA Bull. 130, 1615–1644. https://doi.org/10.1130/B31890.1.
Spray, J.G., Kelley, S.P., Rowley, D.B., 1998. Evidence for a late Triassic multiple impact event on Earth. Nature 392, 171–173. https://doi.org/10.1038/32397.
Stephan, T., Jessberger, E.K., 1992. Isotope systematics and shock-wave metamorphism. III - K-Ar in experimentally and naturally shocked rocks; the Haughton impact structure. Canada. Geochim. Cosmochim. Acta 56, 1591–1605.
Stewart, S.A., 2003. How will we recognize buried impact craters in terrestrial sedimentary basins? Geology 31, 929–932.
Stöffler, D., 1966. Zones of impact metamorphism in the crystalline rocks of the Nordlinger Ries crater. Contrib. Mineral. Petrol. 12, 15–24.
Stöffler, D., 1984. Glasses formed by hypervelocity impact. J. Non-Cryst. Solids 67, 465–502.
Stöffler, D., Grieve, R.A.F., 2007. Impactites. In: Fettes, D., Desmons, J. (Eds.), Metamorphic Rocks. Cambridge University Press, Cambridge, pp. 82–92.
Stöffler, D., Langenhorst, F., 1994. Shock metamorphism of quartz in nature and experiment: 1. Basic observation and theory. Meteoritics 29, 155–181.
Stöffler, D., Artemieva, N.A., Pierazzo, E., 2002. Modeling the Ries-Steinheim impact event and the formation of the moldavite strewn field. Meteorit. Planet. Sci. 37, 1893–1907. https://doi.org/10.1111/j.1945-5100.2002.tb01171.x.
Stöffler, D., Hamann, C., Metzler, K., 2018. Shock metamorphism of planetary silicate rocks and sediments: Proposal for an updated classification system. Meteorit. Planet. Sci. 53, 5–49. https://doi.org/10.1111/maps.12912.
Sturkell, E.F.F., 1998. The marine Lockne impact structure, Jmtland, Sweden: a review. Int. J. Earth Sci. 87, 253.
Svensson, N.B., Wickman, F.E., 1965. Coesite from Lake Mien, southern Sweden. Nat. 205, 1202–1203.

Swisher, C.C.I., Grajales-Nishimura, J.M., Montanari, A., Margolis, S.V., Claeys, P., Alvarez, W., Renne, P.R., Cedillo, P.E., Maurrasse-Florentin, J.M.R., Curtis, G.H., Smit, J., McWilliams, M.O., 1992. Coeval (super 40) Ar/ (super 39) Ar ages of 65.0 million years ago from Chicxulub Crater melt rock and Cretaceous-Tertiary boundary tektites. Science 257, 954–958.

Szokaluk, M., Jagodziński, R., Muszyński, A., Szczuciński, W., 2019. Geology of the Morasko craters, Poznań, Poland—Small impact craters in unconsolidated sediments. Meteorit. Planet. Sci. 54, 1478–1494. https://doi.org/10.1111/maps.13290.

Tauxe, L., Banerjee, S.K., Butler, R.F., van der Voo, R., 2018. Essentials of Paleomagnetism, 5th Web edition.

Therriault, A.M., Fowler, A.D., Grieve, R.A.F., 2002. The Sudbury Igneous Complex: A differentiated impact melt sheet. Econ. Geol. 97, 1521–1540.

Thomas, M.D., Innes, M.J.S., 1977. The Gow Lake impact structure, northern Saskatchewan. Can. J. Earth Sci. 14, 1788–1795.

Thombre, R.S., Shivakarthik, E., Sivaraman, B., Vaishampayan, P.A., Seuylemezian, A., Meka, J.K., Vijayan, S., Kulkarni, P.P., Pataskar, T., Patil, B.S., 2019. Survival of extremotolerant bacteria from the mukundpura meteorite impact crater. Astrobiology 19, 785–796. https://doi.org/10.1089/ast.2018.1928.

Thompson, L.M., Spray, J.G., 1996. Pseudotachylyte petrogenesis: constraints from the Sudbury impact structure. Contrib. Mineral. Petrol. 125, 359–374.

Thomson, O.A., Cavosie, A.J., Moser, D.E., Barker, I., Radovan, H.A., French, B.M., 2014. Preservation of detrital shocked minerals derived from the 1.85 Ga Sudbury impact structure in modern alluvium and Holocene glacial deposits. GSA Bull. 126, 720–737. https://doi.org/10.1130/B30958.1.

Timms, N.E., Erickson, T.M., Pearce, M.A., Cavosie, A.J., Schmieder, M., Tohver, E., Reddy, S.M., Zanetti, M.R., Nemchin, A.A., Wittmann, A., 2017a. A pressure-temperature phase diagram for zircon at extreme conditions. Earth-Science Rev. https://doi.org/10.1016/j.earscirev.2016.12.008.

Timms, N.E., Erickson, T.M., Zanetti, M.R., Pearce, M.A., Cayron, C., Cavosie, A.J., Reddy, S.M., Wittmann, A., Carpenter, P.K., 2017b. Cubic zirconia in > 2370 °C impact melt records Earth's hottest crust. Earth Planet. Sci. Lett. 477, 52–58. https://doi.org/10.1016/j.epsl.2017.08.012.

Timms, N.E., Pearce, M.A., Erickson, T.M., Cavosie, A.J., Rae, Auriol S.P., Wheeler, J., Wittmann, Axel, Ferrière, Ludovic, Poelchau, Michael H., Tomioka, Naotaka, Collins, G.S., Gulick, Sean P.S., Rasmussen, Cornelia, Morgan, Joanna V., Gulick, S.P.S., Morgan, J.V., Chenot, E., Christeson, G.L., Claeys, P., Cockell, C.S., Coolen, M.J.L., Ferrière, L., Gebhardt, C., Goto, K., Green, S., Jones, H., Kring, D.A., Lofi, J., Lowery, C.M., Ocampo-Torres, R., Perez-Cruz, L., Pickersgill, A.E., Poelchau, M.H., Rae, A.S.P., Rasmussen, C., Rebolledo-Vieyra, M., Riller, U., Sato, H., Smit, J., Tikoo, S.M., Tomioka, N., Urrutia-Fucugauchi, J., Whalen, M.T., Wittmann, A., Xiao, L., Yamaguchi, K.E., Scientists, I.-I.E. 364, 2019. New shock microstructures in titanite (CaTiSiO5) from the peak ring of the Chicxulub impact structure, Mexico. Contrib. Mineral. Petrol. 174 https://doi.org/10.1007/s00410-019-1565-7.

Timms, N.E., Kirkland, C.L., Cavosie, A.J., Rae, A.S.P., Rickard, W.D.A., Evans, N.J., Erickson, T.M., Wittmann, A., Ferrière, L., Collins, G.S., Gulick, S.P.S., 2020. Shocked titanite records Chicxulub hydrothermal alteration and impact age. Geochim. Cosmochim. Acta 281, 12–30. https://doi.org/10.1016/j.gca.2020.04.031.

Tornabene, L.L., Watters, W.A., Osinski, G.R., Boyce, J.M., Harrison, T.N., Ling, V., McEwen, A.S., 2018. A depth versus diameter scaling relationship for the best-preserved melt-bearing complex craters on Mars. Icarus 299, 68–83. https://doi.org/10.1016/j.icarus.2017.07.003.

Tuchscherer, M.G., Spray, J.G., 2002. Geology, mineralization, and emplacement of the Foy Offset dike, Sudbury impact structure. Econ. Geol. 97, 1377–1397.

Turtle, E.P., Pierazzo, E., Collins, G.S., Osinski, G.R., Melosh, H.J., Morgan, J.V., Reimold, W.U., 2005. Impact structures: What does crater diameter mean? In: Kenkmann, T., Hörz, F., Deutsch, A. (Eds.), Large Meteorite Impacts III: Geological Society of America Special Paper 384. Geological Society of America, Boulder, pp. 1–24.

Van Ginneken, M., Goderis, S., Artemieva, N., Debaille, V., Decrée, S., Harvey, R.P., Huwig, K.A., Hecht, L., Yang, S., Kaufmann, F.E.D., Soens, B., Humayun, M., Van Maldeghem, F., Genge, M.J., Claeys, P., 2021. A large meteoritic event over Antarctica ca. 430 ka ago inferred from chondritic spherules from the Sør Rondane Mountains. Sci. Adv. 7, eabc1008. https://doi.org/10.1126/sciadv.abc1008.

Vasilyev, N.V., 1998. The Tunguska Meteorite problem today. Planet. Space Sci. 46, 129–150.

Veretennikov, N.V., 2010. The Logoisk impact crater. AIP Conf. Proc. 1205, 185–190. https://doi.org/10.1063/1.3382328.

Warme, J.E., Kuehner, H.-C., 1998. Anatomy of an Anomaly: The Devonian Catastrophic Alamo Impact Breccia of Southern Nevada. Int. Geol. Rev. 40, 189–216. https://doi.org/10.1080/00206819809465206.

Wasson, J.T., 2003. Large aerial bursts: An important class of terrestrial accretionary events. Astrobiology 3, 163–179.

Wasson, J.T., Boslough, M.B., 2000. Large aerial bursts; an important class of terrestrial accretionary events. In: Catastrophic Events and Mass Extinctions: Impacts and Beyond, pp. 239–240.

Wasson, J.T., Ouyang, X., Wang, J., Eric, J., 1989. Chemical classification of iron meteorites: XI. Multi-element studies of 38 new irons and the high abundance of ungrouped irons from Antarctica. Geochim. Cosmochim. Acta 53, 735–744. https://doi.org/10.1016/0016-7037(89)90016-1.

Wasson, J.T., Pitakpaivan, K., Putthapiban, P., Salyapongse, S., Thapthimthong, B., McHone, J.F., 1995. Field recovery of layered tektites in Northeast Thailand. J. Geophys. Res. 100, 14383–14389.

Weeks, R.A., Underwood, J.R., Giegengack, R., 1984. Libyan desert glass: a review. J. Non-Cryst. Solids 67, 593–619.

Whitehead, J., Grieve, R.A.F., Spray, J.G., 2002. Mineralogy and petrology of melt rocks from the Popigai impact structure, Siberia. Meteorit. Planet. Sci. 37, 623–647. https://doi.org/10.1111/j.1945-5100.2002.tb00844.x.

Wieland, F., Gibson, R.L., Reimold, W.U., 2005. Structural analysis of the collar of the Vredefort Dome, South Africa—significance for impact-related deformation and central uplift formation. Meteorit. Planet. Sci. 40, 1537–1554.

Wilshire, H.G., Offield, T.W., Howard, K.A., Cummings, D., 1972. Geology of the Sierra Madera Cryptoexplosion Structure, Pecos County, Texas, United States Geological Survey Professional Paper. United States Government Printing Office, Washington.

Wilson, C.W., Stearns, R.G., 1968. Geology of the Wells Creek Structure, Tennessee, State of Tennessee Department of Conservation Division of Geology Bulletin. State of Tennessee Department of Conservation Division of Geology, Nashville.

Winslow III, F., Rasbury, E., Hemming, S., 2004. Petrologic Complexities of the Manicouagan Melt Sheet: Implications for ^{40}Ar-^{39}Ar Geochronology. Lunar Planet. Inst. Sci. Conf. Abstr. 35, 2034.

Wintle, A.G., 2008. Luminescence dating: where it has been and where it is going. Boreas 37, 471–482. https://doi.org/10.1111/j.1502-3885.2008.00059.x.

Wittmann, A., Kenkmann, T., Schmitt, R.T., Stoffler, D., 2006. Shock-metamorphosed zircon in terrestrial impact craters. Meteorit. Planet. Sci. 41, 433–454.

Wood, C.R., Spray, J.G., 1998. Origin and emplacement of offset dykes in the Sudbury structure: Constraints from Hess. Meteorit. Planet. Sci. 33, 337–347.

Wünnemann, K., Weiss, R., Hofmann, K., 2007. Characteristics of oceanic impact-induced large water waves—Re-evaluation of the tsunami hazard. Meteorit. Planet. Sci. 42, 1893–1903. https://doi.org/10.1111/j.1945-5100.2007.tb00548.x.

Wünnemann, K., Collins, G.S., Osinski, G.R., 2008. Numerical modelling of impact melt production on porous rocks. Earth Planet. Sci. Lett. 269, 529–538.

Wünnemann, K., Zhu, M.-H., Stöffler, D., 2016. Impacts into quartz sand: Crater formation, shock metamorphism, and ejecta distribution in laboratory experiments and numerical models. Meteorit. Planet. Sci. 51, 1762–1794. https://doi.org/10.1111/maps.12710.

Young, G.M., 2002. Stratigraphy and geochemistry of volcanic mass flows in the Stac Fada Member of the Stoer Group, Torridonian, NW Scotland. Trans. Earth Sci. 93, 1–16.

Young, K.E., van Soest, M.C., Hodges, K.V., Watson, E.B., Adams, B.A., Lee, P., 2013. Impact thermochronology and the age of Haughton impact structure, Canada. Geophys. Res. Lett. 40, 3836–3840. https://doi.org/10.1002/grl.50745.

Zellner, N.E.B., 2017. Cataclysm no more: New views on the timing and delivery of lunar impactors. Orig. Life Evol. Biosph. 47, 261–280. https://doi.org/10.1007/s11084-017-9536-3.

Zhao, J., Xiao, L., Xiao, Z., Morgan, J.V., Osinski, G.R., Neal, C.R., Gulick, S.P.S., Riller, U., Claeys, P., Zhao, S., Prieur, N.C., Nemchin, A., Yu, S., IODP 364 Science Party, 2021. Shock-deformed zircon from the Chicxulub impact crater and implications for cratering process. Geology 49, 755–760. https://doi.org/10.1130/G48278.1.